THE UNIVERSITY OF CHICAGO

THE ROLE OF PROTEIN OLIGOMERIZATION IN CELL SURFACE POLARITY

A DISSERTATION SUBMITTED TO
THE FACULTY OF THE DIVISION OF THE BIOLOGICAL SCIENCES
AND THE PRITZKER SCHOOL OF MEDICINE
IN CANDIDACY FOR THE DEGREE OF
DOCTOR OF PHILOSOPHY

COMMITTEE ON GENETICS, GENOMICS, AND SYSTEMS BIOLOGY

BY
CHARLES F LANG

CHICAGO, ILLINOIS
JUNE 2022

TABLE OF CONTENTS

LIST OF FIGURES

ACKNOWLEDGMENTS

I would like to acknowledge the many people who helped me, both scientifically and personally, over the course of my graduate work in Chicago. I'm very grateful to Ed Munro for allowing me to work in his lab and mentoring me. He has had a tremendous impact in shaping me as a scientist and was also a great role model for how to be a productive, generous, and respectful member of the scientific community. I'm also thankful to the Munro lab more broadly for help with experiments and for doing interesting work that I got to hear about in lab meeting. In particular, I want to acknowledge Alex Anneken for training me during my first year in lab and contributing ideas that influenced my thesis work and Seth Donoughe for helpful feedback and encouragement on my dissertation. I also want to acknowledge Younan Li and Jon Michaux for taking me in as senior grad students and for all the great conversations we had over lunch. Outside of lab, I'm very grateful for all my classmates who were wonderful friends and colleagues, and for all the fun things we did together outside of science over my time in Chicago (e.g. camping trips, rock climbing, playing music, hanging out at the pub). I'm also indebted to GGSB administrator Sue Levison for her various forms of support over the years, both personal and logistical (including pushing me to submit this document now as I'm writing the acknowledgments). Finally, I am thankful to the friends and family that made living in Chicago enjoyable over the course of my studies. In particular, it is hard for me to imagine getting through the pandemic lockdown and the final years of my PhD without my girlfriend Ashley Haluck-Kangas, who has been a strong source of support and a great friend and partner.

ABSTRACT

A hallmark of biological life is the cell's apparent ability to orient itself purposefully in space. This property is referred to as cell polarity. Cell polarity is enabled by specific polarity proteins that are asymmetrically distributed on the cell surface. These polarity proteins interact within conserved modules to form biochemical feedback circuits and as result, the asymmetries they form tend to be self-stabilizing. While the constituent parts of these circuits are known in many cell contexts, how they generate self-stabilizing asymmetries remains only partially understood.

In the first chapter of this dissertation, I review the current literature on cell polarity. I discuss three examples of core polarity modules that stabilize asymmetries through various feedback loops. These core modules are utilized across cellular contexts to polarize cells in response to multiple different inputs and produce different asymmetries by interacting with different effector proteins. I show that these core circuits can be abstracted in mass conserved activator substrate (MCAS) models and review the insights we have gained from studying theoretical models. Finally, I discuss the role of protein clustering in core polarity circuits and show how it enables the establishment, maintenance, and elaboration of cell polarities.

In the second chapter of this dissertation, I take a theoretical approach to show how protein oligomerization can modulate the potential for and dynamics of cell polarization. I show that size-dependent binding avidity and mobility of membrane-bound oligomers endow polarity circuits with several key properties. Dynamic oligomerization and size-dependent membrane binding avidity confers local positive feedback on the accumulation of oligomer subunits, which while insufficient by itself, sharply reduces the amount of additional feedback required for spontaneous emergence and stable maintenance of polarized states. Size-dependent oligomer mobility makes symmetry-breaking and stable polarity more robust with respect to variation in subunit diffusivities and cell sizes, and slows the approach to a fi-

nal stable spatial distribution, allowing cells to "remember" polarity boundaries imposed by transient external cues. Given its prevalence and widespread involvement in cell polarity, I speculate that self-oligomerization may have provided an accessible path to evolving simple polarity circuits.

In the third chapter, I apply this mathematical model to PAR protein polarity in the *C. elegans* zygote. Specifically, I consider the role of PAR-3 oligomerization in stabilizing PAR asymmetries. Using fast single molecule imaging, I show that PAR-3 oligomers are larger on the anterior membrane, and measure oligomer size-dependent membrane dissociation. This combination results in PAR-3 more stably associating with the anterior membrane than the posterior. I further show that asymmetries in the distributions of PAR-3 oligomers are dynamically maintained and that the recruitment of new PAR-3 monomers to the cell membrane exhibits an anterior bias. Using a combination of mathematical modeling and experiments, I provide evidence that the combination of feedback on monomer recruitment, dynamic oligomerization, and avidity effects enables PAR-3 asymmetries to self-stabilize, and that these processes are in turn regulated by interactions with other PAR proteins on the anterior membrane. Finally, I show that the positions of PAR-3 domain boundaries are not encoded by a reaction diffusion system, and propose instead that oligomer size-dependent decreases in PAR-3 mobility effectively preserve arbitrary domain boundaries for the duration of polarity maintenance. Together, these results reveal a novel mechanism for stabilizing PAR-3 asymmetries in the *C. elegans* zygote.

In the final chapter, I discuss the implications of this work and future directions in this field. I discuss the potential to apply my modeling work to other polarity systems, the possible sources of feedback on PAR-3 membrane binding, and the potential and pitfalls of constructing mathematical models of PAR polarity. Finally, I outline a potential future project to understand how PAR-3 asymmetries shape PAR-6/PKC-3 distributions.

CHAPTER 1

INTRODUCTION

1.1 An overview of cell polarity

A hallmark of biological life is the cell's apparent ability to orient itself purposefully in space. For example, isolated cells move directionally to find food or mating partners, while groups of cells independently or collectively align activities along one or more spatial axes during fundamental multicellular processes such morphogenesis, organ function, and neural computation. How individual cells sense, store, and act upon directional information is thus a fundamental question in biology.

Cells that possess a spatial orientation are said to be polarized. Cell polarity is often manifested in cell morphology; for example, Santiago Ramón y Cajal famously documented elaborate and complex neuron cells with obvious asymmetries long before the techniques of molecular biology existed. However, in order to polarize, cells must be able to align biochemical processes and/or subcellular structures along specific axes, and cell polarity always emerges from asymmetries in the distributions of intracellular proteins. While some of these proteins can be asymmetrically distributed in the cytoplasm, most commonly these molecular asymmetries are observed on the cell membrane.

Over the past several decades, the study of cell polarity has progressed along two interrelated tracks. One has employed the tools of genetics and biochemistry to produce "parts lists" of the genes that are required for cell polarity, a catalog of their sub-cellular distributions and biochemical functions, and complex interaction diagrams that can be difficult to interpret and have limited predictive value. The other has used mathematical modeling and biophysical characterization to show how complex spatial patterns can arise from fundamental chemical and mechanical processes, identify key control parameters that determine the behaviors of polarity networks, and ultimately place quantitative constraints on those pa-

rameters with precise measurements of reaction and diffusion rates *in vivo*. In this chapter, I will give an overview of what we have learned from each of these approaches and highlight the ways in which clustering of polarity proteins plays a key role in polarizing cells, and how this common motif in polarity circuits has the potential to resolve some key problems in the field.

1.2 Networks of interacting proteins polarize cells

Cell polarity is apparent in the morphologies of many cell types, and early experiments were able to identify the genes that are required for cell polarization by performing forward genetic screens for loss of asymmetry in cell morphology or division. A major conclusion from these screens is that cell polarity is not a property endowed by individual proteins, but rather an emergent property of interacting networks of proteins that constitute feedback circuits. Further, conserved core polarity networks were found to be repurposed in different cellular contexts to achieve different functional outcomes by responding to different upstream cues and interacting with different downstream signaling networks. In this section, I will describe a network of proteins called the PAR proteins that was discovered through this approach in *C. elgans* and later found to polarize cells throughout metazoa. I will also briefly describe the conserved planar cell polarity (PCP) system and the network of GTPases, GEFs, and GAPs that polarize budding yeast, and show how polarity circuits in theses systems are also modular and are repurposed in multiple contexts for distinct functional outcomes.

1.2.1 PAR protein polarity

The PAR proteins were identified in screens for mutations that affect asymmetric cell division in the *C. elegans* zygote [76, 157, 143, 8, 49, 62, 82]. This initial division produces a smaller posterior and larger anterior daughter cell, and is the first in a series of asymmetric cell divisions that distinguish the soma from the germ line [127]. These screens identified a

large number of gene products with diverse molecular functions, including scaffolds, kinases, adaptors, and small GTPases, which are collectively called the *par*-titioning defective (PAR) proteins. A subset of these PAR proteins were found to be themselves polarized on the plasma membrane of the zygote, and a key focus over the past several decades has been to understand how symmetry is broken in this cell and how interactions between these proteins amplify and stabilize their asymmetric localization.

The PAR proteins are separated into two groups in the *C. elegans* zygote, which localize to opposing anterior and posterior domains on the cell surface. The anterior PARs (aPARs) include the oligomeric scaffold PAR-3, the adaptor PAR-6, the kinase PKC-3 (aPKC in other species) and the small GTPase CDC-42. The posterior PARs (pPARs) include the kinase PAR-1, the RING domain protein PAR-2, the GTPase activating protein (GAP) CHIN-1, and LGL-1. Two additional proteins (the kinase PAR-4 and the 14-3-3 protein PAR-5) are not asymmetrically localized but are required for proper asymmetric localization of the other PARs.

The process of polarization is separated into distinct phases called *polarity establishment* and *polarity maintenance* [30]. During polarity establishment phase, which corresponds to interphase of the cell cycle, embryonic symmetry is broken by a sperm-derived spatial cue and PAR proteins segregate into complementary cell surface domains. During polarity maintenance phase, which corresponds to M phase, PAR protein asymmetries are dynamically stabilized in the absence of the original polarizing cue. The cell ultimately divides at the boundary between aPARs and pPARs, enriching aPARs and pPARs in the anterior and posterior daughter cells, respectively.

Prior to polarity establishment, the aPARs PAR-3, PAR-6, and PKC-3 are uniformly enriched on the cell membrane. PAR-3 binds peripherally to the cell membrane and oligomerizes into clusters of indeterminate stoichiometry [88, 130, 34]. PAR-6 and PKC-3 form an obligate heterodimer which localizes to the cell surface by binding to PAR-3 [84]. PKC-

3 phosphorylates and dissociates PAR-1, PAR-2, and LGL-1 [118], and as a consequence pPARs are initially uniformly cytoplasmic. Approximately 20 minutes after fertilization as the zygote enters mitotic interphase, a spatial cue closely associated to the sperm-derived centrosomes triggers redistribution of aPARs to the anterior membrane and pPARs to the posterior membrane [15, 29, 56, 111] (Fig. 1.1A). The centrosomes localize near the future posterior of the embryo and break symmetry through two parallel mechanisms. In one mechanism, the centrosome locally inhibits actomyosin contractility in the posterior of the embryo through inactivation of the RHO-1 GEF ECT-2 by the kinase Aurora-A [106, 169, 77]. This local inhibition of contractility results in anisotropic tension on the cell cortex that produces anterior-directed actomyosin flows [109, 99]. aPARs are transported by these flows and consequently become concentrated in the anterior of the embryo [109, 23, 44]. pPARs bind to the posterior membrane as aPARs are cleared from the posterior membrane and local inhibition of pPAR membrane binding is relieved. In a second mechanism, microtubules emanating from the centrosome load the pPAR PAR-2 onto the posterior membrane [107]. PAR-2 recruits PAR-1 to the cell membrane, which phosphorylates and drives the aPAR PAR-3 off the cell membrane [107, 118].

In addition to these centrosome-dependent mechanisms, there is evidence that PAR-2 preferentially binds to regions of high membrane curvature. In embryos depleted of Aurora-A, PAR-2 localizes to both high-curvature poles of the ellipsoid embryo [77]. Further, when Aurora-A mutant embryos are forced into triangular PDMS chambers, PAR-2 preferentially localizes to the corners [77], providing direct evidence that it senses curvature. However, while this effect is interesting, it is suppressed in wild type embryos by an unknown mechanism, preventing PAR-2 from localizing to the anterior pole [77]. Therefore, curvature sensing is unlikely to play a significant role in polarizing the zygote.

Once symmetry is broken, interactions between aPARs and pPARs, as well as between PAR proteins and actomyosin contractility amplify and stabilize the resulting asymmetries

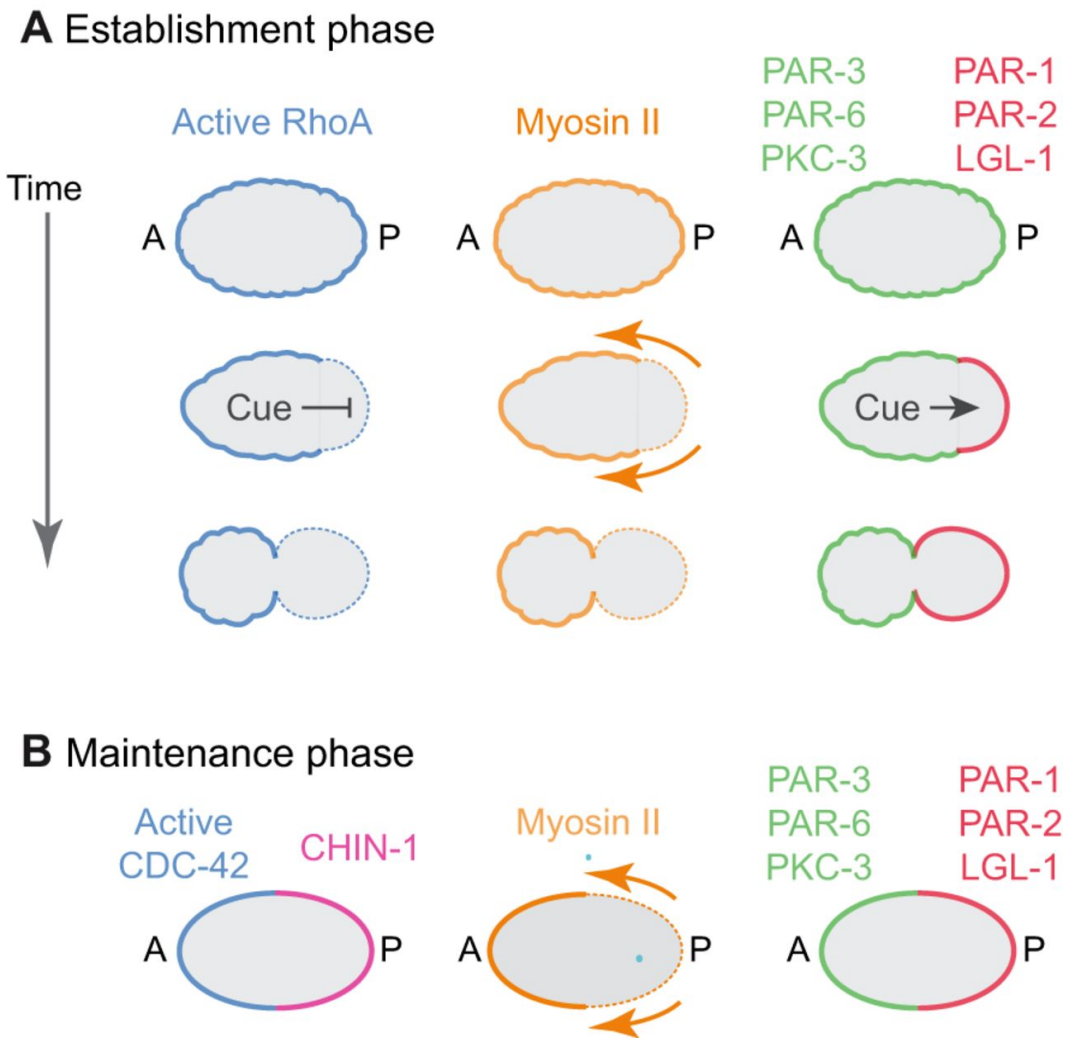

Figure 1.1: **Overview of polarization in the *C. elegans* zygote.** Polarization of the *C. elegans* zygote involves two distinct phases: establishment phase **(A)** and maintenance phase **(B)**. **(A)** Before polarity establishment, anterior PAR proteins (green), active RhoA and Myosin II are uniformly enriched at the cell cortex. During polarity establishment, a transient sperm-derived cue acts locally to inhibit RhoA activity and induce actomyosin-based cortical flows that segregate anterior PAR proteins towards the anterior pole, and to promote local accumulation of posterior PAR proteins (red) on the posterior cortex where they act to inhibit local accumulation of anterior PAR proteins. **(B)** During maintenance phase, complementary distributions of anterior PAR proteins and posterior PAR proteins are maintained in the absence of a cue. RhoA activity is low, and CDC-42 activity becomes enriched at the anterior cortex, while the CDC-42 GAP CHIN-1 becomes enriched on the posterior cortex. CDC-42 acts through the kinase MRCK-1 to activate Myosin II on the anterior cortex, leading to persistent cortical flows.

during polarity establishment. Mutual antagonism between aPARs and pPARs enforce complementary anterior and posterior PAR domains [52, 38, 16, 143, 157]. Further, aPARs locally promote actomyosin contractility while pPARs locally inhibit contractility. This results in PAR asymmetries strengthening the cortical flows that generate the asymmetries in a mechanochemical feedback loop [109, 51]. As a result of these feedback interactions, the centrosome cue that triggers polarization is not continuously required throughout polarity establishment and if ablated early in the polarization process, polarity is established normally [29, 51]. Quantitative analyses have shown that while extrinsic cues are required to trigger polarization, the intrinsic feedback mechanisms that amplify PAR asymmetries determine the dynamics of polarization shortly after symmetry breaking [51].

Some evidence suggests PAR polarization can be rescued in the absence of actomyosin flow [107]. Attenuation of establishment phase flows through genetic knockdown of either NOP-1 [128, 148], the RHO-1 GEF ECT-2 [174], or myosin regulatory light chain MLC-1 [107] slows the process of polarization, but does not ultimately prevent the establishment of polarized PAR domains or asymmetric cell division. Loading of PAR-2 on to the posterior membrane and phosphorylation of PAR-3 by PAR-1 have been shown in these cases to be required polarization [107], leading to a model where redundant mechanisms polarize the zygote that are dependent on actomyosin flows and dissociation of PAR-3 respectively. However, while it is true that PAR-2 is loaded onto the membrane at the posterior pole in the absence of flow, there is controversy as to whether this flow-independent mechanism is sufficient to polarize the cell as other studies show that myosin depletion eliminates asymmetric division PAR-3 asymmetries [53, Lang and Munro unpublished observations].

As the embryo enters mitosis (polarity maintenance phase), the sperm-derived centrosome that triggers and orients polarization migrates from the posterior to the center of the embryo [84]. Nonetheless, PAR asymmetries are maintained through mitosis (Fig. 1.1B). Further, PAR asymmetries persist if the centrosome is ablated after polarity establishment is complete

[29]. Therefore, PAR polarity is self-stabilizing in the absence of any known extrinsic cues.

In contrast with polarity establishment, polarity maintenance does not require cortical actomyosin flows and asymmetries are stable even when the actin cytoskeleton is disassembled [43]. Instead, a growing body of evidence suggests that during maintenance phase, PAR protein asymmetries are dynamically stabilized by a reaction-diffusion mechanism involving biochemical feedback. PAR proteins have been shown to exchange between membrane-bound and cytoplasmic pools on a faster timescale than that of polarity maintenance and diffuse laterally at the cell membrane [43, 125, 130]. In the face of turnover and diffusion, complimentary PAR asymmetries are actively reinforced by mutual antagonism between aPARs and pPARs [84]. While there is overlap between how mutual antagonism works in establishment phase and maintenance phase, there are also some key differences.

As in polarity establishment phase, PAR-3 binds directly to the cell membrane in maintenance phase and recruits PAR-6/PKC-3, which phosphorylates and dissociates PAR-1, PAR-2, and LGL-1 [44, 43, 130, 5] (Fig. 1.2). PAR-1 reciprocally phosphorylates and inhibits the accumulation of PAR-3. However, unlike in polarity establishment phase, PAR-2 is not required to recruit PAR-1 to the membrane, and plays no role in mutually inhibitory feedback [130]. Instead, PAR-2 plays a secondary role in polarity maintenance by inhibiting posterior-directed cortical flows that redistribute aPARs to the posterior. In addition to this PAR-3/PAR-1 feedback circuit, a second feedback mechanism operates specifically in maintenance phase. Early in maintenance phase active (GTP-bound) CDC-42 becomes enriched with other aPARs at the anterior membrane [82]. CDC-42 binds directly to PAR-6 and recruits PAR-6/PKC-3 to the membrane. At the same time, the CDC-42 GAP protein CHIN-1 becomes highly enriched in a complementary posterior domain. CHIN-1 accumulation is inhibited by PKC-3 in the anterior membrane [130] and CDC-42 is reciprocally inactivated by CHIN-1 in the posterior (Fig. 1.2), completing a mutual inhibition feedback circuit.

Genetic epistasis experiments have shown that the combination of these two overlapping mutual inhibition circuits results in redundant inhibition of PAR-6/PKC-3 in the posterior membrane. While in establishment phase most PAR-6/PKC-3 is tethered to the membrane by PAR-3, in maintenance phase most of it is bound to active CDC-42 [1, 10]. Nonetheless, PAR-3 and CDC-42 are both required for robust accumulation of PAR-6/PKC-3 on the membrane [10, 130]. While it is not known why PAR-3 and CDC-42 are jointly required to recruit PAR-6/PKC-3 to the membrane since PAR-6/PKC-3 can bind directly to either, the consequence is that posterior inhibition of either active CDC-42 or PAR-3 is sufficient to maintain PAR-6/PKC-3 asymmetries [130] (Fig. 1.2). While neither *chin-1* nor *par-1* mutant embryos exhibit loss of PAR-6/PKC-3 asymmetries, the combination leads to rapid depolarization in maintenance phase [130].

One unsolved question is how PAR-3 asymmetries are reinforced through polarity maintenance phase. While PAR-1 inhibits accumulation of PAR-3 in the posterior membrane during maintenance phase, it is not required to maintain PAR-3 asymmetries and there is relatively weak accumulation of PAR-3 in the posterior membrane in *par-1* mutant embryos [130]. This strongly suggests the presence of additional feedback mechanisms, which is the focus of the third chapter of this dissertation.

Consistent with the model that posterior inhibition acts directly on PAR-3 and CDC-42 rather than PAR-6/PKC-3, single molecule imaging experiments show that PAR-6/PKC-3 asymmetries are accounted for entirely by an anterior bias in its recruitment to the cortex, rather than a bias its dissociation rates [125]. Surprisingly, even the very slight accumulation of PAR-3 that occurs in *par-1/chin-1* double mutants is sufficient to totally eliminate the anterior bias in appearance rates, suggesting that PAR-3 acts to catalytically load PAR-6/PKC-3 onto molecules of CDC-42, and pointing to very sharp nonlinearities in the system [130]. How this might work is an outstanding question in the field, which is discussed briefly in the fourth chapter.

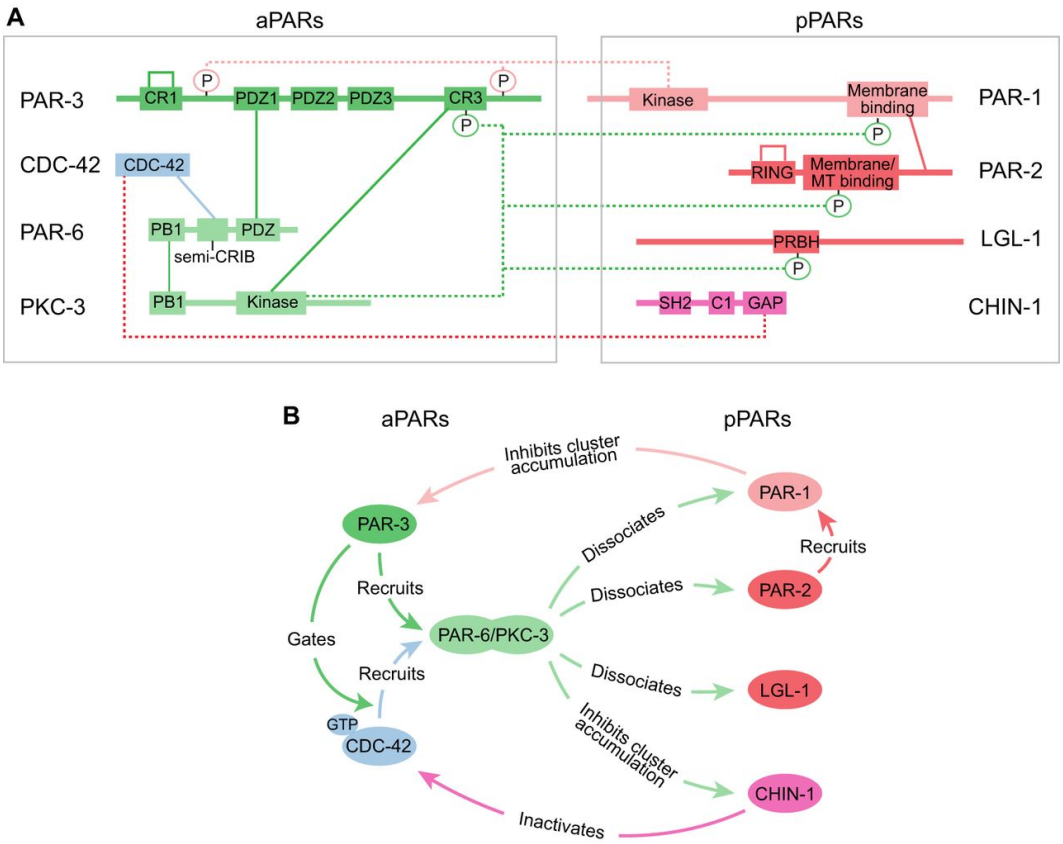

Figure 1.2: **Core molecular interactions that underlie the dynamic stabilization of PAR asymmetries.** **(A)** A schematic view of the PAR network indicating key domains and phosphorylation sites involved in protein-protein interactions. Solid lines indicate direct binding interactions, whereas dotted lines terminating in circles represent enzymatic action, either phosphorylation or GAP activity. In the case of PAR-3 and PAR-2, self-connecting loops indicate oligomerization. **(B)** A functional view of the same circuit emphasizing the consequences of protein-protein interactions. For clarity, some interactions documented in other contexts (e.g. inhibition of aPKC by LGL or by PAR-3) have been omitted here.

While mechanochemical interactions are unlikely to play a dominant role in polarity maintenance, there is evidence that they play a secondary role in stabilizing the boundaries of polarized CHIN-1 distributions. In addition to interacting directly with other PAR proteins, CDC-42 acts through the conserved kinase MRCK-1 to activate myosin, creating a gradient of contractility that drives anterior-directed cortical flows in polarized cells [82, 130], albeit weaker ones than those observed in establishment phase. These flows continuously transport CHIN-1 clusters anteriorly and may contribute to the stable positioning of PAR domain

boundaries [130].

In all, many similarities exist between the mechanisms for polarity establishment and polarity maintenance. Both mechanisms involve mutually antagonistic interactions between aPARs and pPARs and mechanochemical feedback between PAR proteins and actomyosin contractility, and the dynamics of both phases are dominated by self-organized processes. However, there are also some key differences. Polarity establishment initially requires an extrinsic signal (the sperm centrosome) while polarity maintenance is an entirely self-sustaining process. Mechanochemical feedback and transport of PAR proteins plays a key role in polarity establishment, but a secondary role in polarity maintenance. Finally, while the topology of feedback circuits is similar in both phases, the molecular interactions between and among aPARs and pPARs, as well as between PARs and actomyosin contractility, are slightly different.

PAR polarity across different cell types

While best studied in the *C. elegans* zygote, the PAR network described there, with the exception of PAR-2, is conserved across metazoa and polarizes a wide range of different cell type [45, 142, 33, 110, 146, 158]. As in the *C. elegans* zygote, antagonism between PAR proteins localizing to complementary membrane domains is found in other early embryonic cells as well as epithelial cells [100]. However, in other cells such as neurons and neuroblast stem cells, aPAR proteins localize in a unipolar fashion, without an opposing domain [84]. Other feedback mechanisms independent of mutual antagonism have been shown to exist in other cell types. In at least one example, PAR-1 is involved both in mutual antagonism, and unexpectedly in a positive feedback loop that polarizes PAR-3 to the apical junctions of epithelia [73]. In all, what seems to be most conserved across these many different instances of PAR polarity is that feedback interactions amplify and stabilize PAR asymmetries. In contrast, the mechanisms and spatial landmarks that trigger polarization and even the types

of spatial patterns formed by PAR proteins vary considerably. For example, while the sperm centrosomes serves as spatial landmark for polarization of PAR proteins in the *C. elegans* zygote by inducing long range cortical flows, cell-cell interfaces serve as the polarity landmark in the 4-cell embryo by locally recruiting a the GAP PAC-1, which inactivates CDC-42 [4, 78].

Another motif that is found in multiple examples of PAR polarity is partitioning of PAR-6/aPKC into distinct pools bound to PAR-3 and CDC-42 respectively. In the *C. elegans* zygote both pools localize to overlapping domains. However, in *Drosophila* epithelial cells, PAR-3 localizes to adherens junctions while CDC-42/PAR-6/aPKC complexes localize to the apical cell membrane. In both cases, PAR-3 is required for PAR-6/aPKC polarization even when the majority of PAR-6/aPKC is bound to CDC-42 [104]. Reciprocally, in epithelial cells phosphorylation of PAR-3 by aPKC is required to restrict PAR-3 to cell junctions [104, 155, 138], and PAR-6/aPKC is required for maintaining PAR-3 asymmetries in the *C. elegans* zygote (see chapter 3). The difference in patterns between worms and flies may be a result of epithelia-specific interactions between PAR-3 and adherens junctions and aPKC and Crumbs [104], but in both cases it is tempting to hypothesize that PAR-3 acts as a local "source" for PAR-6/aPKC at the membrane without remaining in a stable complex with it. Overall the interplay between these proteins, as well as functional differences between different pools of PAR-6/aPKC, remains only partially understood and should be a focus for investigation in the future.

While the PAR proteins are capable of sustaining stable asymmetries required for cell polarity, they do not independently define subcellular identities. Further, they do not define one single type of axis across cell types, and in some cases are polarized across multiple axes. Thus a key question is how do PAR proteins interact with downstream effectors to achieve diverse functional outcomes in cells.

One of the best studied examples of a functional asymmetry downstream of the PAR module is the polarization of cytoplasmic proteins in the *C. elegans* zygote, which are asym-

metrically inherited by its daughter cells and specify the anterior-posterior axis of the embryo. In this cell, the pPAR PAR-1 provides the key link between the PAR network and its downstream effectors. PAR-1 localizes to the posterior of the embryo where it phosphorylates the cytoplasmic protein MEX-5 [50]. This causes MEX-5 to locally switch from a slow-diffusing state to a fast-diffusing state, resulting in its accumulation in the anterior cytoplasm through a diffusion trap mechanism [50]. MEX-5 in turn locally increases the mobility of POS-1 and PIE-1 in a PLK-1 dependent manner, causing them to be enriched in the posterior cytoplasm [165, 164, 57]. In addition, MEX-5 induces the posterior localization of phase separated liquid-like RNA-protein compartments called P granules by dissolving them in the anterior cytoplasm, potentially by competing with P granule components for binding to RNA [17, 137, 129]. However, unlike the PAR network, this appears to be a linear signaling pathway that follows from PAR-6/PKC-3-dependent membrane asymmetries in PAR-1. These cytoplasmic asymmetries are established downstream of PAR asymmetries at the cell membrane there is no evidence that, once established, they are self-stabilizing.

In other cell types, the PAR module interacts with different sets of proteins for entirely different ends. For example, PAR proteins partition a totally different set of cell fate determinants in neuronal stem cells [158], position adherens junctions in epithelial cells [59], bundle microtubules in the axons of neurons [24], and define the site of lumen formation in *Ciona* tubulogenesis [33] and cultured MDCK cells [97]. This observation combined with the plethora of different cues that define the axis of PAR polarity in different cells suggests a conceptual picture of the PAR module as a core polarity circuit that can interface with diverse inputs and outputs to function in a very wide range of cellular contexts.

1.2.2 Planar cell polarity

While PAR proteins polarize a wide range of cells through primarily intracellular feedback mechanisms, a different module of proteins called the planar cell polarity (PCP) proteins

cells coordinate polarities that are reinforced through a combination of intracellular feedback and interactions across cell-cell junctions. PCP refers to asymmetries in epithelial sheets that are orthogonal to the apical-basal axis. These asymmetries are coordinated between cells such that the planar polarities of all cells in a tissue are aligned. Current models [116] posit the existence of three distinct modules that give rise to PCP: 1) a global module that determines the axis of polarity on the tissue level, 2) the core module that amplifies and stabilizes asymmetries in individual cells and communicates polarity information between cells, and 3) tissue-specific effectors that translate the asymmetric distributions of polarity proteins into functional cell-level polarity.

As with the PAR proteins, the core PCP module is highly conserved across metazoans and is a self-organizing system. In contrast, the modules that orient PCP and produce functional asymmetries vary considerably across cellular contexts. The core PCP proteins were initially identified in genetic screens for disruption of the coordinated orientation of bristles in *Drosophila* wings [116, 19], and this system remains the best studied example of PCP. These screens identified Frizzled (Fz), Flamingo (Fmi), Disheveled (Dsh), Diego (Dgo), Van Gogh (Vang), and Prickle (Pk) as the components of the core module. Mutants for these proteins caused loss of planar polarity, and with the exception of Fmi, they localize in polarized distributions at the apical junctions of cells.

In each cell, core PCP proteins segregate into complementary domains that define the proximal and distal end of the cell. Hairs are produced at the distal end of each cell. Dsh, Dgo, and Fz localize to distal junctions, while Vang and Pk localize to proximal junctions. Fmi localizes to both distal and proximal junctions.

This core module is further broken down into distinct mechanisms that mediate intercellular communication and intracellular, cell-autonomous polarization. Intercellular communication depends on the transmembrane proteins in the module: Fmi, Fz, and Vang [152, 144]. Fmi interacts at the junctions with either Fz or Vang and dimerizes across ap-

posing cell junctions, but its binding affinity is affected by intracellular binding partners [25]. Specifically, Fmi bound to Fz dimerizes much more readily with Fmi bound to Vang, and since dimerization across cells promotes its stabilization at junctions, Fz localization at one junction promotes Vang localization at the other [25, 141].

While these interactions align polarized axes between cells, both modeling and experiments show that they are not sufficient on their to produce planar polarity [147, 3]. In addition, intracellular feedback involving mutual inhibition between proximal and distal proteins is required to polarize cells [147, 3]. While the mechanisms involved in this mutual inhibition are poorly understood, they are likely to involve the cytoplasmic PCP proteins Dsh, Dgo, and Pr [116, 19]. These proteins bind to and cluster transmembrane PCP proteins [139]. Pr has been shown to inhibit the localization of distal proteins in the proximal junctions [147] perhaps by binding directly to Dsh and preventing its association with Dgo [72]. Overall, understanding the mechanisms that provide intracellular feedback in this circuit remains an active focus for PCP research.

While the core PCP module can promote local polarity alignment, an additional global PCP module is required to produce tissue-level polarity. Genes in the global PCP module are characterized by mutant phenotypes where cells exhibit similar polarities to their neighbors, but swirl randomly over longer length-scales [93, 116]. While the mechanisms by which global polarity information is transduced are not well understood and are beyond the scope of this chapter, they involve expression gradients of proteins in the Fat/Dachous/Four-jointed module, diffusion gradients in Wnt ligand, and anisotropic strain in different tissue contexts [116]. Thus, as with PAR proteins, multiple polarizing cues can orient asymmetries in PCP proteins.

As with PAR proteins, the core PCP module can also interact with a range of different proteins to produce different functional outcomes. While distal PCP proteins specify where bristles form in the *Drosophila* wing, the same proteins inhibit Notch signaling and control

cell fate specification in asymmetric cell division in the developing *Drosophila* eye [116, 19]. In fish and frogs, PCP promotes gastrulation by driving convergent extension, which requires interaction with cytoskeleton regulatory proteins such as Cdc42 and RhoA [116, 19]. And in a number of mammalian contexts, PCP proteins interact with ODF2 and centrin 2 to produce directional beating of ciliated cells [116, 19]. In all, core PCP proteins, like the PAR proteins, form a highly conserved polarity module that amplifies and stabilizes asymmetries specified by a number of different polarizing cues, and that is utilized to produce a wide range of polarized states in different contexts.

1.2.3 Polarity in budding yeast

The PAR and PCP modules are specific to multicellular organisms. However, unicellular organisms polarize as well, and there is evidence at least in budding yeast *S. cerevisiae* that the same core polarity circuit can be reused for different functions. Budding yeast cells have been observed to polarize in two contexts. In one, the cell selects a bud site on the cell membrane to produce a new cell. In the other, haploid yeast spores extend protrusions (termed "shmoos") in the direction of mating partners in order to fuse membranes and become diploid. Interestingly, these two very different functions both involve the same core feedback mechanisms to polarize the activity of the small GTPase Cdc42 at the cell membrane.

In this module, Cdc42 switches between an active GTP-bound form, which binds tightly to the cell membrane, and an inactive GDP-bound form, which rapidly dissociates from the cell membrane. The GEF Cdc24 and the GAP Pak1 promote activation and inactivation of Cdc42 respectively, and together locally regulate levels of active Cdc42. Feedback comes into the system via the scaffold protein Bem1, which binds to both active Cdc42 and to the GEF Cdc24, which results in the Cdc42 activation rate being higher in patches of membrane with more active Cdc42.

During bud site selection in wild-type yeast, biochemical feedback amplifies Cdc42 activity at sites marked by the small GTPase Rsr1. Interestingly, in rsr1 mutants, Cdc42 spontaneously polarizes without an extrinsic cue, albeit along a random axis, and yeast cells form buds and proliferate normally. Several lines of evidence suggest that the feedback involved in bud site selection is independent of relatively slow dynamics of cytoskeletal transport and endocytosis and instead involve dynamic turnover of Cdc42 at the membrane due to GTP hydrolysis and regulation of local activity through Bem1 and Cdc24 (and possibly other proteins) [66, 71].

During yeast mating, the characteristic protrusion is formed at a site of Cdc42 enrichment at the membrane, similar to budding. In this context, the feedback mechanism responds to inputs from a shallow gradient of pheromone released by other yeast cells of complementary mating type. Importantly, yeast cell are still able to polarize in the absence of a gradient of pheromone, and therefore the intrinsic capacity of the cell to polarize through a biochemical feedback mechanism is simply harnessed by a distinct input cue than the one that generates polarity in budding. Therefore, like the PAR network, the yeast polarity network is modular and can be elaborated in at least two distinct ways to execute different functions.

1.3 Mathematical modeling of cell polarity

Since Alan Turing, mathematicians have been interested in whether and how mathematical models of biochemical reaction-diffusion systems can describe the emergence of biological patterns [150]. More recently, interest in applying these types of models to cell polarity has been bolstered by the discovery of multiple experimental systems where there is strong evidence that polarity is established and/or maintained by reaction-diffusion mechanisms [48, 43, 125]. In these systems, polarity proteins exchange dynamically between the cell membrane and the cytoplasm, with asymmetries building up primarily at the cell surface (hereafter referred to as cell surface polarity). While both pools diffuse freely, the cytoplas-

mic pool diffuses much more rapidly. Membrane-bound protein locally promotes its own accumulation through either direct or indirect interactions, and accumulation is ultimately limited by a finite amount of total protein. Together, this collection of reactions forms the basis of a class of widely studied reaction-diffusion models of cell surface polarity called mass conserved activator substrate (MCAS) models (Fig. 1.3).

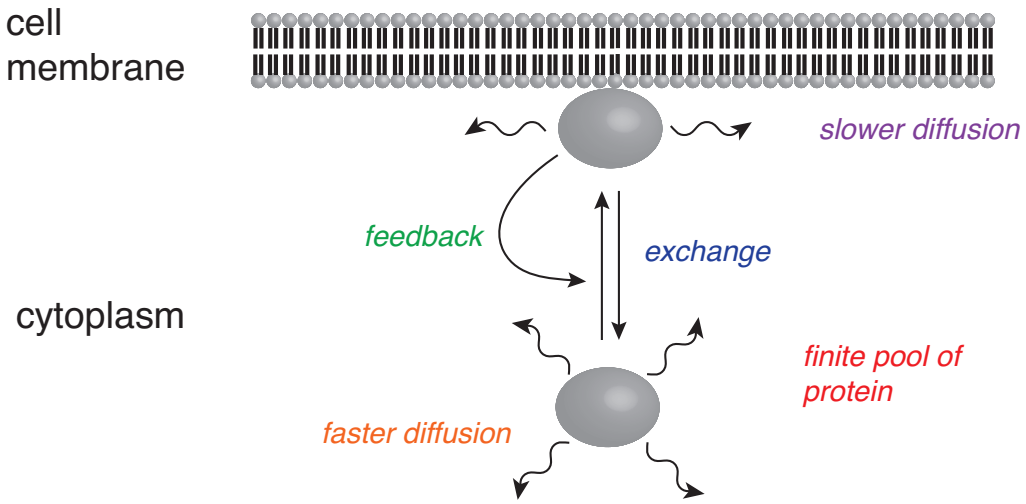

Figure 1.3: **Schematic of a generic MCAS model.** Schematic highlighting the key components of a mass-conserved activator substrate (MCAS) model. Polarity proteins exchange between fast diffusing cytoplasmic and slow diffusing membrane-bound states. Local feedback on exchange rates concentrates protein in subcellular domains and a finite amount of protein limits its accumulation on the membrane.

MCAS models have been applied to several different cell contexts where polarity proteins form self-stabilizing cell surface asymmetries, most notably small GTPase polarity [114, 105, 48, 47] and PAR protein polarity [44, 130]. In some of these contexts, cells spontaneously polarize, presumably by amplifying noisy spatial heterogeneities in protein concentration. In others, unpolarized states are stable, but polarization can be triggered by a transient perturbation of sufficient magnitude. By tuning model parameters, MCAS models can reproduce both of these behaviors [63]. Nonetheless, there is substantial experimental evidence from a number of cell contexts that physical processes beyond reaction-diffusion can contribute to cell polarity. For example, polarity proteins are redistributed by intracellular

actomyosin flows [109, 44, 21], can sense membrane tension and local curvature [149, 64, 77], and interact across cell junctions [3]. As a result, recent studies have elaborated these fundamental reaction-diffusion models to include mechanics, cell geometry [136], and intercellular communication. In this section, I will discuss some general principles of self-stabilizing cell surface polarity that emerge from studying MCAS models. I will also discuss how processes beyond reaction and diffusion can both fulfill minimum requirements for stable polarity in MCAS systems, and also endow them with additional properties.

1.3.1 Local positive feedback loops counteract diffusion and turnover to reinforce polarity

In MCAS models, cell surface asymmetries are dispersed by dissociation of protein from cell membrane and diffusion. Therefore, some form of energy-consuming feedback on the local accumulation of polarity proteins is required to maintain what is by definition a gradient in chemical potential. In MCAS models, feedback comes from having the rates at which polarity proteins switch between membrane bound and cytoplasmic states be dependent on the local concentrations of these species [115]. In some models, feedback loops involve a membrane-bound protein directly promoting the local binding of cytoplasmic molecules to the membrane [105, 48]. In others, double negative feedback between two proteins that mutually promote the other's dissociation from the membrane results in bipolar cell surface asymmetries [44, 130]. However it is built into equations, the strength of feedback, defined as the ratio of feedback-dependent rates to basal reaction rates, is a control parameter in these models that determines whether stably polarized states exist, and whether polarization will occur spontaneously by amplifying noisy fluctuations or only in response to a sufficiently large perturbation [63].

More recently, empirical evidence suggests that a similar paradigm can be applied to cytoplasmic proteins [115]. Instead of switching between membrane-bound and cytoplasmic

states, asymmetrically distributed proteins in the cytoplasm of the *C. elegans* zygote have been shown to switch between fast and slow diffusing states [164] or diffuse and condensed states [163, 35]. However, while these models are in principle able to produce self-stabilizing cytoplasmic asymmetries, evidence of this *in vivo* is lacking.

While feedback in classical MCAS models results purely from biochemical reactions, it is likely that many positive feedback loops in real cells also incorporate elements that generate and/or sense mechanical forces. One example of this type of mechanochemical feedback comes from the *C. elegans* zygote, where PAR asymmetries promote cortical actomyosin flows that in turn locally concentrate PAR proteins through polarized transport (discussed above). A similar kind of feedback likely operates in migratory cells, where directional migration results in retrograde actomyosin flow that transports polarity proteins to the trailing edge [95]. This in turn reinforces cell polarity and promotes directional migration. This mechanism may explain the observation that migration speed and directional persistence are correlated across a wide range of cell types and conditions [95].

Another example of mechanochemical feedback comes from fibroblast cells, in which membrane protrusions are polarized [149]. In this context, the WASP/WAVE complex locally generates Arp2/3-dependent actin protrusions at the leading edge of the cell. The force generated by these protrusions generates a local positive curvature in the membrane. The F-BAR protein FBP17 senses and accumulates at sites of positive curvature, and thus localizes to the leading edge. Finally, FBP17 recruits the WASP/WAVE complex, closing the positive feedback loop [149]. Therefore, realistically capturing experimentally observed positive feedback systems in models of cell polarity may require invoking mechanical forces and cell geometry in addition to biochemical reactions and diffusion.

1.3.2 Long-range negative feedback is required to limit the spread of polarized domains

While feedback is necessary to amplify and/or reinforce asymmetries against dispersion by turnover and diffusion, it begs the question of how the effects of feedback can be focused in a subcellular domain if the source of feedback is a diffusible molecule. In MCAS models, this is accomplished by coupling local positive feedback to global negative feedback. Since the total number of protein molecules in the cell is held constant, as the protein accumulates in a polarized membrane domain, the amount of the cytoplasmic protein decreases. Since the cytoplasmic protein diffuses rapidly, it is often assumed in these models to be well mixed, and since the membrane binding rate is dependent on the amount of locally available cytoplasmic protein, local accumulation protein at the membrane is coupled to global decreases in membrane binding rates. The broad consequence of this is that if certain conditions are satisfied (discussed further below), local domains of the cell with more protein will be better able to compete for a shared pool of cytoplasmic protein and will accumulate protein at the expense of regions with even slightly less protein. This competition counteracts the dispersal of asymmetries through diffusion [48, 27]. However, how a finite pool of protein limits the size of a polarized domain depends on how positive feedback is formulated in the model [27].

Chiou et al. distinguish between "Turing-like" and "wave-pinning" sub-types of MCAS models based on whether the feedback is far from or near saturation respectively [27]. In Turing-like models, the patch of the membrane with the highest concentration of protein has the strongest feedback and is best able to compete for a limiting cytoplasmic pool. Lateral diffusion at the cell membrane disperses protein out of this patch, producing a polarized gradient of protein. However, the weaker positive feedback in the region outside of this polarized domain is unable to compensate for the global negative feedback induced by accumulation in the domain. Therefore, at steady state, there is net flux of protein from the cytoplasm into the center of the polarized domain, net diffusive flux along the membrane

out of polarized domain, and net flux off of the membrane outside of the domain into the cytoplasm [27]. The shape of the domain is always peaked and the half-width is determined by the diffusion and dissociation rates of protein.

In contrast, in wave-pinning models accumulation of protein on the membrane is stalled by locally saturating feedback rates, rather than global negative feedback alone [105, 27]. As a result, these systems exhibit one high and one low local steady state even in the absence of cytoplasmic depletion. Starting from a small polarized domain with protein levels at the high steady state, diffusive flux causes protein levels in the adjacent regions to jump from the low to the high state. As the polarized domain spreads, it depletes the pool of cytoplasmic protein, which in turn slows the spread of the domain until it stops [105]. Therefore, at steady state, this mechanism will produce a flat "mesa-like" domain, the length of which is determined by the limiting pool of protein in the cell [105, 27]. A number of studies have invoked wave-pinning models to explain how the boundary that separates aPAR and pPAR domains is specified in the *C. elegans* zygote, although I will show evidence in chapter 3 that calls this interpretation into question.

An interesting consequence of models where the domain boundary is determined by a reaction diffusion system is that the parameters that control domain size will also determine whether or not polarization in a cell of a given size is possible. In both models, the intrinsic diffusion and dissociation rates of membrane-bound protein will set a cell-length threshold, below which polarization is impossible [69]. There is evidence that this mechanism determines the shift from asymmetric to symmetric cell divisions in progressively smaller germ-line blastomeres in the *C. elegans* embryo [69].

Finally, while cells necessarily have a finite amount of protein, it is not always that case that domain size is determined by a limiting cytoplasmic pool. Two additional mechanisms for stabilizing a polarized domain boundary that do not rely on depletion of cytoplasmic polarity proteins and have been demonstrated to function *in vivo* are global inhibition through

increased membrane tension [64] and persistent transport of polarity proteins by cortical actomyosin flows [130]. Additionally, under certain conditions it may be the case that reaction diffusion systems effectively preserve boundaries imposed by transient extrinsic cues. This possibility is discussed in depth in chapter 2.

1.3.3 Nonlinear dynamics are required for stable asymmetries

While local positive feedback and global negative feedback are ubiquitous models of cell polarity, they are not on their own sufficient to generate stable asymmetries. In addition, it must be the case that there exists some form of cooperativity in the dynamics of local protein accumulation. Formally, if $F(X) = k_1X^m + k_2$ is the function that determines the local accumulation of protein X and $G(X) = k_3X^n$ is the function that determines the local turnover of protein X, it must be the case that $m > n$ in the model both for spontaneous symmetry breaking to be possible and for polarity to be stably maintained [90, 47, 27]. In a system with no feedback, $m = 0$ and $n = 1$, so stable polarity is impossible. Perhaps counterintuitively, if $F(X)$ is linearly dependent on X (positive feedback resulting from a simple first order reaction) $m = n = 1$ and stable polarity is still impossible. This conclusion thus begs the question: What systems of plausible chemical reactions produce the kind of feedback needed for stable polarity? In many models, m is simply set to 2 or n is set to < 0 over some range of values for X without explicit justification with chemical reactions [105, 44, 63, 5, 51, 69]. However, several models have specifically invoked plausible biological mechanisms to satisfy this requirement.

One way to increase $m > 1$ is to combine multiple feedback loops [114, 47]. Crucially, the multiple feedback loops must converge, rather than act independently, as described by Goryachev and Leda [47]. To illustrate this point, consider a scenario where protein X locally modifies the cell membrane to increase the number of binding sites for other molecules of X. If X recruits two different enzymes that catalyze reactions that independently increase

membrane binding, then the total binding rate F will be equal to the sum of those reaction rates, which are each proportional to X. In contrast, if X recruits two components of a higher order reaction, or two enzymes in different steps of a multi-step reaction, F will be proportional to the product of those individual rates, and since each is proportional to X, F will be proportional to X^2. Converging feedback loops have been included in several MCAS models for polarization of small GTPases [114, 47, 48]. Additionally, the combination of first order feedback loops that affect the association and dissociation rates of X can generate stable asymmetries by making $m = 1$ and $n < 1$. This scenario has been explored in synthetic polarity circuits [22].

A notable exception to the rule that feedback circuits must contain some nonlinearity is a class of models in the literature involving linear feedback and intrinsic noise [2, 74]. While in deterministic models it is always impossible to spontaneously break symmetry with linear feedback, these models show that if the number of molecules of polarity protein is sufficiently low, it is likely that spontaneous polarization will occur. While this mechanism can reliably generate spontaneous asymmetries given a small enough number of molecules, the asymmetries are not stable over time and there is little evidence supporting this kind of model in experimental literature.

1.3.4 Modeling the dynamics of polarization

In addition to exploring the conditions under which stable asymmetries are possible, mathematical models can be used to explore what factors determine the dynamics of polarization. Two interesting questions that come out of this line of inquiry are 1) how fast are asymmetries established? and 2) how fast do multipolar states resolve into a single polarized domain?

The speed at which polarization occurs in MCAS models can be quantified based on reaction and diffusion rates. For example, in the case of wave pinning models discussed above,

the speed at which a polarized domain expands is determined by the model parameters and progressively slows as it approaches a stable position. However, evidence in *C. elegans* zygote suggests that while polarization can occur though reaction and diffusion alone, the dynamics of polarity establishment are determined by polarized actomyosin flow [107, 44, 51]. Therefore, in this cell the speed of polarization is relatively insensitive to diffusivities of polarity proteins and biochemical feedback rates, and is instead determined by mechanochemical feedback between PAR proteins and contractility. This type of mechanism may be necessary in biological contexts where large cells need to polarize quickly (such as the *C. elegans* zygote) as physical constraints may put a hard limit on how quickly reaction-diffusion mechanisms can polarize a cell of that size. In contrast, it may be advantageous in other cell contexts to preserve distributions imposed by transient polarizing cues by slowing the approach of a reaction diffusion system to its intrinsic steady state. One mechanism for achieving this slowing down diffusion of polarity proteins through molecular clustering, which is discussed in chapters 2 and 3 and which is also described in Dine et al., discussed below [35].

An analogous situation exists for resolution of multipolar cells to a singularly polarized state. In different cell types, it may be advantageous to either stabilize multiple polarized domains, or polarize along only one axis. Modeling work has shown that the timescale over which multi-polar states can be maintained depends on the turnover rate of membrane-bound polarity protein [66], but also on the degree to which feedback is saturated [27, 26]. Both *in silico* and *in vivo*, saturation emerges as a key control parameter for whether multipolar states resolve into unipolar distributions or are effectively stable [27, 26]. It will be interesting in the future to explore how this and other control parameters are tuned to modulate polarization dynamics and achieve qualitatively distinct outcomes.

1.4 Protein clustering in cell polarity

A common motif that is observed in several distinct polarity modules is that polarity proteins assemble into discrete clusters at the cell membrane [85]. In the PAR network, PAR-3 [34, 130, 60], CHIN-1 [130], and PAR-2 [5] are all reported to oligomerize *in vivo*. In planar polarized epithelia, proximal and distal polarity protein both assemble into clusters with variable stoichiometry [139]. In fission yeast, Pom1, Mid1, Cdr1, Tea1/4, and Mod5 are all reported to oligomerize [131, 37, 14]. In migrating fibroblasts, FBP17 oligomerizes at the cell membrane [149]. And in Arabidopsis cells, the polarized protein SOSEKI oligomerizes [151]. Why does this motif reoccur so frequently in unrelated polarity modules? One simple explanation could simply be that there is a non-adaptive evolutionary tendency to produce oligomeric proteins [61]. However, several lines of evidence from both theory and experiments suggest there may be general functions endowed by oligomerization that are particularly advantageous for polarizing cells.

1.4.1 Clustering entrains polarity proteins in cortical flows

In several different contexts, distributions of proteins are shaped by cortical actomyosin flows. As noted above, during establishment of PAR protein asymmetries in the *C. elegans* zygote, PAR-3, PAR-6, and PKC-3 are concentrated in the anterior of the cell through anterior-directed cortical actomyosin flows [23, 109, 44] and non-muscle myosin is required for asymmetric division [53]. Similarly, polarity establishment in *Drosophila* neuroblasts involves transport of PAR-3 puncta towards the apical pole of the cell through cortical actomyosin flow [112, 113], and in activated leukocytes, signaling proteins are transported to the immunological synapse by cortical actomyosin flows [36]. However, classical experiments in motile macrophage cells demonstrated that cortical flows do not induce bulk flow of the cell membrane and that membrane proteins are not necessarily transported by cortical flows [135, 81]. Thus, how polarity proteins become entrained in cortical flows is a key question

in the field of cell polarity.

A number of recent studies conducted in the *C. elegans* zygote suggest that only clustered proteins are efficiently transported by flow [126, 34, 21]. These studies have focused on the aPAR PAR-3, an oligomeric peripheral membrane protein which, along with PAR-6 and PKC-3, becomes enriched in the anterior of the embryo following transport by anterior-directed cortical flows. PAR-6 and PKC-3 do not bind directly to phospholipids and are tethered to the membrane by binding to either PAR-3 or active CDC-42. During polarity establishment, PAR-6/PKC-3 co-clusters with PAR-3. However, inhibition of PKC-3 kinase activity causes it to instead associate with monomeric CDC-42 during polarity establishment through an unknown mechanism [126]. While PAR-3 clusters are still polarized by cortical flows under these conditions, diffuse PAR-6/PKC-3 is not. Further, multiple different PAR-3 mutants that lack the ability to homo-oligomerize all fail to polarize in response to cortical flows [21, 34, 126, 88] and rescue experiments show that PAR-3 clusters must contain at least three subunits to be polarized by cortical flows [21]. While similar experiments have not been done with PAR-3/PAR-6/aPKC in Drosophila neuroblasts, they are similarly co-clustered in these cells [112, 113]. Therefore, protein clustering may be a general mechanism for entraining proteins in cortical flows.

How might molecular clustering entrain polarity proteins in cortical actomyosin flows? One mechanism that has been proposed is that efficient transport is simply a consequence of the increase in membrane avidity with the number of subunits in an oligomer [86, 34, 21]. Assuming an oligomer is perfectly entrained in cortical flow, the distance it will be transported is proportional to the length of time it is bound to the membrane, and therefore oligomers can be transported longer distances than monomers. This mechanism has been proposed to be at play in the case of PAR-3 polarization in the *C. elegans* zygote, where avidity effects has been demonstrated *in vivo* [34, 21]. However, this simple interpretation is challenged by the observation that monomeric PAR-3 artificially tethered to the cell membrane fails to

polarize during polarity establishment in the *C. elegans* zygote [126].

Another way in which oligomerization could promote coupling to cortical flow are oligomer size-dependent decreases in protein mobility. A common measure in physical systems for the degree to which an object is entrained in a flow over some length scale is the ratio of the rates of advective and diffusive transport, i.e. the Péclet number. In the context of cell polarity, it will only be possible to build up an asymmetry if the Péclet number is high and advective transport dominates.

Oligomer size-dependent mobility has been demonstrated empirically in cell polarity systems [130, 34, 21] as well as *in vitro* [159, 172, 79] and outside the context of cell polarity [70]. A simple explanation then for why only clusters are entrained in cortical flows is that while all molecules at the cell surface are subjected to a fluid drag force generated by flows, monomers diffuse more rapidly than oligomers due to greater mass and increased number membrane binding sites [34, 21]. This basic model is supported by studies showing that lateral diffusion coefficients of particles bound to the cell membrane at multiple sites are proportional to the inverse of the number of binding sites [172, 79]. Further, Chang and Dickinson showed through simulations that the inferred diffusivities and dissociation rates of PAR-3 trimers, but not dimers, are sufficiently slow for cortical flows to build up asymmetries in PAR-3, a finding consistent with observations *in vivo* [21]. However, this simple model predicts that oligomers undergo pure diffusion, i.e. mean squared displacement scales linearly with lag time. In contrast, PAR-3 clusters, as well as CHIN-1 clusters, have been shown to undergo subdiffusive motion, where mean squared displacement scales less than linearly with lag time [130]. Crucially, this subdiffusive motion depends on an intact actin cytoskeleton, suggesting a model where size-dependent interactions between PAR-3 clusters and the actin cortex sharply restrict their diffusion [130].

One explanation for actin-dependent decreases in PAR-3 cluster mobility is that PAR-3 clusters could bind directly to the actomyosin cortex [173]. While this type of mechanism

likely operates at the immunological synapse [36], super-resolution imaging shows that PAR-3 and actin fail to co-localize in the *C. elegans* zygote [21]. Therefore, perhaps the most likely model is the "membrane skeleton fence" model, from classic literature [124]. In this model, cell surface proteins are free to diffuse freely over short distances, but are confined to membrane compartments by steric interactions with the cortical actin cytoskeleton, from which they infrequently escape. The result of this process of "hop diffusion" is sub-linear scaling of mean squared displacement with lag time, and studies suggest that larger proteins may be more likely to be subject to steric restriction from the cytoskeleton [70]. This model is therefore best able to explain all aspects of the phenomenology of PAR-3 polarization by cortical flows.

While further study is needed to determine whether viscous drag and decreased diffusivity are sufficient to entrain PAR-3 clusters in cortical flows or whether additional steric interactions with the actin cytoskeleton are required, experiments to distinguish between models are complicated by the fact that flows are generated by actomyosin. One promising way forward may be combine actin depolymerization with ectopic flows generated by focused-light-induced cytoplasmic streaming [103] to determine whether polarity proteins can be redistributed by flows in the absence of steric interactions with the cytoskeleton.

1.4.2 Clustering stabilizes asymmetries by introducing nonlinear dynamics

Another way protein clustering could function in polarity circuits is by introducing nonlinear dynamics to the accumulation of polarity proteins on the cell membrane. If protein clustering is driven by the local concentration of protein and clustering stabilizes the association of polarity proteins with the membrane through avidity effects [86], a negative relationship will exist between the local concentration of a polarity protein and its effective dissociation rate constant. This in turn results in sub-linear scaling of the dissociation flux with protein concentration. As established above, one insight from mathematical modeling of cell polarity

is that self-stabilizing polarity circuits require that the order of the function defining the local on-flux of polarity protein must be greater than the order of the function defining the local off-flux. This sub-linear scaling of off-flux with protein concentration therefore stabilizes asymmetric cell surface distributions of clustered polarities protein when combined with any additional form of linear feedback [85].

As with the connection between cortical flow and clustering, the context in which this idea has been explored most directly is in the *C. elegans* zygote, where multiple PAR proteins cluster at the cell membrane. Bipolar PAR asymmetries are stabilized at least in part by mutual antagonism between proteins localizing in complementary and opposing domains. However, modeling shows that the first order phosphorylation reactions that form the biochemical basis for mutual inhibition do not satisfy the conditions for stable polarity. Most modeling studies deal with this by simply making phosphorylation rates proportional to the square of the kinase, without biochemical justification. However, three studies deal with this by introducing homo-oligomerization of PAR proteins and avidity effects.

In one of these studies, Dawes and Munro focused on mutual antagonism between PAR-3/PKC-3 and PAR-1 in the PAR network [32]. PAR-3 oligomerizes via an N-Terminal PB1-like domain, which forms linear filaments *in vitro* [39, 168]. In multiple experimental systems, PAR-3 oligomerization is necessary for its enrichment on the cell surface, suggesting that avidity effects stabilize PAR-3 interactions with the cell membrane. Dawes and Munro considered a simplified model where PAR-3 dimerizes at the cell membrane according to mass action kinetics, with dimers dissociating more slowly than monomers [32]. When this effect is combined with first order mutual inhibition with PAR-1, local dynamics of PAR-3 accumulation can become bistable (i.e. PAR-3 can be in either a stably high or stably low state) and bipolar PAR domains can be stabilized. However, bistability was only observed in a small region of possible parameter space, and general conditions required for the emergence of bistability were not identified.

In a second study, Sailer et al. focused on the CDC-42/CHIN-1 subcircuit of the PAR network [130]. CHIN-1 localizes to the cell membrane in clusters of various sizes, although the mechanism by which it self-associates is unknown. As noted above, CHIN-1 is a GAP that acts on CDC-42. CDC-42 recruits PKC-3 to the cell surface, where it inhibits accumulation of CHIN-1 on the membrane. Sailer et al. showed that CHIN-1 clusters respectively condense or dissolve on opposite sides of a spatial boundary in the cell that corresponds to a threshold level of PKC-3 [130]. Based on this observation, they propose a model where CHIN-1 clusters grow when the monomer concentration is above a critical threshold, which is in turn determined by the local concentration of PKC-3. Clusters are assumed to be long-lived at the membrane, while monomers rapidly exchange with the cytoplasm. Experimental constraints on the threshold level of PKC-3 that dissolves CHIN-1 clusters and the strength with which CHIN-1 inhibits CDC-42 demonstrate that mutual inhibition between CHIN-1 clusters and CDC-42/PKC-3 was sufficient to endow the circuit with bistable dynamics and stabilize PAR asymmetries [130].

In a third study, Arata et al. explore the role of oligomerization in stabilizing PAR-2 asymmetries. They show that PAR-2 forms oligomers with up to four subunits, and use single molecule imaging to show that oligomers dissociate from the membrane more slowly than monomers. However, while oligomer size-dependent dissociation is implicit in the nonlinear functions used in their model that determine the flux of PAR-2 off the membrane [5], oligomerization is not built explicitly into their model, and the dynamic emergence of bistability in this model is not explored.

All three of these examples point to a key role for oligomerization in introducing nonlinear dynamics to polarity circuits. However, none of them systematically demonstrate how oligomerization of membrane proteins, and its effects on lateral mobility and dissociation, shapes their abilities to form and stabilize asymmetric distributions on the cell surface. This point is explored in depth in the second chapter of this dissertation as well as in the as-

sociated manuscript [85]. Further, while Dawes and Munro show that oligomerization of PAR-3 combined with mutual antagonism between PAR-3/PKC-3 and PAR-1 can produce stable asymmetries, the model they propose is not a realistic depiction of PAR-3 oligomers (PAR-3 forms oligomers of various sizes, not dimers) and is not experimentally constrained. In the third chapter of this dissertation I will present an experimentally constrained model of PAR-3 asymmetries in the *C. elegans* zygote that explains the observation that PAR-3 asymmetries are stable even in the absence of PAR-1.

In addition to this specific idea that clustering of peripheral membrane proteins amplifies asymmetries through avidity effects and can introduce nonlinearities necessary to stabilize polarity, clustering has been proposed to act as a form of positive feedback in the core PCP module [28]. This view is supported by the observations that for some core PCP proteins, clustered but not diffuse protein is asymmetrically distributed at cell junctions [28], and that in at least some contexts, PCP clustering is required for functional polarization [162, 166]. While core PCP proteins are tethered to the membrane through transmembrane domains and thus are not subjected to the avidity effects of clustering like peripheral membrane proteins, an analogous role for clustering could exist for PCP proteins if clustered PCP proteins are less likely to be endocytosed that monomeric proteins. Support for this kind of relationship comes from the observation that integral PCP proteins accumulate to higher levels on the membrane when they are clustered by cytoplasmic binding partners [116]. Further, the effects of clustering on lateral mobility apply to both peripheral and integral membrane proteins, and thus clustering could amplify PCP asymmetries through a diffusion trap mechanism. Either way, it may be interesting in the future to build models of PCP asymmetries that explicitly consider the physical consequences of molecular clustering.

Another context where clustering plays a key yet currently unknown role in stabilizing asymmetries is the SOSEKI polarity proteins in plant cells [167, 151]. SOSEKI proteins oligomerize through conserved DIX domains that are functionally equivalent to those

found in Dsh proteins [151]. While not required for membrane localization, these domains are required for SOSEKI protein polarization [167, 151]. While this polarity system was only recently discovered [167] and it is yet unknown whether it is even a component of a self-stabilizing polarity module, it will be interesting in the future to determine what role molecular clustering plays in stabilizing SOSEKI protein asymmetries.

One interesting exception to the rule that clustering needs to be paired with active feedback to stabilize asymmetries comes from a model proposed by Dine et al. [35] involving phase separated protein clusters. This model lacks any active feedback and instead relies on the fact that due to a physical process called Ostwald ripening, there is no thermodynamic tendency for phase separated droplets to equalize in size. Instead large droplets slowly grow at the expense of smaller droplets [35]. This effect, combined with the slow diffusion of large, phase separated droplets leads to metastable polarity through a mechanism termed "kinetic trapping" if an asymmetry in the size of droplets is initially established by some extrinsic cue. While the steady state of this mechanism is technically one very large droplet randomly located in the cell, the time scale for achieving that steady state is very slow under certain conditions [119] and a number of biological mechanisms can further slow the approach to this steady state in cells [40, 175, 42]. While this model does not include energy-consuming feedback, positive dependence of droplet growth rate and negative dependence of droplet diffusion on droplet size are analogous to the feedback loops found in traditional reaction diffusion models. Dine et al. demonstrated that this mechanism can stabilize protein asymmetries in principle using a synthetic optogenetic system, and it will be interesting in the future to determine the degree to which this type of mechanism is utilized in cells.

1.4.3 Clustering regulates the shapes of asymmetric distributions

In addition to establishing and maintaining asymmetric distributions of polarity proteins, a more subtle way clustering plays a role in cell polarity mechanisms is by regulating the shapes

of asymmetric distribution. For example, clustered peripheral membrane proteins often exhibit very sharp domain boundaries [130, 126]. In the case of CHIN-1 in *C. elegans* zygote (see above), CHIN-1 clusters rapidly dissolve across a threshold level of inhibitory PKC-3. Since CHIN-1 monomers dissociate from the membrane much more rapidly than clusters, this is accompanied by a sharp increase in effective dissociation rate across this threshold. When combined with the slow diffusion of CHIN-1 clusters, this results in CHIN-1 domain boundaries that are much sharper than the opposing gradients of PKC-3, (particularly in the absence of transport by cortical flow) [130]. This effect is not specific to peripheral membrane proteins and also generalizes to cytoplasmic asymmetries of phase-separated proteins. Phase separated P granules in the *C. elegans* zygote similarly dissolve or grow across an axial boundary in the cell, which may correspond to a threshold level inhibitory MEX-5 [17]. As a result, P granules exhibit much sharper domain boundaries than other proteins that form cytoplasmic asymmetries in the *C. elegans* zygote.

Another general way that clustering can regulate the shapes of polarized distributions is that it may enable polarity modules to "remember" arbitrary polarized distributions that are imposed by transient extrinsic cues, which is primarily a consequence of slow diffusivity of clustered proteins. Dine et al. demonstrated this effect in an optogenetic system where phase separation of a synthetic protein could be controlled through exposure to blue light [35]. The authors could generate polarized cytoplasmic distributions of these proteins by patterning light in space, and found that boundaries of these polarized domains persisted for hours in the absence of sustained spatial cues [35]. This idea is further explored in chapters 2 and 3 of this dissertation.

A more specific example of protein clustering regulating the shape of a polarized distribution comes from fission yeast. Pom1p is loaded onto the plasma membrane on the poles of fission yeast cells by the Tea1p/Tea4p/Dis2p complex [54]. Dis2p dephosphorylates Pom1p, which increases its affinity for the plasma membrane. Pom1p diffuses laterally away from

the pole forming a gradient from the pole to the midline [131]. In individual cells, this gradient is well fitted by an exponential decay function with a maximum intensity at the cell pole I_0 and a characteristic decay length λ [131]. Surprisingly, I_0 and λ were shown to be anti-correlated in measurements across cells, suggesting that some mechanism buffers the absolute concentrations of Pom1p in the middle of the cell against fluctuations in the amount of Pom1p at the poles [131]. To explain this phenomenon, Saunders et al. proposed a model where dynamic clustering of Pom1p at the cell poles both slows down lateral diffusion D of Pom1p, and also increases its dissociation rate k_{off} through auto-phosphorylation [131]. Since $\lambda = \sqrt{\frac{D}{k_{off}}}$ [156], and since clustering reactions are proportional to the product of local concentrations of clustered and monomeric Pom1p, Pom1p clustering causes λ and I_0 become anti-correlated [131].

1.4.4 Clustering can amplify functional asymmetries

Protein clustering has been proposed to act as a pervasive mechanism for introducing hypersensitivity into biochemical signaling pathways [161, 7, 68, 80]. In general terms, hypersensitivity can emerge from the combination of 1) positive relationship between some signal and protein clustering and 2) a nonlinear relationship between the number of molecules in a cluster and the downstream response. One recent and prominent example of this effect comes from T cell receptor (TCR) signaling in the immunological synapse. TCR activation triggers phosphorylation of the transmembrane scaffold protein LAT at multiple tyrosine residues. The adaptor protein Grb2 binds to these sites and recruits the guanine nucleotide-exchange factor (GEF) SOS to the cell membrane. Interaction between SOS and phospholipids relieves SOS autoinhibition and allows it to activate Ras GTPase processively. Each molecule of SOS can bind to two molecules of Grb2, so in addition to its enzymatic function, it crosslinks two molecules of LAT. As a result of these interactions, multi-site phosphorylation of LAT induces co-clustering of LAT, Grb2, and SOS through multivalent assembly.

While Grb2 has stronger affinity for phosphorylated as opposed to unphosphorylated LAT, it is still a relatively weak interaction (mean dwell time 0.1 seconds). However, Grb2 molecules bound to LAT molecules within a cluster dissociate much more slowly (mean dwell time 10 seconds) and SOS molecules with clusters dissociate even more slowly (mean dwell time 30 seconds) [67]. Therefore, through avidity effects, clustering increases the steady state amount of SOS on the membrane more than two orders of magnitude over what you would get from a simple linear response to phosphorylating LAT.

While this avidity effect alone introduces a nonlinearity into the signal response, another layer of nonlinearity is introduced from the observation that the activation time for membrane-associated SOS molecule follows a gamma distribution indicating slow, multi-step reaction. The mean activation time (55 seconds) is much longer than the dwell time of a monovalant interaction between pLAT and Grb2 [68]. As a result, SOS activity has a sharply nonlinear relationship SOS dwell time [68]. The combination of these effects ensures that the amount of clustered pLAT, rather than just the concentration of pLAT, exerts a very strong influence on SOS activity simply by increasing its dwell time at the membrane through avidity effects. Interestingly, an similar paradigm is found in the Nephrin-Nck-N-WASP signaling pathway, where clustering regulates downstream signaling by increasing N-WASP dwell time [20].

There are several examples that suggest that clustering of polarity proteins could amplify functional asymmetries downstream of polarity modules. As noted above, core PCP proteins Fz and Dsh co-cluster at cell junctions [94, 28, 140]. Fz recruits Dsh to the cell membrane, locally increasing its concentration and thus triggering oligomerization through a conserved DIX domain [133]. When Fz is activated by its extracellular ligand Wnt, the downstream signaling response is preceded by clustering of Fz and Dsh at the cell membrane [94] and oligomerization of Dsh is required in several contexts for generating a robust signaling response [133, 134, 94]. Dsh clustering have been proposed to activate downstream signaling

by increasing the avidity of low affinity effectors, such as Axin [133, 134, 41]. In a parallel with the pLAT-Grb2 interaction, single molecule imaging shows that clustering significantly increases Dsh dwell time at the membrane [94]. While the connection between clustering and signaling has not been worked out in as great detail as in TCR signaling, it seems likely that clustered Dsh is better able to transmit signals to downstream effectors than monomeric Dsh, and therefore asymmetries in Dsh clusters sizes will amplify asymmetries in downstream signaling beyond simply the asymmetry in Dsh concentration.

Another example of clustering potentially amplifying functional asymmetries comes from the SOSEKI proteins in plants. While the functional effectors of SOSEKI polarity are currently unknown, the ANGUSTIFOLIA protein colocalizes with SOSEKI at the cell membrane in *Arabidopsis* root tips. ANGUSTIFOLIA polarity is dependent of SOSEKI, while SOSEKI polarity is independent of ANGUSTIFOLIA, suggesting that SOSEKI is a component of a core polarity module while ANGUSTIFOLIA is an effector. While oligomerization of SOSEKI has relatively mild effects its membrane localization [167], clustering of SOSEKI proteins is shown to be required for co-localization of SOSKEI and ANGUSTIFOLIA [151]. Whether this is mediated by multivalent interactions and avidity effects or some other mechanism remains to be seen, but this will be an interesting system in the future to study the role of oligomerization in cell polarity.

A final example comes from the *C. elegans* zygote. Single molecule pull-down experiments show that PAR-3 oligomers co-localize with PAR-6/PKC-3 dimers more frequently than would be expected given independent recruitment to each oligomer subunit [34]. Since PAR-6 and PKC-3 both interact with PAR-3, it is possible multivalent interactions within PAR-3/PAR-6/PKC-3 trimers introduce avidity effects where PKC-3 binds much more stably to oligomeric than monomeric PAR-3. Whether PAR-3 oligomerization is required for its downstream functions remains an open question in the *C. elegans* zygote and is a promising avenue for future research.

CHAPTER 2

OLIGOMERIZATION OF PERIPHERAL MEMBRANE PROTEINS PROVIDES TUNABLE CONTROL OF CELL SURFACE POLARITY

2.1 Introduction

Cells rely on morphological and functional polarity to execute a wide range of biological tasks, including asymmetric cell division, polarized growth and secretion, and cell migration. Cell polarity typically emerges from underlying asymmetries in the intracellular distributions of specific molecules or molecular activities. These asymmetries can form spontaneously or in response to transient localized "symmetry-breaking" cues that determine the axis of polarity.

In many cells, asymmetries are formed at the cell surface by molecules that exchange dynamically between a rapidly diffusing cytoplasmic pool and binding sites at the plasma membrane where they undergo slower diffusion that can be further hindered by interactions with a submembrane cytoskeleton [125, 43, 130], and where they interact to promote or inhibit one another's binding or activity [66, 44, 130, 14, 123, 153]. These mutual interactions define biochemical feedback circuits, which encode the ability to respond to external cues by establishing and stabilizing asymmetric distributions of their component molecules. In the past several decades, a relatively small number of such circuits have been shown to underlie the formation and stabilization of polarity in a wide range of cellular and organismal contexts. Examples include circuits formed by small GTPases such as RhoA and Cdc42, their activators (GEFs), inhibitors (GAPs) and effectors [160, 132], the conserved PAR polarity circuit [84],

. Citation for chapter: Charles F Lang and Edwin Munro. Oligomerization of peripheral membrane proteins provides tunable control of cell surface polarity. Biorxiv, 2022

the Min proteins in bacteria [120, 91], and a collection of proteins in fission yeast, including Pom1p and Mid1p, that differentiate the pole from the mid-cell [123, 54, 14].

Cell surface asymmetries can emerge spontaneously, or they can be induced by transient local cues acting in various ways – for example through locally biased activation or inhibition of recruitment [75, 170, 98, 112] or through polarized transport [109, 44, 112]. However, positive feedback is required to amplify the effects of these symmetry-breaking cues and to stabilize asymmetries once the cues are gone against dissipation by dissociation and lateral diffusion. Thus, a key challenge is to understand how asymmetric distributions of membrane proteins are amplified and stabilized by the dynamic interplay of local exchange, lateral mobility, and feedback.

Theoretical efforts to address this challenge have focused on simple abstractions of known circuits or circuit "motifs" expressed as mass-conserved reaction-diffusion models [114, 48, 105, 27, 55, 47].These efforts have revealed how simple polarity circuits can manifest qualitatively different dynamics, depending upon the types and strengths of feedback, protein abundance, binding rates and mobilities, and the forms of nonlinearities that appear in model equations. For example, the same model can exhibit a spatially uniform stable state, a stably polarized state, or both, depending on model parameters [63, 47]. The positions of stable domain boundaries, or the rates at which competition between multiple domains is resolved, can be continuously tuned by tuning the strength and/or saturation of feedback interactions, the lateral diffusion of proteins at the cell membrane, or the total abundance of proteins [44, 27, 171].

A general conclusion from these studies is that while linear positive feedback can generate transient noisy asymmetries when the numbers of molecules are sufficiently low [2, 74], stable polarity requires some form of nonlinear positive feedback [90, 47, 27]. But how specific forms of nonlinearity and feedback, arising through specific molecular interactions, shape polarization dynamics, remains poorly understood.

One potentially important source of nonlinearity in polarity circuits is the oligomerization of peripheral membrane proteins. In recent years, an increasing number of polarity proteins have been observed to form discrete clusters on the cell membrane [121, 123, 149, 130, 37, 131] suggesting that oligomerization may play a general role in polarity circuits. Oligomerization confers size-dependent membrane binding avidity [86, 34], and can also lead to size-dependent restriction of mobility through the interactions of oligomers with a submembrane cytoskeleton [159, 130, 83, 70, 124]. A few previous modeling studies have considered oligomerization reactions [130, 32, 131, 14], but these have focused on special cases [130, 32], or on how oligomerization shapes gradients formed by a local source of protein recruitment [131, 65]. To date there has been no systematic analysis of how oligomerization of membrane proteins, and its effects on lateral mobility and dissociation, shapes their abilities to form and stabilize asymmetric distributions on the cell membrane.

Here we study a class of simple polarity models in which monomers bind reversibly to the membrane, and oligomerize in the presence of positive feedback governed by first order (linear) mass action kinetics. We find that nonlinear dissociation kinetics emerge generically from size dependence of membrane binding avidity, and that this, combined with weak linear positive feedback, is sufficient for polarization. We show that the strengths of oligomerization and feedback define phase boundaries separating regimes in which stable polarity is impossible to achieve, is inducible, or occurs spontaneously. Furthermore, modulating oligomerization strength provides a simple way to tune the speed of polarization, allowing the same system to rapidly approach a uniquely stable polarized state, or to preserve polarized domains of arbitrary sizes as quasi-stable states over biologically relevant timescales. These basic findings extend to multiple circuit architectures and different modes of positive feedback. Given its widespread occurrence, our results suggest that oligomerization of peripheral membrane proteins may play a key role in facilitating and tuning polarization dynamics across a wide range of evolutionarily distinct polarity circuits and cell types.

2.2 Results

2.2.1 A kinetic model for membrane-binding and oligomerization with feedback on monomer recruitment

We consider a simple and general scenario in which monomers exchange between a well-mixed 2D cytoplasmic pool with area $A = HL$ and a 1D membrane of length L, where they undergo reversible assembly into simple linear oligomers (Fig 2.1A). Cytoplasmic monomers also bind directly and reversibly to membrane associated monomers and oligomers. We will distinguish these two modes of binding as indirect (to the membrane) and direct (to membrane-bound monomers and oligomers). Oligomers dissociate from the membrane at a rate that decreases with oligomer size [86, 34]. To simplify the analysis, we assume that the dissociation rate is zero for oligomers with size $n \geq 2$. Finally, we assume positive feedback on monomer recruitment, proportional to the total density of oligomer subunits at the membrane.

Letting x be the local position along the membrane, $m_n(x)$ be the density of n-mers, $N(x)$ be the density of all oligomers, $M(x)$ the density of all subunits, C be the concentration of cytoplasmic subunits, and M_{tot} be the constant total number of subunits in the system, we write the following system of equations:

$$\begin{aligned} \frac{dm_1}{dt} &= D_1\frac{\partial^2 m_1}{\partial x^2} + (k_{on}^m + k_f M)C - k_{off}^m m_1 - k_{ass}m_1 + \\ &\qquad k_{diss}m_2 - k_{on}^p m_1 N + k_{off}^p(N - m_1) \\ \frac{dm_n}{dt} &= D_n\frac{\partial^2 m_n}{\partial x^2} + k_{ass}m_{n-1} - (k_{ass} + k_{diss})m_n + k_{diss}m_{n+1}, \quad n > 1 \\ A(M_{tot} - C) &= \int_0^L M(x)dx \end{aligned} \tag{2.1}$$

where $k_{ass} = k_{on}^p m_1 + k_{on}^c C, k_{diss} = k_{off}^p + k_{off}^c$ and the third equation enforces conservation of total subunits.

The spatially uniform steady states of this system are characterized by exponential distributions of oligomer sizes (see Methods) :

$$m_n = \alpha^{n-1} m_1, \quad \alpha = \frac{k_{ass}}{k_{diss}}$$

with mean cluster size:

$$s = \frac{1}{1-\alpha}$$

2.2.2 Reduction to a one-species model

Our goal is to determine conditions in which this system will form and stabilize asymmetric distributions of membrane bound oligomers. To this end, we first consider a simpler limiting case in which oligomerization kinetics on the membrane are fast relative to the exchange of subunits between the cytoplasm and membrane. Invoking a quasi-steady state approximation to study the slower dynamics of subunit exchange, and choosing appropriate units of length, time and concentration/density (see Methods), we obtain a simpler equation for the total density of membrane-bound subunits M (see Methods):

$$\begin{aligned} \frac{\partial M}{\partial t} &= D\frac{\partial^2 M}{\partial x^2} + F(M)C - G(M) \\ C_{tot} &= C + \int_0^L M(x)dx \end{aligned} \tag{2.2}$$

where

$$F(M) = K_M\left(1 + BN + fM\right), \quad G(M) = m_1\left(1 + \gamma BN\right)$$

and $D = \frac{D_M}{k_{off}^m L^2}$, $K_M = \frac{k_{on}^m}{L k_{off}^m}$, $B = \frac{k_{on}^c}{k_{on}^m}$, $f = \frac{k_f}{k_{on}^m}$, $\gamma = \frac{k_{on}^m k_{on}^p k_{off}^c}{k_{off}^m k_{off}^p k_{on}^c}$ and $C_{tot} = \frac{M_{tot}}{L}$ are scaled parameters. D_M is the mean diffusivity of M, which will depend on mean oligomer size (see below), B quantifies the relative rates of direct and indirect monomer binding, f is the scaled feedback strength, γ is a dimensionless number that equals unity when the

basal exchange and oligomerization kinetics (i. e. excluding feedback) (2.1) satisfy detailed balance, and C_{tot} is the density of membrane-bound subunits when all subunits are on the membrane.

For this simpler system, the effective dissociation rate constant for membrane-bound subunits, $\frac{G(M)}{M}$, is a nonlinear decreasing function of M (Fig. 2.1E, dark curve), reflecting the dependence of membrane binding avidity on oligomer size and the dependence of oligomer size on M (Fig. 2.1E, lighter curve). Thus the combination of oligomerization and size dependent binding avidity confers nonlinear negative feedback on dissociation of M.

2.2.3 Conditions for spontaneous and inducible polarization

Plotting binding and unbinding fluxes ($F(M)(M_{tot} - M)$ and $G(M)$) vs M shows that, for most choices of parameter values, the reduced system (and thus the full kinetic model) has a single spatially uniform steady state (Fig. 2.1F, 2.7). For different choices of model parameters, numerical solutions predict one of three qualitatively distinct behaviors (Fig 2.2A-C): **Spontaneous polarization** - the uniform steady steady state is unstable to all perturbations, **Inducible polarization** - the uniform steady state is stable, but stable polarity can be triggered by a sufficiently large transient perturbation, and **No polarization** - the uniform steady state is globally stable.

Using linear stability analysis (see Methods), we determined general conditions for spontaneous polarization:

$$\left(\frac{\partial F}{\partial M}C - \frac{\partial G}{\partial M}\right)_{M=M_{ss}} > 4\pi^2 D_M \tag{2.3}$$

The terms on the left hand side of Eq 2.3 measures how the attachment and detachment rates vary with density of M near the steady state. In words, Eq 2.3 states that to amplify local asymmetries in M, the net accumulation rate must increase with increasing density near M, and it must do so sufficiently fast to overcome the dispersive effects of diffusion.

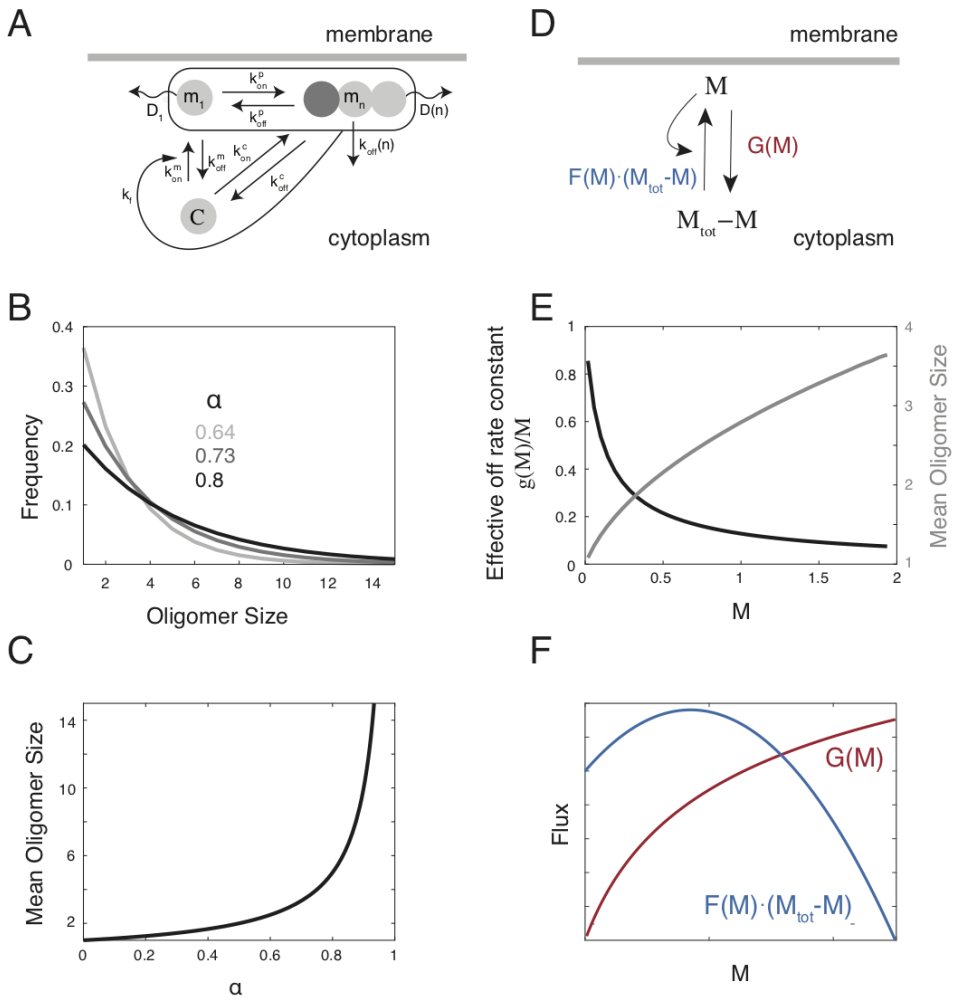

Figure 2.1: **A kinetic model for membrane binding and oligomerization. (A)** Schematic overview of the kinetic scheme. Cytoplasmic monomers bind reversibly to the plasma membrane with rate constants (k^m_{on}, k^m_{off}), where they self-associate to form linear oligomers with rate constants (k^p_{on}, k^p_{off}). Cytoplasmic monomers also bind directly and reversibly to membrane-associated subunits with rate constants (k^c_{on}, k^c_{off}). We assume that oligomer dissociation rates $k_{off}(n)$ and diffusivities $D(n)$ are decreasing functions of oligomer size. Curved line indicates positive feedback on membrane binding at a rate $k_f(M)$ which depends on the local density of membrane-bound subunits M. **(B)** Examples of steady state oligomer size distributions corresponding to different values of the parameter α. **(C)** Plot showing the fixed relationship between α and the mean oligomer size. **(D)** A simpler model for the total density of subunits M, which is valid when oligomerization kinetics are sufficiently fast (see Methods for details). $F(M)(M_{tot} - M)$ and $G(M)$ represent total binding and unbinding rates. (legend continued on next page)

Figure 2.1: (continued) **(E)** Effective unbinding rate (black curve) and mean oligomer size (grey curve) decrease and increase respectively as a function of M, reflecting size-dependent oligomer dissociation. **(F)** Representative flux balance plot showing one uniform steady state for the model. The blue line represents flux onto the membrane and the orange flux represents flux off of the membrane.

Mean oligomer size and feedback strength determine the potential for polarization

We first considered the case in which diffusion is slow ($D_M \approx 0$) and direct binding of cytoplasmic monomers to membrane-bound oligomers can be neglected ($B \approx 0$). Under these conditions (see Methods), spontaneous symmetry-breaking occurs when:

$$J_{feedback} > \frac{(1-\alpha)}{2\alpha} \tag{2.4}$$

where $J_{feedback} = fM_{ss}$ quantifies feedback strength as the ratio of binding flux due to feedback and the basal binding flux, and $J_{feedback}$ and α are evaluated at the uniform steady state. For $J_{feedback} < \frac{(1-\alpha)}{2\alpha}$, we determined the threshold for inducible polarization using Local Perturbation Analysis (LPA; [63]; see Methods). Plotting different polarization regimes in the $J_{feedback}$ vs α plane (Fig. 2.2D-E), highlights several conclusions: First, both indirect positive feedback ($J_{feedback} > 0$) and negative dependence of dissociation rate on oligomer size ($\alpha > 0$) are required for spontaneous symmetry-breaking. However, the strength of feedback required for spontaneous symmetry-breaking decreases rapidly with an increase in mean oligomer size, such that for mean oligomer sizes greater than a few subunits, positive feedback must only deliver a fractional increase over the basal on-rate to induce spontaneous polarization. Finally, when the uniform state is stable, stable polarity can always be induced by a sufficiently large local input, and the threshold for induction decreases with increasing $J_{feedback}$ or α, reaching zero at the spontaneous polarization boundary.

We then assessed how increasing diffusivity affects the potential for both spontaneous

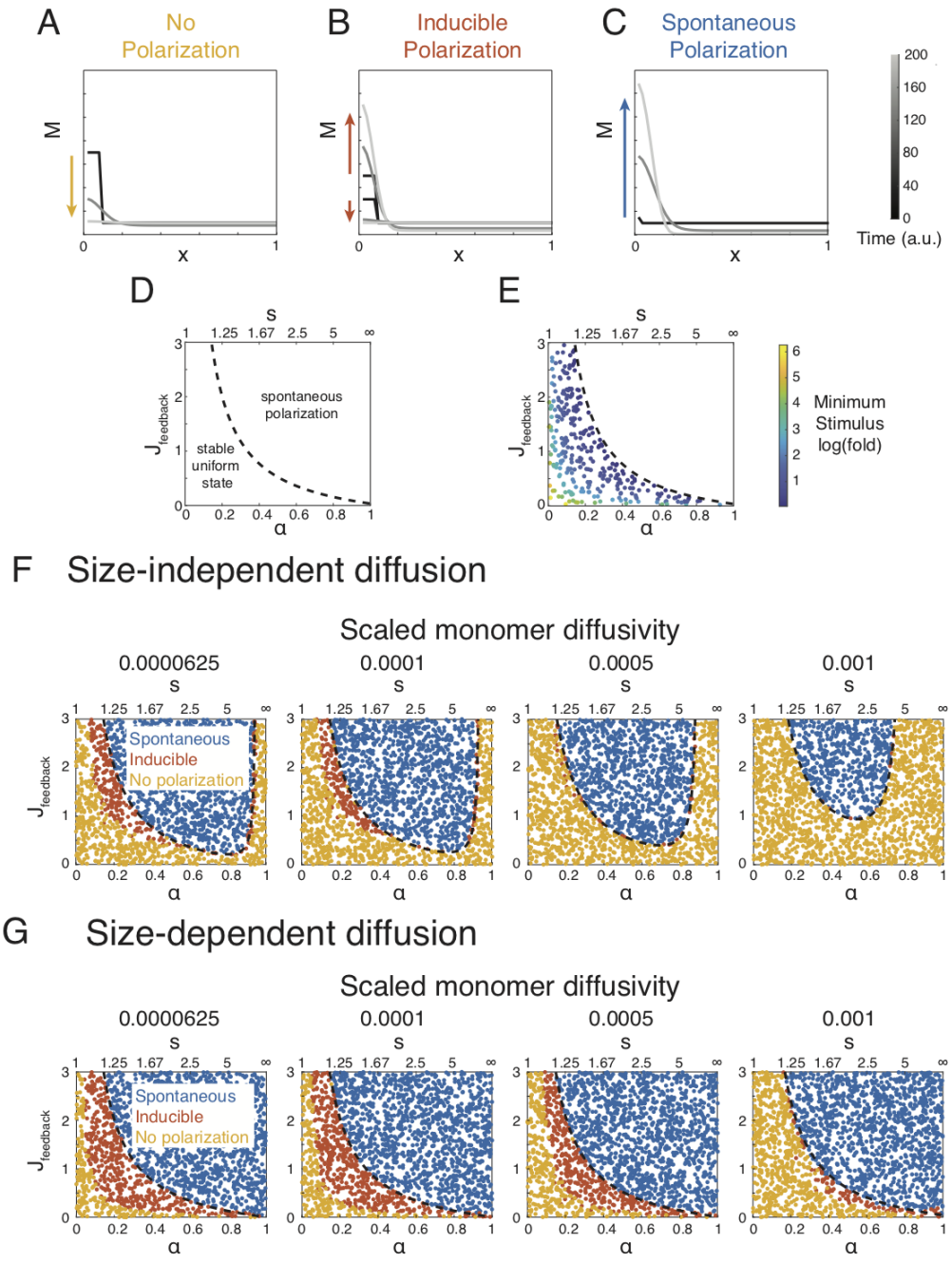

Figure 2.2: **Strength of oligomerization and positive feedback define the potential for polarization.** **(A-C)** Examples of three qualitatively distinct polarization regimes: **(A) No Polarization**, in which the uniform steady state is globally stable; **(B) Inducible Polarization**, in which uniform steady state is stable, but it coexists with a stably polarized state that can be accessed by a sufficiently large transient local perturbation; and **(C) Spontaneous Polarization**, in which the uniform steady state is unstable and the system will spontaneously polarize. (legend continued on next page)

Figure 2.2: (continued) **(D)** Spontaneous symmetry breaking as a function of α and mean oligomer size s and feedback strength $J_{feedback}$. The dotted line indicates the boundary between regimes in which the uniform steady state is stable (respectively unstable) to small perturbations. **(E)** The minimum size of a local perturbation (measured as local fold increase over steady state concentration) required to induce polarization under conditions where symmetry-breaking is not spontaneous, as determined by Local Perturbation Analysis (see Methods). **(F,G)** Dependence of spontaneous and inducible polarization on scaled monomer diffusivity $D = \frac{D_1}{k_{off}^m L^2}$. For a typical length scale $L = 40\mu m$, and monomer dissociation rate $k_{off}^m = 1$, the scaled values represent (left to right) $D_1 = (0.1, 0.16, 0.4, 1.6)\,\frac{\mu m^2}{s}$. For a typical monomer diffusivity $D_1 = 0.1\frac{\mu m^2}{s}$, and dissociation rate $k_{off}^m = 1$, the scaled values represent (left to right) $L = (40, 30, 20, 10)\,\mu m$. The dotted line indicates the predicted boundary for spontaneous symmetry breaking from linear stability analysis. **(F)** represents a scenario in which diffusion is size-independent ($D_M = D_1$), while **(G)** represents a scenario in which oligomers of size greater than one do not diffuse. ($D_M = D_1(1-\alpha)^2$).

and inducible polarization. Recent studies suggest that the mobility of membrane-bound oligomers can decrease sharply with oligomer size [130, 131]. Therefore we considered two limiting scenarios: Size-independent diffusivity in which oligomers diffuse at the same rate as monomers ($D_M = D_1$), and size-dependent diffusivity in which oligomers of size ≥ 2 are immobile ($D_M = D_1(1-\alpha)^2$). When diffusivity is non-negligible, the conditions for spontaneous polarization are given by

$$\begin{aligned} J_{feedback} &> \frac{D^* \frac{1+\alpha}{(1-\alpha)^2} + (1-\alpha)}{2\alpha - D^* \frac{1+\alpha}{(1-\alpha)^2}} \\ 2\alpha - D^* \frac{1+\alpha}{(1-\alpha)^2} &> 0 \end{aligned} \tag{2.5}$$

We plotted the spontaneous polarization boundary in the $J_{feedback} - \alpha$ phase plane and used numerical simulations to assess the threshold for inducing polarity when the uniform steady state is stable (Fig. 2.2 F,G). Consistent with intuition, we found that for size-independent diffusion, increasing scaled monomer diffusivity $D_1^* = \frac{D_1}{k_{off}^m L^2}$ makes it harder for the system to undergo both spontaneous and induced polarization: For a given value of α, as monomer diffusivity increases, the feedback strength $J_{feedback}$ required for spontaneous

polarization increases, especially for large values of α or oligomer size s, and the region of the $J_{feedback} - \alpha$ phase plane in which polarity can be induced shrinks progressively (Fig. 2.2F). These effects are relatively mild for typical diffusivities of membrane proteins ($D = 0.1\frac{\mu m^2}{sec}$), cell lengths ($L = 10 - 40\mu m$) and monomer dissociation rates ($k^m_{off} \approx \frac{1}{sec}$) (see Fig. 2.2 legend for scaled diffusivities corresponding to these typical values). Importantly, for the size-dependent diffusion scenario, these effects become negligible (Fig. 2.2 G). Thus, while diffusion can degrade the potential for spontaneous and/or induced polarization, this effect is relatively mild and it can be further reduced by a size-dependent decrease in oligomer mobility.

Numerical simulations of the full kinetic model reveal that equation 2.3 continues to yield an accurate prediction of spontaneous polarization when we relax the assumption that oligomerization kinetics are very fast relative to membrane exchange, i.e. when $k^p_{off} \geq k^m_{off}$ (Fig. 2.5). Similarly, relaxing the sharp size dependence of oligomer dissociation (Fig. 2.5), or allowing formation of cytoplasmic oligomers (Fig. 2.5), produced only minor shifts in the dependence of spontaneous and inducible polarization on $J_{feedback}$ and α. Thus simple oligomerization plus linear feedback provides a robust mechanism for spontaneous polarization of membrane bound proteins.

Direct binding of cytoplasmic monomers to membrane-bound oligomers can promote or antagonize polarization under different conditions.

In addition to binding the membrane, cytoplasmic monomers can bind directly to membrane-bound monomers and oligomers. In this case, the ability to polarize will depend on three factors: The strength of positive feedback $Jfeedback$; the ratio of direct to indirect binding rates, determined by the relative abundances of membrane binding sites and membrane bound oligomers [13], and quantified by $B_{dir} = \frac{k^c_{on} N_{ss}}{k^m_{on}}$, where N_{ss} is oligomer density at uniform steady state; and whether the basal oligomerization and exchange reactions obey

detailed balance.

We first asked how direct binding affects polarization driven by indirect positive feedback when basal oligomerization and exchange reactions obey detailed balance (i.e. $\gamma = 1$) (Fig. 2.3A ; see Methods).Neglecting the effects of diffusion, the conditions for spontaneous polarization are then given by (see Methods):

$$J_{feedback} > \frac{(1-\alpha)(1+B_{dir})^2}{2\alpha(1+B_{dir}) - B_{dir}} \tag{2.6}$$

Plotting the phase boundary for spontaneous polarization (Fig. 2.3B) shows that when detailed balance is enforced, direct binding to oligomers makes it more difficult to polarize. Increasing B_{dir} from 0 to 1 increases the strength of positive feedback required to polarize by more than two-fold. The increase is largest when oligomerization is weak (i.e. α is small). Numerical simulations confirm this result for the full kinetic model when oligomerization is faster than exchange. As oligomerization kinetics become slower, the phase boundary shifts upwards in the $J_{feedback}$ vs α plane (2.5). However, the effect of increasing direct binding on polarization persists. Thus direct binding to oligomers opposes polarization driven by indirect positive feedback when the basal oligomerization and exchange kinetics obey detailed balance.

We then considered an alternative scenario in which there is no indirect positive feedback ($f = 0$ in Eq 2.2), but one or more of the basal exchange and oligomerization reactions are driven in a way that breaks detailed balance ($\gamma \neq 1$). This could arise, for example, if phosphorylation of subunits within oligomers increase their affinity for the membrane. In this scenario, spontaneous polarization can occur when $\gamma < 1$ (see Methods: Conditions for Spontaneous Polarization). When $\gamma < 1$, at steady state, there will be a net flux J_{net} of subunits from the cytoplasm into oligomers, from oligomers onto the membrane, and then back into the cytoplasm (Fig. 2.3 C). Defining $J_{feedback} = \frac{J_{net}}{K_M C_{ss}}$ to be the ratio of this net flux to the basal rate of monomers binding to the membrane, and again neglecting diffusion,

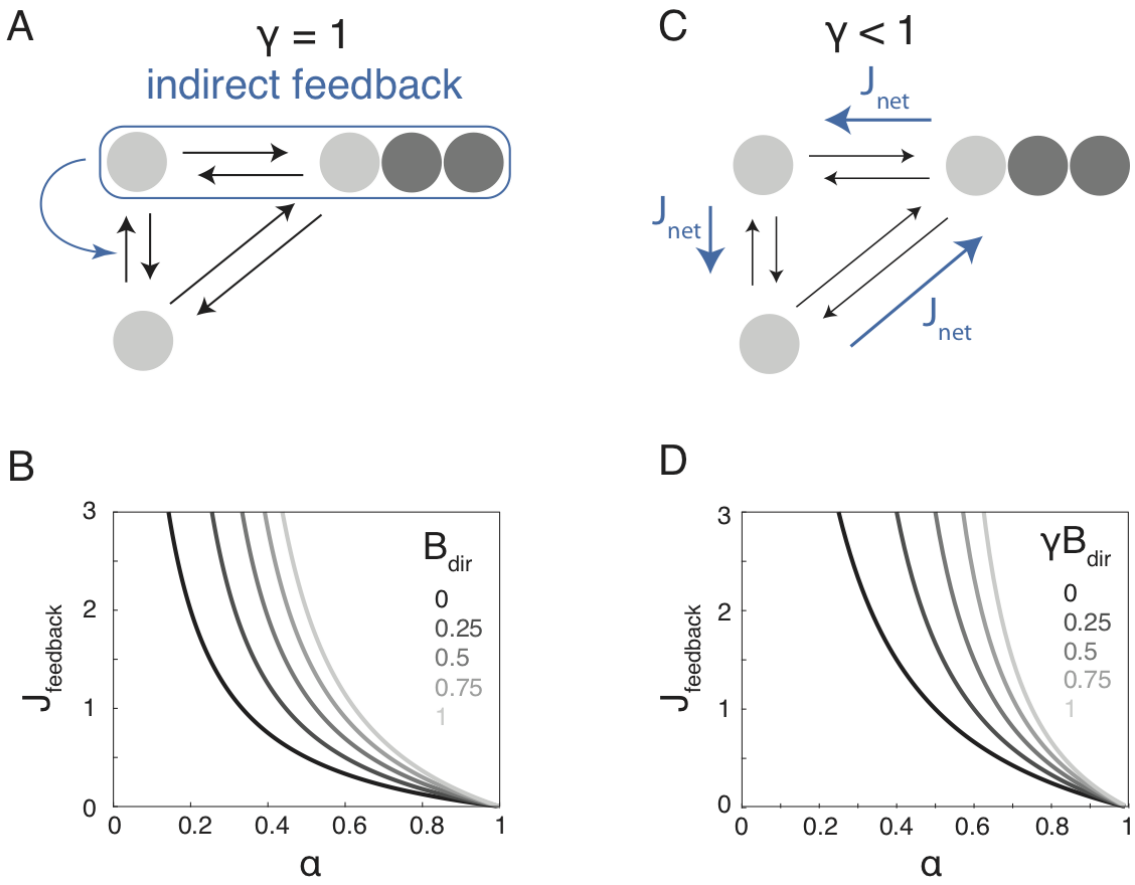

Figure 2.3: **Direct binding of cytoplasmic monomers to membrane-bound oligomers can promote or antagonize polarization.** **(A)** Schematic view of the scenario in which there is indirect feedback on monomer recruitment and detailed balance is enforced for membrane binding and oligomerization $\gamma = 1$. **(B)** Spontaneous symmetry breaking as a function of α or mean oligomer size s and $J_{feedback}$ for different values of B_{dir}, measured at the uniform steady state. The gray scale lines indicate the boundary across which the uniform steady state goes from stable (bottom left) to unstable (top right) for different values of B_{dir}. **(C)** Schematic illustrating the case where there is no indirect positive feedback and the basal kinetics obey $\gamma < 1$. **(D)** Spontaneous symmetry breaking as a function of α or mean oligomer size s and $J_{feedback}$ for different values of γB_{dir}. The dotted line indicates the phase boundary separating regimes in which the uniform steady state is stable (bottom left) and unstable (top right).

the conditions for spontaneous polarization are (see Methods):

$$J_{feedback} > \frac{(1+\gamma B_{dir})(1-\alpha)}{1-(1+\gamma B_{dir})(1-\alpha)} \tag{2.7}$$

Plotting the conditions for spontaneous polarization in the $J_{feedback}$ vs α phase plane for different values of γB_{dir} (Fig. 2.3 D) reveals that, for relatively small mean oligomer sizes, the net flux delivered by breaking detailed balance must only be a small fraction of the basal monomer binding rate to support spontaneous symmetry-breaking (Fig. 2.3 D). Thus when $\gamma < 1$, a net flux of subunits into membrane-bound oligomers constitutes a form of positive feedback. Numerical simulations show that these result hold approximately for the full kinetic model when oligomerization kinetics are sufficiently fast (Fig. 2.5). For slower oligomerization kinetics, and a fixed value of γB_{dir}, there still exists a well-defined phase boundary in the $J_{feedback}$ vs α plane, but it becomes harder to polarize (Fig. 2.5). Altogether, these results show that when $\gamma = 1$, direct binding opposes polarization driven by indirect positive feedback. However, when $\gamma < 1$, direct binding can drive polarization.

2.2.4 Mean oligomer size tunes the speed of polarization and the stability of polarity boundaries

Thus far, we have characterized the conditions in which polarized states can arise through spontaneous or induced symmetry-breaking. To study how oligomerization affects the dynamic evolution of polarized states, we turned to numerical simulations. We again considered a simple model with indirect positive feedback and no direct binding, and we focused on two features of polarization dynamics: the rate at which asymmetries grow during spontaneous or induced symmetry-breaking, and the rate at which the spatial distribution of membrane-bound oligomers evolve towards a final steady state profile.

Simulations confirm that for this system, stably polarized states are characterized by

single-peaked distributions (Fig. 2.4A). For a given choice of parameter values, the time to reach the stably polarized state depends strongly on initial conditions (Fig. 2.5). However, for both spontaneous and induced polarization, the growth of asymmetries proceeds through an intermediate exponential phase (Fig. 2.4B, Fig. 2.5). Although the growth rate depends on the choice of initial conditions, variation in growth rate with model parameters is tightly correlated across different initial conditions (Fig. 2.5). Therefore we used exponential growth rate following a transient local perturbation (3-fold increase in local protein level) of the uniform steady state as a measure of polarization speed.

Polarization speed was weakly sensitive to variation in feedback strength, but strongly sensitive to variation in mean oligomer size. Increasing the mean oligomer size s from 1.5 to 6 produced an order of magnitude decrease in polarization speed (Fig. 2.4C, blue curve; solid line represents mean speed for a given oligomer size; error bars indicate the maximum and minimum values measured for different values of J). The observed decrease in polarization speed is close to the predicted decrease in effective dissociation rate ($\approx \frac{1}{s^2}$ = 16-fold), suggesting that size dependence of oligomer exchange determines how oligomerization shapes polarization speed. Indeed, scaling the monomer off-rate (k^m_{off}) to enforce a size-independent dissociation (at steady state) completely abolished the dependence of polarization speeds on mean oligomer size (Fig. 2.4C, orange curve). In contrast, nullifying size-dependence of diffusivity had no effect on polarization speed (Fig. 2.4C, magenta curve). Therefore, size-dependent oligomer release sets polarization speed for this simple system. Increasing mean oligomer size reduces the need for strong feedback, but at the cost of slowing down polarization.

In some biological contexts (e.g. in *C. elegans* zygotes and certain neuroblast stem cells[109, 112, 113]), a transient response to external cues can induce the rapid enrichment of polarity proteins within a broad spatial domain. Once this cue is gone, the initial distribution will evolve further through diffusion and exchange. For the system considered here, a broad

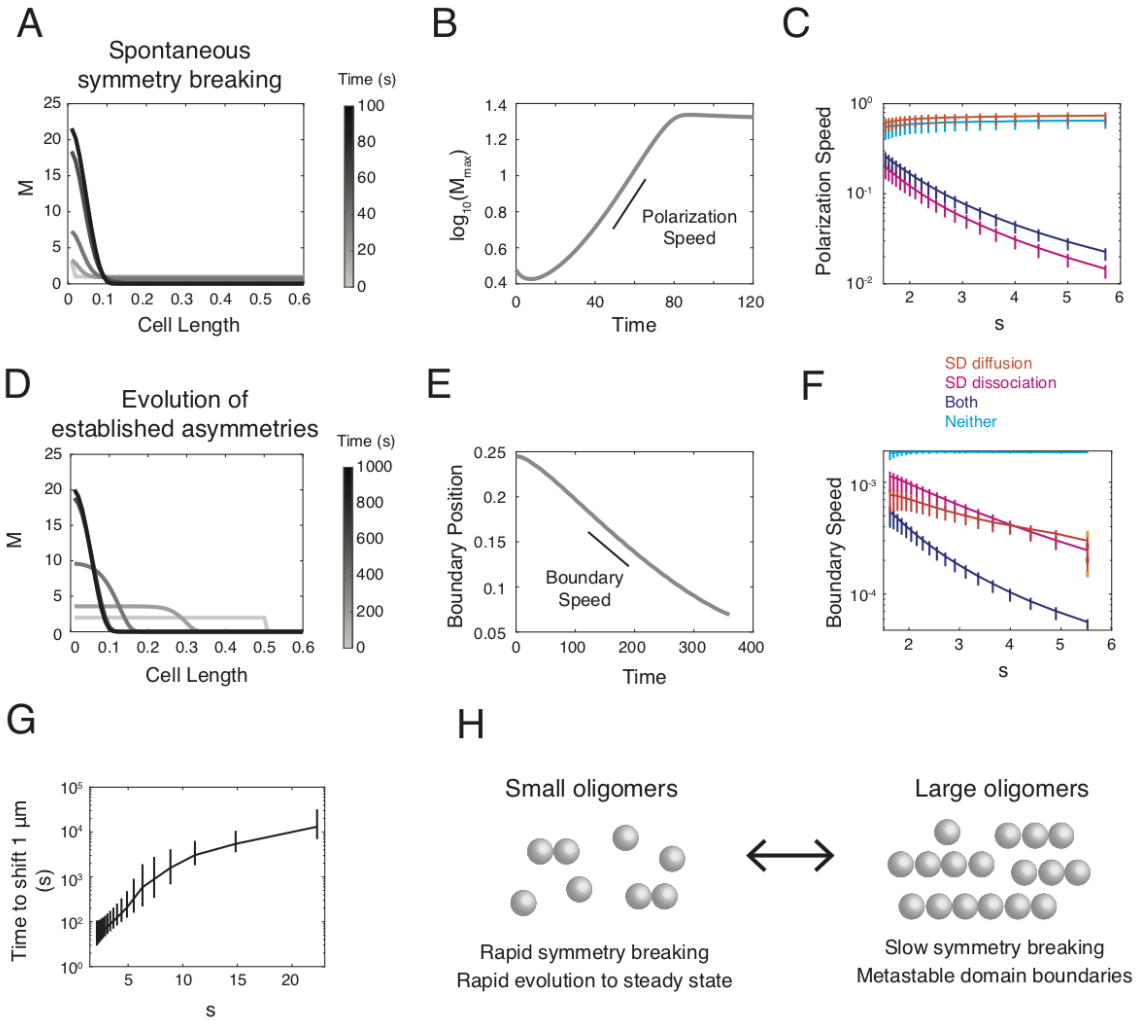

Figure 2.4: **Mean oligomer size tunes polarization dynamics. (A)** Example dynamics of polarization when symmetry-breaking is induced by a local 3-fold increase in membrane protein concentration M in a single point in space. Each line represents the spatial distribution of protein at a different time point **(B)** The logarithm of maximum local value of M over time, showing a region in which M_{max} grows exponentially (polarization speed). **(C)** Polarization speed plotted as a function of mean oligomer size s, given different relationships between oligomer size, effective diffusivity and effective subunit dissociation rates. The bold lines indicate the average of values measured while sampling J between 2 and 10, and the error bars represent the maximum and minimum values. The orange line represents the case where only diffusion is size-dependent, the magenta line represents the case where only the dissociation rate is size dependent, and the dark blue line represents the case where both are size dependent. **(D)** Example of the temporal evolution of a step-change distribution that is stable in the absence of diffusion. **(E)** The boundary position, measured as the inflection point in the spatial profile of the distribution, as a function of time. The position moves at a constant rate (boundary speed). (legend continued on next page)

Figure 2.4: (continued) **(F)** Boundary speed plotted as a function of mean oligomer size s, given different relationships between oligomer size and effective diffusivity and effective dissociation. The bold lines indicate the average of values measured sampling J between 2 and 10 and the error bars represent the maximum and minimum values. Orange line: size-dependent diffusion; Magenta line: size dependent dissociation; Dark blue line: size dependent diffusion and dissociation; Light blue line: no size dependence. **(G)** Plot showing the time it would take for the boundary to shift 1 μm as a function of mean oligomer size s, given $J = 1$, $D = 0.1\ \mu m^2 s^{-1}$, $k^p_{off} = 0.1\ s^{-1}$, and $k^m_{off} = 1\ s^{-1}$. **(H)** Schematic illustrating the trade-offs that emerge from tuning the mean oligomer size.

initial distribution will evolve towards the stably peaked distribution described above (Fig. 2.4D). To determine how oligomerization and feedback shape the timescale on which this occurs, we initialized simulations with broad plateau-shaped distributions that are stable in the absence of diffusion. Then we tracked the position of the domain boundary over time in the presence of diffusion. In all such simulations, the domain boundary position moves at an approximately constant speed towards the stable peaked steady state (Fig. 2.4E). Therefore, we quantified how boundary speed varies with mean oligomer size (Fig. 2.4F). Like polarization speed, boundary speed showed very weak dependence on positive feedback and strong dependence on mean oligomer size, decreasing by more than an order of magnitude as the mean oligomer size increases from 1.5 to 6 (Fig. 2.4F). In this case, the size-dependence of boundary speed depends on multiplicative contributions from size-dependent dissociation and mobility (Fig. 2.4F). Slowing depolymerization kinetics further decreases both polarization and boundary speed (2.5). For typical diffusivities of membrane proteins ($D = 0.1\frac{\mu m^2}{sec}$), and cell sizes ($L = 50\mu m$), a mean oligomer size of 4, and $\frac{k^p_{off}}{k^m_{off}} = 0.1$ a shift in boundary position by 2 percent of cell length would take > 250 times the monomer binding lifetime, and for a mean oligomer size of 20, the same shift would take > 5000 times the monomer lifetime (Fig. 2.4G). Therefore, oligomerization of membrane proteins can allow a cell to effectively stabilize polarized domains of different sizes in response to transient inputs over times much longer than the residence times of individual proteins.

When boundary speed is slow relative to polarization speed, the quasi-stability of a

step-change asymmetry can be assessed in a simpler two-compartment model in which two membrane compartments of varying relative lengths compete for a shared pool of cytoplasmic monomers in the absence of lateral membrane diffusion (see Methods). This analysis shows that when oligomerization and feedback strengths are tuned for spontaneous symmetry breaking (upper right domain in Fig. 2.2D), there is no limit to the size of the domain that a cell can stabilize. When the uniform steady state is stable (but stable polarity can still be induced; lower left domain in Fig. 2.2E), the maximum size of the quasi-stable domain that can be induced depends on both oligomerization and feedback strength and becomes smaller with increasing distance from the phase boundary (Fig. 2.5). Therefore, the ability to stabilize a domain of arbitrary size is only a property of systems in which polarization would occur spontaneously

Together, these findings reveal how size-dependent oligomer dynamics produce an intrinsic trade-off between an ability to polarize rapidly in response to small cues or noisy fluctuations, and the ability to stabilize a domain boundary at an arbitrary position (Fig. 2.4H). Increasing mean oligomer size pushes the system towards slow polarization and stable boundaries.

2.2.5 Saturating feedback slows polarization speed but has weak effects on boundary speed relative to oligomerization

Previous studies show that introducing saturating feedback kinetics into simple mass-balanced reaction diffusion models can lead to slower polarization and slower resolution of multipolar states by competition [27]. To ask how the effects of saturation compare to those that arise through oligomerization, we modified the above model (linear indirect feedback and no direct binding) by introducing a simple form of saturating feedback proportional to $\frac{M}{M+K_{sat}}$ (Fig. 2.5A). Introducing $S = \frac{M_{ss}}{K_{sat}}$ as a simple measure of saturation at the uniform steady state,

the conditions for spontaneous polarization become (see Methods):

$$J_{feedback} > \frac{D^* \frac{1+\alpha}{(1-\alpha)^2} + 1 - \alpha}{\alpha\left(\frac{2+S}{1+S}\right) - \left(\frac{S}{1+S}\right) - D^* \frac{1+\alpha}{(1-\alpha)^2}} \tag{2.8}$$

where $J_{feedback}$ is again the ratio of monomer binding flux due to positive feedback over the basal monomer binding rate, evaluated at the uniform steady state.

Using a combination of local perturbation analysis and simulations, we find that introducing saturation increases the strength of feedback and/or oligomerization required for spontaneous polarization, and reduces the range of parameter values for which polarity can be induced through local perturbation (Fig. 2.5B). Consistent with previous reports [27], both the polarization speed and boundary speed decrease with the strength of saturation (Fig. 2.5C,D). However, while the effect on polarization speed is significant relative to the effects of oligomerization(Fig. 2.5C), the effect on boundary speed is modest(Fig. 2.5D). Thus increasing the degree of saturation makes it more difficult to polarize, both by increasing the strength of feedback and/or oligomerization required to polarize, and by slowing down polarization speed. In contrast, while saturating feedback makes boundaries of established asymmetries slightly more stable, its effects are relatively weak compared to those of increasing mean oligomer size.

2.2.6 The role of oligomerization in shaping polarization dynamics extends to different feedback topologies

Thus far, we considered forms of feedback in which a protein acts locally to promote its own accumulation on the cell membrane. To explore the generality of these results, we considered an alternative model in which two peripheral membrane proteins A and B bind the membrane at constant rates and act locally to promote one another's dissociation at rates that are linear functions of their local densities (Fig. 2.6A). We assume that A forms oligomers while B

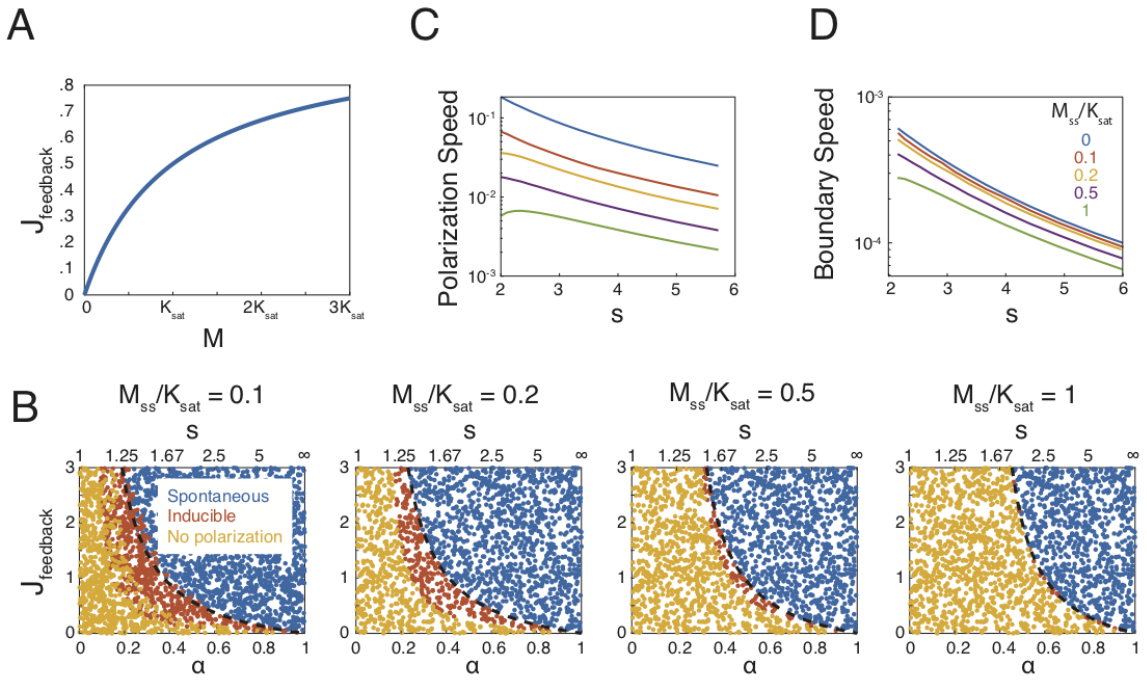

Figure 2.5: **Saturating feedback reduces the potential for polarization and slows polarization speed but has weak effects on boundary speed.(A)** Plot of simple saturating feedback. **(B)** Phase diagrams produced using LPA and showing how regimes with spontaneous, inducible, or no polarity shift with increasing saturation at uniform steady state, measured by $S = \frac{M_{ss}}{K_{sat}}$. **(C,D)** The effect of increasing M relative to the saturation constant on the dynamics of polarization and boundary stability, assessed by numerical simulations. **(C)** Polarization speed plotted as a function of mean oligomer size s, for different values of $S = \frac{M_{ss}}{K_{sat}}$. **(D)** Boundary speed plotted as a function of mean oligomer size s, for different values of $S = \frac{M_{ss}}{K_{sat}}$.

does not, and that only monomers dissociate. Assuming that oligomerization of A is fast relative to exchange, we can write equations for a two-species model:

$$\begin{aligned}
\frac{\partial A}{\partial t} &= k_{on}^{A} C_A - (k_{off}^{A} + k_{BA} B) m_1(A) + D_A \frac{\partial^2 A}{\partial x^2} \\
\frac{\partial B}{\partial t} &= k_{on}^{B} C_B - (k_{off}^{B} + k_{AB} A) B + D_B \frac{\partial^2 B}{\partial x^2} \\
C_A &= A_{tot} - \int_0^L A(x) dx \\
C_B &= B_{tot} - \int_0^L B(x) dx
\end{aligned} \tag{2.9}$$

Considering a limiting form of this model in which diffusion is slow and B monomers dissociate far more rapidly than A monomers, we find that spontaneous polarization occurs when:

$$J_{feedback} = \left(\frac{J_A}{1 + J_A} \right) \left(\frac{J_B}{1 + J_B} \right) > \frac{1 - \alpha}{1 + \alpha} \tag{2.10}$$

where J_A and J_B are the ratios of feedback-dependent to basal dissociation rates for A and B respectively. Plotting $J_{feedback}$ vs α (Fig. 2.6B) shows that as for models with positive feedback on local recruitment, combinations of relatively weak oligomerization and feedback are sufficient for spontaneous polarization. For example, when the mean oligomer size is 2.5, mutual inhibition must only double the dissociation rates of A and B for polarization to occur. Local perturbation analysis reveals that even when polarization does not occur spontaneously, it can be induced by sufficiently large local perturbations for a broader range of $J_{feedback}$ and α values (Fig. 2.6C). Finally, as for models with positive feedback on recruitment, the polarization speed and the boundary shift speed decrease as a function of mean oligomer size (Fig. 2.6D). Thus, oligomerization enables polarization and shapes polarization dynamics in very similar ways for networks with very different feedback topologies.

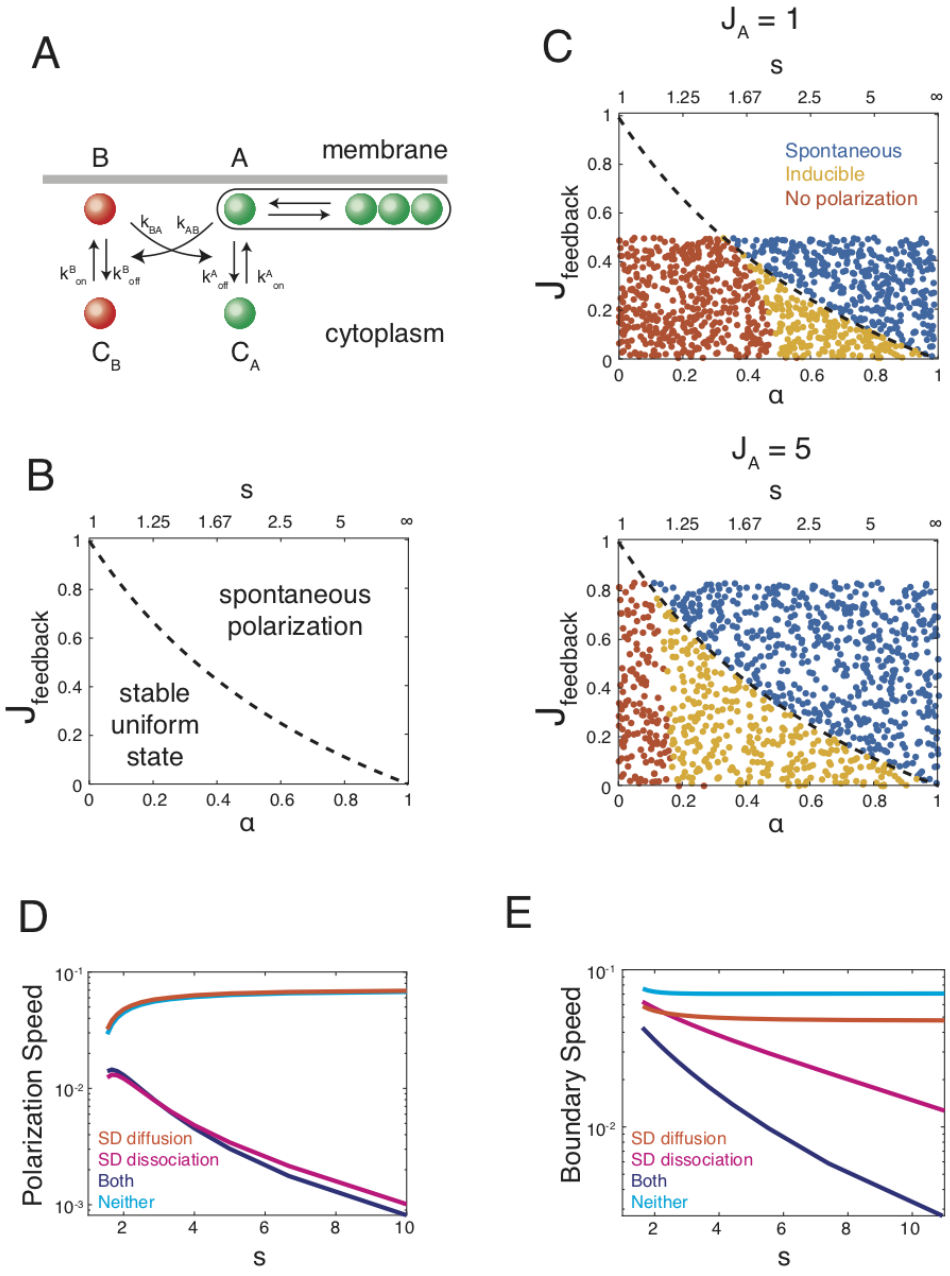

Figure 2.6: **Oligomerization promotes polarization and slows polarization dynamics when combined with mutual antagonism. (A)**Reaction diagram showing mutually antagonistic effects between two membrane-binding proteins. **(B)** Analytical solution for the boundary between unstable and stable uniform states in phase space determined by α and $J_{feedback} = \frac{J_A}{1+J_A}\frac{J_P}{1+J_B}$. **(C)** The potential for polarization, as assessed by LPA, plotted in terms of α or s and $J_{feedback}$ for $J_A = 1$ (top) and $J_A = 5$ (bottom). Blue indicating spontaneous polarization, yellow indicating inducible polarization, and orange indicating no polarization. (legend continued on next page)

Figure 2.6: (continued) **(D)** Polarization speed plotted as a function of mean oligomer size S, given different relationships between oligomer size and effective diffusivity and effective dissociation. The orange line represents the case where only diffusion is size-dependent, the magenta line represents the case where only the dissociation rate is size dependent, and the dark blue line represents the case where both are size dependent. **(E)** Boundary speed plotted as a function of mean oligomer size S for $J_{feedback} = 0.64$, given different relationships between oligomer size and effective diffusivity and effective dissociation. Orange line: size-dependent diffusion only; Magenta line: size dependent dissociation only; Dark blue line: size dependent diffusion and dissociation; Light blue line: no size dependence.

2.3 Discussion

The ability to self-oligomerize is common to many peripheral membrane proteins that adopt asymmetric distributions in polarized cells. Here we have explored how this ability shapes the performance of simple feedback circuits that underlie cell polarization. We focused on two properties that emerge as natural consequences of oligomerization – size-dependent membrane binding avidity [86, 34] and size-dependent mobility [124]. We find that both properties sharply enhance the ability of simple circuits to form and stabilize cell surface polarity. Both also contribute to controlling the rate at which asymmetries grow spontaneously or in response to local cues and the rate at which they evolve towards stably polarized states. Overall, our results reveal how strength of oligomerization, which determines mean oligomer size, can act as a physiological control parameter that determines if, when and how fast polarization can occur.

Oligomerization promotes symmetry breaking through positive feedback and by reducing the dissipative effect of diffusion.

Cell surface asymmetries are formed and maintained by the local differences in the relative rates of binding and unbinding [55] working against the dissipative effects of diffusion. Theoretical studies have established that both spontaneous emergence and maintenance of stable asymmetries require nonlinear positive feedback on accumulation [90, 47, 27]. For

peripheral membrane proteins, this can involve either increased binding rates, or decreased unbinding rates, with increasing density. To amplify local asymmetries around a spatially uniform steady state, the net rate of accumulation must increase with cell surface density at the steady state (see Eq. 2.3, [47, 27]). For a typical protein that binds the membrane with zero-order (density-independent) kinetics and unbinds with first order (linear in density) kinetics, this implies that the combination of positive feedback on binding and detachment must contribute stronger than linear dependence of net accumulation rate on density, to amplify local asymmetries.

Here, we find that size dependent membrane binding avidity endows oligomers generically with a form of positive feedback in which the effective dissociation rate constant decreases with increasing density. This form of feedback is insufficient, on its own, to drive spontaneous symmetry-breaking. However, it strongly reduces the amount of additional positive feedback required to break symmetry to an extent that increases with increasing oligomer size. Even for weak oligomerization, characterized by a mean oligomer size of 2.5, positive feedback on monomer binding (resp. unbinding) need only deliver an approximately 50% increase (resp. decrease) over basal rates to drive symmetry breaking. As a simple comparison, achieving the same result (with the same feedback strength) with cooperative positive feedback on monomer recruitment would require greater than fourth order dependence (Fig. 2.5).

We also find that the size-dependent decrease in oligomer mobility can sharply reduce the dissipative effects of diffusion which would otherwise degrade the potential for symmetry-breaking. This effect would be weak for the weak size-dependence of proteins observed in pure membranes. However, interactions with a submembrane cytoskeleton can lead to much sharper size dependence, and thus much sharper reduction in mobility. Moreover, the magnitude of this effect will increase with the strength of oligomerization. Thus oligomerization of peripheral membrane proteins provides a tunable form of feedback, and tunable control of protein mobility that can greatly enhance the potential for symmetry breaking and po-

larization. Importantly, the strength of this effect can be readily controlled by modulating the equilibrium binding constant for self-association, e.g through phosphorylation.

Direct binding of cytoplasmic monomers to oligomers can either inhibit or drive polarization.

For proteins that can bind membranes and self-oligomerize, there are two paths by which a cytoplasmic monomer can join membrane-bound oligomers – either indirectly by first binding the membrane and then diffusing into contact with an oligomer, or by direct binding to the oligomer. Classical studies [13, 102] have characterized the relative contributions of these two binding modes to protein absorption on membranes [102] or to ligand binding and uptake [13].

Here we characterized the relative contributions of direct and indirect binding modes to polarization. We find that the contribution of direct binding depends on whether or not the basal membrane binding and oligomerization kinetics obey detailed balance (i.e. whether or not they consume energy). When detailed balance is satisfied and polarization is driven by positive feedback on monomer binding to the membrane, direct binding to oligomers reduces the potential for polarization. However, another unanticipated mode of feedback emerges when detailed balance is broken in a way that favors a steady state flux of monomers from the cytoplasm into oligomers. This could occur in many ways. For example, oligomers could recruit an enzyme that locally modifies monomers or phospholipids to promote association between monomers and the cell membrane. Regardless of how it arises, net flux from cytoplasm into oligomers at steady state is a form of positive feedback because its magnitude increases with overall density of membrane-bound subunits. As with other forms of feedback, we find that the potential for polarization increases with feedback strength (measured as the ratio of the net flux from cytoplasm into oligomers (J_{net}) over basal monomer binding rate), and increasing oligomerization strength reduces the amount of

additional feedback required for polarization. However, in this case, increasing direct binding increases feedback strength because it increases (J_{net}).

Our results therefore highlight two general modes of positive feedback on recruitment that could drive symmetry breaking and polarization: One relies on increasing the effective number of membrane binding sites for cytoplasmic monomers; the other relies on breaking detailed balance to favor a net flux into oligomers. Because binding to the cell surface is a diffusion limited process, the relative densities of membrane binding sites and oligomers will determine which of these two modes are more effective drivers of cell polarity.

Oligomerization provides tunable control over the speed and mode of polarization.

Our results also reveal how oligomerization allows tunable control over the speed of polarization. Weak oligomerization favors rapid growth of asymmetries and a rapid approach to a steady state in which the position of polarity boundaries are dictated by binding/unbinding kinetics and diffusivities intrinsic to the polarity circuit through mechanisms such as wave-pinning [105]. Stronger oligomerization reduces the rate at which local asymmetries grow, and the rate at which they approach steady state. This allows external cues that promote local binding [98, 96, 54, 122] or unbinding [107] of polarity factors, or their rapid transport by actomyosin flows [109, 112, 113] to impose spatial asymmetry patterns that are then maintained as quasi-stable states over much longer timescales, and which are no longer dictated by the internal reaction/diffusion kinetics of the polarity circuit. While increasing oligomerization strength to maintain asymmetries far from steady state will also necessarily decrease the rate at which asymmetries grow, this can be readily overcome through the rapid control of local binding/unbinding or transport by external inputs. Thus, modulating the strength of oligomerization can allow tunable control, across different cells or within the same cell over time, over the relative extents to which circuit-specific reaction diffusion dynamics and

external inputs determine the spatial distributions of polarity proteins.

Homo-oligomerization as a versatile source of nonlinear feedback and tunable mobility for cell polarity.

The ability to self-oligomerize is common to a large fraction of peripheral membrane proteins. By recent estimates, something like 50% of cytoplasmic and membrane proteins form homo-oligomers [46, 87], although the majority of these form homo-oligomers of fixed size. This abundance is thought to be driven at least in part by the ease with which homodimeric interfaces can arise through random mutation and through selection for the many functional advantages (unrelated to polarization) conferred by homo-oligomerization [46, 92], and also through entrenchment of randomly occurring, selective neutral mutations [61]. Therefore, the frequent presence of oligomeric proteins in polarity circuits may be the result from exaptation of a frequently occurring property of proteins for an essential function in polarization. Importantly, because the generic form of nonlinear positive feedback and tunable control of mobility conferred by oligomerization do not depend on polarity circuit architecture, or other modes of feedback, the barrier to exaptation is low.

2.4 Methods

Mathematical Model

We consider a simple 2D "cell" consisting of a 1D membrane of length L adjacent to a cytoplasmic compartment with height H and area A = HL. Without loss of generality, we assume $H = L$. We assume that monomers bind reversibly to the membrane from a single well-mixed cytoplasmic pool with rate constants (k^m_{on}, k^m_{off}), and they self-associate at the membrane with rate constants (k^p_{on}, k^p_{off}) to form simple linear oligomers. In addition, cytoplasmic monomers can bind directly and reversibly with rate constants (k^c_{on}, k^c_{off}) to monomers or

the ends of membrane-bound oligomers. We assume that there is simple positive feedback on monomer recruitment, proportional to the total density of oligomer subunits at the membrane. Finally, we assume that oligomers dissociate from the membrane at a rate that decreases with oligomer size. We assume initially that oligomers with size > 2 are stably bound.

Letting:

$m_n(x)$	be the concentration of oligomers of size i,
$N(x)$	be the total density of oligomers at the membrane,
$M(x)$	be the total density of oligomer subunits at the membrane
C	be the total concentration of cytoplasmic subunits,
M_{tot}	be the total number of all oligomer subunits

we write the following system of equations

$$\begin{aligned}
\frac{\partial C}{\partial t} &= (k_{on}^m + k_f M + k_{on}^c N)C - k_{off}^m m_1 - k_{off}^c (N - m_1) \\
\frac{\partial m_1}{\partial t} &= D_1 \frac{\partial^2 m_1}{\partial x^2} + (k_{on}^m + k_f M)C - k_{off}^m m_1 \\
&\quad - k_{ass} m_1 + k_{diss} m_2 - k_{on}^p m_1 N + k_{off}^p (N - m_1) \\
\frac{\partial m_n}{\partial t} &= D_n \frac{\partial^2 m_n}{\partial x^2} + k_{ass} m_{n-1} - k_{ass} m_n - k_{diss} m_n + k_{diss} m_{n+1}, \quad n > 1
\end{aligned}$$

where $k_{ass} = k_{on}^p m_1 + k_{on}^c C, k_{diss} = k_{off}^p + k_{off}^c$. Note that these equations are not independent, given the conservation of total subunits:

$$M_{tot} = CA + \int_0^L M(x)dx$$

Steady state analysis

Setting time and space derivatives to 0 in Eq 2.11 , we obtain:

$$
\begin{aligned}
0 &= (k_{on}^m + k_f M + k_{on}^c N)C - k_{off}^m m_1 - k_{off}^c (N - m_1) \\
0 &= (k_{on}^m + k_f M)C - k_{off}^m m_1 - k_{ass} m_1 + k_{diss} m_2 - k_{on}^p m_1 N + k_{off}^p (N - m_1) \\
0 &= k_{ass} m_{n-1} - k_{diss} m_n - k_{ass} m_n + k_{diss} m_{n+1},\ n = 2, 3, ...
\end{aligned}
$$

The bottom equations imply:

$$
k_{ass} m_n - k_{diss} m_{n+1} = k_{ass} m_{n+1} - k_{diss} m_{n+2} = K,\ n = 1, 2, ...
$$

Combining the top two equations yields:

$$
0 = k_{ass} m_1 - k_{diss} m_2 + \sum_{n=1}^{\infty} (k_{ass} m_n - k_{diss} m_{n+1}) = \sum_{n=0}^{\infty} K
$$

It follows that K must be identically 0, and at any uniform steady state, we must have

$$
\begin{aligned}
m_{i+1} &= \alpha m_i,\ i = 1, 2, ..., \\
\alpha &= \frac{k_{ass}}{k_{diss}} = \frac{k_{on}^p m_1 + k_{on}^c C}{k_{off}^p + k_{off}^c}
\end{aligned}
\tag{2.11}
$$

Summing $N = m_1 \sum_{i=0}^{\infty} \alpha^i$ and $M = m_1 \sum_{i=0}^{\infty} i\alpha^i$ yields the following simple identities relating m_1, N, M and α that we use below:

$$
N = \frac{m_1}{1 - \alpha}, \quad M = \frac{N}{1 - \alpha} = \frac{m_1}{(1 - \alpha)^2} \tag{2.12}
$$

Enforcing detailed balance for basal binding kinetics

If basal membrane binding and oligomerization reactions satisfy detailed balance, then the free energy change associated with incorporating a cytoplasmic monomer into a membrane-bound oligomer is path-independent:

$$-\log\left(K_M\right)RT - \log\left(K_P\right)RT = -\log\left(K_C\right)RT$$

where

$$K_m = \frac{k_{on}^m}{k_{off}^m}, \quad K_c = \frac{k_{on}^c}{k_{off}^c}, \quad K_p = \frac{k_{on}^p}{k_{off}^p}$$

and therefore detailed balance is satisfied when:

$$\gamma = \frac{K_M K_P}{K_C} = 1,$$

Reducing to a simple one species model

We start by rewriting:

$$\alpha = \frac{K_p m_1 (k_{off}^p + \frac{K_C C}{K_p m_1} k_{off}^c)}{k_{off}^p + k_{off}^c} \tag{2.13}$$

If oligomerization kinetics are sufficiently fast, i.e if they satisfy:

$$k_{off}^p \gg max\left(k_{off}^m, k_{off}^c, \frac{K_C C}{K_P m_1} k_{off}^c\right) \tag{2.14}$$

Then $\alpha \approx K_p m_1$, and we can invoke a quasi-steady state assumption to write the single equation for M:

$$\frac{\partial M}{\partial t} = D_M \frac{\partial^2 M}{\partial x^2} + (k_{on}^m + k_{on}^c N(M) + k_f M)C - k_{off}^m m_1(M) - k_{off}^c (N(M) - m_1(M)) \tag{2.15}$$

$$M_{tot} = CA + \int_0^L M(x)dx$$

where

$$N(M) = M(1 - K_P m_1), \quad m_1(M) = \frac{1 + 2MK_P - \sqrt{1 + 4MK_P}}{2MK_P^2},$$

and where D_M represents the average subunit diffusivity, reflecting the dependence of oligomer mobility on oligomer size.

Rearranging terms and using $N - m_1 = K_P m_1 N$:

$$\frac{\partial M}{\partial t} = k_{off}^m \left[\frac{D_M}{k_{off}^m} \frac{\partial^2 M}{\partial x^2} + \frac{k_{on}^m}{k_{off}^m} \left(1 + \frac{k_{on}^c}{k_{on}^m} N + \frac{k_f}{k_{on}^m} M \right) C - m_1 \left(1 + \frac{k_{off}^c}{k_{off}^m} K_P N \right) \right] \tag{2.16}$$

Choosing units of time $\tau = \frac{1}{k_{off}^m}$, length $l = L$ and membrane density ρ we obtain:

$$\begin{gathered} \frac{dM}{dt} = D \frac{\partial^2 M}{\partial x^2} + K \left(1 + BN + fM\right) C - m_1 (1 + \gamma BN) \\ C_{tot} = C + \int_0^1 M(x)dx \end{gathered} \tag{2.17}$$

where:

$$D = \frac{D_M}{k_{off}^m L^2}, \; K = \frac{k_{on}^m}{L k_{off}^m}, \; B = \frac{k_{on}^c}{k_{on}^m}, \; f = \frac{k_f}{k_{on}^m}, \; \gamma = \frac{K_p K_m}{K_c}, \text{ and } C_{tot} = \frac{M_{tot}}{L}$$

General conditions for spontaneous polarization

Eq 2.17 has the general form:

$$\frac{dM}{dt} = D\frac{\partial^2 M}{\partial x^2} + F(M)\left(C_{tot} - \int_0^1 M(x)dx\right) - G(M) \tag{2.18}$$

where $F(M)$ and $G(M)$ define membrane binding and unbinding kinetics, respectively, as a function of M. Spatially uniform steady state solutions of the form $M(x) = M_{ss}$ must satisfy:

$$0 = F(M_{ss})\left(C_{tot} - M_{ss}\right) - G(M_{ss}) \tag{2.19}$$

We consider stability with respect to small perturbations of the form:

$$M(x) = M_{ss} + \Delta(x) \tag{2.20}$$

Any such perturbation can be written as $\Delta(x) = \bar{M} + v(x)$, where $\bar{M}$ is a spatially uniform perturbation and $v(x)$ is a spatially varying perturbation satisfying

$$\int_0^1 v(x)dx = 0$$

Combining Eqs 2.18 and 2.19:

$$\frac{\partial M}{\partial t} = \frac{\partial \Delta}{\partial t} = D\frac{\partial^2 \Delta}{\partial x^2} + F\left(M_{ss} + \Delta\right)\left(C_{tot} - \int_0^1 (M_{ss} + \Delta)dx\right) - G(M_{ss} + \Delta) \tag{2.21}$$

Using a Taylor's series expansion, we obtain:

$$\frac{\partial \Delta}{\partial t} = D\frac{\partial^2 v}{\partial x^2} + \left(F(M_{ss}) + \frac{\partial F}{\partial m}(M_{ss})\Delta + o(\Delta^2)\right)\left(C_{tot} - M_{ss} - \bar{M}\right) \\ -G(M_{ss}) - \frac{\partial G}{\partial m}(M_{ss})\Delta + o(\Delta^2) \tag{2.22}$$

Neglecting higher order terms and using

$$\Delta(x) = \bar{M} + v(x) \text{ and } C_{ss} = C_{tot} - M_{ss} = \frac{G(M_{ss})}{F(M_{ss}}$$

we have:

$$\frac{\partial \Delta}{\partial t} = D \ + \alpha\bar{M} + \beta v \tag{2.23}$$

where:

$$\alpha = \left(\frac{\partial F}{\partial m}\frac{G}{F} - F - \frac{\partial G}{\partial m}\right)_{M=M_{ss}} \text{ and } \quad \beta = \left(\frac{\partial F}{\partial m}\frac{G}{F} - \frac{\partial G}{\partial m}\right)_{M=M_{ss}} \tag{2.24}$$

The general solution to Eq 2.23 can be written:

$$\Delta(x,t) = M(t) + v(x,t) = M_0 e^{\alpha t} + \sum_{n=1}^{\infty} a_n e^{\beta - k^2 D} cos(kx), \ k = 2\pi n \tag{2.25}$$

For any small perturbation $\Delta(x,0) = M_0 + \sum_{n=1}^{\infty} a_n cos(kx)$, the spatially uniform part, $M(t) = M_0 e^{\alpha t}$, decays over time if $\alpha < 0$, whereas the spatial differences

$$v(x,t) = \sum_{n=1}^{\infty} \alpha_n e^{\beta - k^2 D} cos(kx) \tag{2.26}$$

can grow only if $\beta > k^2 D$ for some $n \geq 1$. Therefore, the conditions for spontaneous polarization are:

$$\left(\frac{\partial F}{\partial m}\frac{G}{F} - \frac{\partial G}{\partial m}\right)_{M=M_{ss}} > D^*, \quad \text{where} \quad D^* = 4D\pi^2 \tag{2.27}$$

Conditions for inducible polarization

We used Local Perturbation Analysis (LPA) to evaluate coexistence of stable spatially uniform and polarized steady states. Briefly, we consider the dynamic response to a finite-amplitude perturbation from a stable spatially uniform steady state $M = M_{ss}$ within an infinitesimally small spatial domain. We assume that diffusion is sufficiently slow ($D_M \approx 0$) that local changes within this domain do not affect the bulk pools of membrane-bound or cytoplasmic protein. The equation for the local response M_l then writes:

$$\frac{dM_l}{dt} = F(M_l) * C_{ss} - G(M_l) \tag{2.28}$$

where

$$C_{ss} = \frac{G(M_{ss})}{F(M_{ss})}$$

Eq 2.28 has a fixed point at $M_l = M_{ss}$ corresponding to the spatially uniform steady state. When $D_M = 0$, spontaneous polarization occurs when this fixed point is unstable, i.e when:

$$\left(\frac{\partial F}{\partial M_l}\frac{G}{F} - \frac{\partial G}{\partial M_l}\right)_{M_l = M_{ss}} > 0$$

consistent with the result from linear stability analysis when $D_M = 0$.

If the fixed point at $M_l = M_{ss}$ is stable, then a stably polarized steady state exists when Eq 2.28 has an unstable steady state at $M_l = M_{th}$, for $M_{th} > M_{ss}$. M_{th} then defines the threshold size of a perturbation required to induce a transition to the polarized steady state (neglecting diffusion).

In practice, we used MATLAB to identify a point $M_l = M_{th} > M_{ss}$ where:

$$\frac{dM_l}{dt} = F(M_{th}) * C_{ss} - G(M_{th}) = 0$$

within the range:

$$M_{ss} \leq M_l \leq M_{ss} * 1000$$

and we assessed its stability by determining the sign of:

$$\left(\frac{\partial F}{\partial M_l} * C_{ss} - \frac{\partial G}{\partial M_l}\right)_{M_l=M_{th}}$$

Specific conditions for spontaneous polarization

Case 1: Indirect positive feedback; basal kinetics satisfy detailed balance.

If basal kinetics satisfy detailed balance, then $\gamma = 1$,

$$F(M) = K(1 + fM + BN), \quad G(M) = m_1(1 + BN), \tag{2.29}$$

and the uniform steady state is unstable when

$$\left(\frac{m_1(1+BN)}{1+fM+BN}\right)\left(f + B\frac{\partial N}{\partial M}\right) - \left(\frac{\partial m_1}{\partial M}(1+BN) + \frac{\partial N}{\partial M}Bm_1\right) > D^* \tag{2.30}$$

where m_1, N and M are evaluated at the uniform steady state.

Using:

$$\frac{\partial m_1}{\partial M} = \frac{m_1}{M}\left(\frac{1-\alpha}{1+\alpha}\right), \quad \frac{\partial N}{\partial M} = \frac{\partial m_1}{\partial M}\frac{M}{m_1} = \frac{1-\alpha}{1+\alpha}, \quad \frac{m_1}{M} = (1-\alpha)^2 \tag{2.31}$$

gives:

$$\frac{\frac{m_1}{M}\left(fM(1+BN) - \frac{1-\alpha}{1+\alpha}\left(fM(1+BN+\frac{BN}{1-\alpha}) + (1+BN)^2\right)\right)}{1+fM+BN} > D^* \tag{2.32}$$

Introducing $J_{feedback} = fM$, and $B_{dir} = BN$, this becomes:

$$\begin{aligned} J_{feedback}(1+B_{dir}) - \left(\frac{1-\alpha}{1+\alpha}\right)\left(J_{feedback}\left(1+B_{dir}+\frac{B_{dir}}{1-\alpha}\right)+(1+B_{dir})^2\right) \\ > D^* \frac{1+J_{feedback}+B_{dir}}{(1-\alpha)^2} \end{aligned} \tag{2.33}$$

Solving for $J_{feedback}$ yields conditions for spontaneous polarization:

$$\begin{aligned} J > \frac{D^*(1+B_{dir})\frac{1+\alpha}{(1-\alpha)^2} + (1-\alpha)(1+B_{dir})^2}{2\alpha(1+B_{dir}) - B_{dir} - D^*\frac{1+\alpha}{(1-\alpha)^2}} \\ 2\alpha(1+B_{dir}) - B_{dir} - D^*\frac{1+\alpha}{(1-\alpha)^2} > 0 \end{aligned} \tag{2.34}$$

The simpler conditions cited in the main text follow directly from setting $D^* = 0$ and/or $B_{dir} = 0$ in Eq 2.34

Case 2: No indirect positive feedback; detailed balance not satisfied

Assume now that there is no positive feedback ($f = 0$) and that detailed balance is not satisfied ($\gamma \neq 1$):

$$F(M) = K(1+BN), \quad G(M) = m_1(1+\gamma BN) \tag{2.35}$$

The uniform steady state is unstable when

$$\frac{m_1(1+\gamma\beta N)}{1+BN}\left(B\frac{\partial N}{\partial M}\right) - \left(\frac{\partial m_1}{\partial M}(1+\gamma\beta N) + \frac{\partial N}{\partial M}\gamma B m_1\right) > D^* \tag{2.36}$$

Using

$$\frac{\partial N}{\partial M} = \frac{\partial m_1}{\partial M}\frac{M}{m_1}, \ \frac{\partial m_1}{\partial M} = \frac{(1-\alpha)^3}{1+\alpha}, \ \text{ and } M = \frac{N}{1-\alpha}$$

and simplifying yields:

$$\frac{(1-\gamma)BN-(1+\gamma\beta N)(1-\alpha)(1+BN)}{1+BN} > \frac{1+\alpha}{(1-\alpha)^2}D^* \tag{2.37}$$

Note that this inequality can only be satisfied if $\gamma < 1$. Thus detailed balance must be broken in a particular direction for spontaneous symmetry breaking to occur.

To simplify this inequality, we consider the net flux of monomers from the cytoplasm to membrane oligomers (or from the membrane back to the cytoplasm) at steady state. From eq 2.17, we have:

$$J_{net} = BN(KC - \gamma m_1) = m_1 - KC \tag{2.38}$$

Eliminating KC and solving for J_{net} yields:

$$J_{net} = \frac{m_1(1-\gamma)BN}{(1+BN)} \tag{2.39}$$

or

$$(1-\gamma)BN = \frac{(1+BN)J_{net}}{m_1} \tag{2.40}$$

Using $J_{net} = m_1 - KC$ and introducing $J_{feedback} = \frac{J_{net}}{KC}$, this becomes:

$$(1-\gamma)BN = (1+BN)\frac{J_{feedback}}{J_{feedback}+1} \tag{2.41}$$

Substituting 2.41 into 2.37, and using $B_{dir} = BN$ gives:

$$\frac{J_{feedback}}{1+J_{feedback}} - (1+\gamma B_{dir})(1-\alpha) > \frac{1+\alpha}{(1-\alpha)^2}D^* \tag{2.42}$$

Solving for J_{ratio} yields the final result:

$$J_{feedback} > \frac{\frac{1+\alpha}{(1-\alpha)^2}D^* + (1+\gamma B_{dir})(1-\alpha)}{1-(1+\gamma B_{dir})(1-\alpha) - \frac{1+\alpha}{(1-\alpha)^2}D^*} \tag{2.43}$$

When $D^* = 0$, this reduces to the simpler form:

$$J_{ratio} > \frac{(1+\gamma B_{dir})(1-\alpha)}{1-(1+\gamma B_{dir})(1-\alpha)} \tag{2.44}$$

Case 3: Saturating feedback and no direct binding

We now consider a model in which there is no direct binding and positive indirect feedback on M recruitment is governed by a saturating function of the form:

$$H(f, K_{sat}, M) = \frac{fM}{K_{sat} + M} \tag{2.45}$$

With these assumptions, we have:

$$F(M) = K\left(1 + H(f, K_{sat}, M)\right), \quad G(M) = m_1(M) \tag{2.46}$$

Thus the conditions for spontaneous polarization are:

$$\left(\frac{\frac{\partial H}{\partial M}m_1}{1+H} - \frac{\partial m_1}{\partial M}\right)_{M=M_{ss}} > D^* \tag{2.47}$$

One can readily verify that::

$$\frac{\partial H}{\partial M} = \frac{fK_{sat}}{(K_{sat}+M)^2} = \frac{K_{sat}}{K_{sat}+M}\frac{H}{M}$$

Using

$$\frac{m_1}{M} = (1-\alpha)^2$$

and introducing:

$$S = \frac{M_{sat}}{K_{sat}}, \quad J_{feedback} = H(M_{ss})$$

we have:

$$\left(\frac{1}{1+S}\right)\left(\frac{J_{feedback}}{1+J_{feedback}}\right) > \frac{D^*}{(1-\alpha)^2} + \frac{1-\alpha}{1+\alpha}$$

Finally, solving the inequality for $J_{feedback}$, we find that spontaneous polarization occurs when:

$$J_{feedback} > \frac{D^*\frac{1+\alpha}{(1-\alpha)^2} + 1 - \alpha}{\alpha\left(\frac{2+S}{1+S}\right) - \left(\frac{S}{1+S}\right) - D^*\frac{1+\alpha}{(1-\alpha)^2}} \tag{2.48}$$

Case 4: Feedback through cross-inhibition

We consider a model in which two distinct proteins A and B bind reversibly to the membrane from well-mixed cytoplasmic pools. We assume that A, but not B, oligomerizes at the membrane, and that cytoplasmic monomers of A do not bind directly to membrane-bound oligomers. We assume that A and B monomers bind to the membrane at constant rates, and that A promotes the dissociation of the B monomers, and B promotes the dissociation of A monomers, in each case at rates proportional to the total density of membrane bound protein. Assuming that oligomerization of A is much faster than exchange, and invoking a quasi steady state approximation described above, we can write:

$$\begin{aligned}
\frac{\partial A}{\partial t} &= k_{on}^A C_A - (k_{off}^A + k_{BA}B)m_1(A) + D_A\frac{\partial^2 A}{\partial x^2} \\
\frac{\partial B}{\partial t} &= k_{on}^B C_B - (k_{off}^B + k_{AB}A)B + D_B\frac{\partial^2 B}{\partial x^2} \\
C_A &= A_{tot} - \int_0^L A(x)dx \\
C_B &= B_{tot} - \int_0^L B(x)dx
\end{aligned} \tag{2.49}$$

Where k_{AB} and k_{BA} are cross-inhibition rates and:

$$m_1(A) = \frac{1 + 2AK_P^A - \sqrt{1 + 4AK_P^A}}{2A\left(K_P^A\right)^2}$$

One can verify that this system of equations has a single spatially uniform steady state. Assuming that diffusion of A and B is negligible, we can determine the conditions for spontaneous symmetry breaking by considering the dynamic response of A and B to a local perturbation to this steady state within an infinitesimally small domain. The time evolution of local densities of A and B are then given by:

$$\begin{aligned} \frac{dA_L}{dt} &= k_{on}^A C_{SS}^A - (k_{off}^A + k_{BA}B_L)m_1(A_L) \\ \frac{dB_L}{dt} &= k_{on}^B C_{SS}^B - (k_{off}^B + k_{AB}A_L)B_L \end{aligned} \tag{2.50}$$

Assuming that the membrane-binding dynamics of B are much faster than those of A and making a quasi-steady state approximation for B_L:

$$B_L \approx \frac{k_{on}^B C_{ss}^B}{k_{off}^B + k_{AB}A_L}$$

we obtain:

$$\frac{dA_L}{dt} = k_{on}^A C_{SS}^A - \left(k_{off}^A + \frac{k_{BA}k_{on}^B C_{ss}^B}{k_{off}^B + k_{AB}A_L}\right) m_1(A_L) = F(A_L) \tag{2.51}$$

Eq 2.51 has a steady state at $A_L = A_{ss}$. If diffusion is infinitely slow and membrane dynamics of B are infinitely fast, a small perturbation to the steady state in equations 2.49 will grow iff this steady state is unstable:

$$\left(\frac{dF(A_L)}{dA_L}\right)_{A_L = A_{ss}} > 0 \tag{2.52}$$

Thus we have:

$$\left(\frac{k_{AB}k_{BA}k_{on}^{B}C_{ss}^{B}}{(k_{off}^{B}+A_{ss}k_{AB})^{2}}\right)m_{1}\left(A_{ss}\right)-\frac{dm_{1}(A_{ss})}{dA_{L}}\left(k_{off}^{A}+\frac{k_{BA}k_{on}^{P}C_{ss}^{B}}{k_{off}^{B}+A_{ss}k_{AB}}\right)>0 \tag{2.53}$$

using

$$m_{1}(A_{ss})=A_{ss}\left(1-\alpha\right)^{2},\quad \frac{dm_{1}(A_{ss})}{dA_{L}}=\frac{(1-\alpha)^{3}}{1+\alpha},\quad C_{ss}^{B}=\frac{(k_{off}^{B}+k_{AB}A_{ss})B_{ss}}{k_{on}^{B}}$$

we have:

$$\frac{k_{AB}A_{ss}k_{BA}B_{ss}}{k_{off}^{P}+A_{ss}k_{AB}}\left(1-\alpha\right)^{2}-\left(k_{off}^{A}+k_{BA}B_{ss}\right)\left(\frac{(1-\alpha)^{3}}{1+\alpha}\right)>0 \tag{2.54}$$

and thus:

$$\left(\frac{A_{ss}k_{AB}}{A_{ss}k_{AB}+k_{off}^{B}}\right)\left(\frac{B_{ss}kBA}{B_{ss}kBA+k_{off}^{A}}\right)>\frac{1-\alpha}{1+\alpha} \tag{2.55}$$

Finally, introducing $J_A=\frac{k_{BA}B_{ss}}{k_{off}^{A}}$ and $J_B=\frac{k_{AB}A_{ss}}{k_{off}^{B}}$ we obtain the final result:

$$\left(\frac{J_A}{1+J_A}\right)\left(\frac{J_B}{1+J_B}\right)>\frac{1-\alpha}{1+\alpha} \tag{2.56}$$

Numerical simulations

We performed all numerical simulations using custom scripts written in MATLAB. We discretized the 1D membrane domain into 100 equally-sized compartments and used a center-difference approximation to estimate diffusive flux between compartments. We used periodic boundary conditions in simulations to test for symmetry breaking, and no-flux boundary conditions in simulations to determine dynamics. In simulations of the full kinetic model, We allowed oligomers a maximum size of 50. We solved the resulting systems of ordinary

differential equations using MATLAB's built-in ode45 function using default settings. In all simulations, we chose k_{off}^{m} and membrane length L to be the units of time and length respectively, and selected values for other model parameters as described below.

Mapping the parameter space for spontaneous and inducible polarization in simple one- and two-species models

Linear positive feedback and no direct binding

For this scenario, we set $B = 0$ and $\gamma = 1$ in Eq 2.17. We randomly sampled values for K_M between 0.2 and 2, α between 0 and 1 and $J_{feedback}$ between 0 and 3. We constrained the uniform steady state density to be $M_{ss} = 1$, and then we computed the values of all other model parameters. For the case with no diffusion ($D = 0$, Fig. 2.2E), we used LPA as described above to determine the threshold for inducible polarization. For the case where $D > 0$ (Fig. 2.2F), we chose values for D as specified in the figure legend, sampled all other parameter values as described above, and then assessed the potential for spontaneous and inducible polarization using simulations. To look for spontaneous polarization, we initialized simulations from the uniform steady state with a small perturbation to the density in one membrane compartment. To look for polarity induction, we initialized simulations with an asymmetry predicted to be stable without diffusion based on phase plane analysis (see below). In both cases, we ran simulations for 5000 units of time and then scored the outcome as polarized when the ratio of the maximum and minimum densities, assessed across all membrane compartments, was greater than the initial value.

Saturating positive feedback and no direct binding

We fixed values for the saturation factor $S = \frac{M_{ss}}{K_{sat}}$ as specified in Fig. 2.5, and sampled values for all other parameters as in the case for linear positive feedback described above.

Model with mutual antagonism

For the model with mutual antagonism, we sampled values for α and $J_{feedback}$ uniformly between 0 and 1. We constrained the uniform steady state densities for proteins A and B to be $A_{ss} = 1, B_{ss} = 1$. We fixed a value for J_A as indicated in figure panels. We sampled values for k^a_{on}, k^p_{on}, and k^p_{off} randomly between 0.1 and 1, then computed the values of all other parameters. We used LPA as described above to test for spontaneous and inducible polarization for the scenario in which diffusion is negligible.

Relaxing the assumption of fast oligomerization kinetics

We used simulations of the full kinetic model to determine the effect of relaxing the assumption of fast oligomerization kinetics.

Linear positive feedback and no direct binding

We fixed k^p_{off} as indicated in (2.5(A)), sampled values for all other parameters as described above for the one-species model, and tested for spontaneous symmetry breaking as described above.

Scenarios with direct binding

For the cases where $\gamma = 1$ and indirect positive feedback is active ($k_f \geq 0$), we fixed $k^m_{on} = 0.05$ and $k^c_{off} = 0.1$; we assigned values to $\frac{k^p_{off}}{k^c_{off}}$ and B_{dir} as indicated in (2.5). We randomly sampled values for $J_{feedback}$ between 0 and 3 and α between 0 and 0.95. Then we computed the values of all other parameters. For the cases where $\gamma < 1$ and $k_f = 0$, we fixed $k^m_{on} = 0.05$ and $k^c_{off} = 0.1$; we assigned values to $\frac{k^p_{off}}{k^c_{off}}$ and γB_{dir} as indicated in (2.5). We sampled values for $J_{feedback}$ between 0 and 3 and α between 0 and 0.95. Then we computed the values of all other parameters. For both cases, we used numerical simulations to test for spontaneous polarization as described above.

Relaxing the assumption that oligomers of size ≥ 2 do not dissociate from the membrane

To relax this assumption, we modified the full kinetic model so that oligomer dissociation rate decreases exponentially with size:

$$k^i_{off}(n) = k^m_{off}\beta^{(n-1)}$$

and the parameter β sets the rate of decrease. We fixed values for β as indicated in (2.5(B)). We set $k^c_{on} = k^c_{off} = 0$, and $k^p_{off} = 1$. We sampled values for k^m_{on} between 0.2 and 2, k_f between 0 and $3k^m_{on}$ and $K_p = \frac{k^p_{on}}{k^p_{off}}$ between 0 and ∞. Then we computed values for $J_{feedback}$ and mean oligomer size s at the uniform steady state, assessed by allowing simulations to reach steady state in a single spatial compartment. We then assessed spontaneous symmetry breaking as described above.

Relaxing the assumption that oligomerization occurs only at the cell membrane

To relax this assumption, we modified the full kinetic model so that oligomerization occurs both in the cytoplasm and on the membrane with different equilibrium constants K^p_{mem} and K^p_{cyt}. We assumed that oligomerization in the cytoplasm is at quasi-steady state, such that the distribution of cytoplasmic oligomer sizes is given by $C_n = C_1\alpha^{n-1}$ where $\alpha = C_1K^p_{cyt}$. We set $k^p_{off} = 1$ and we fixed the ratio $\frac{K^p_{cyt}}{K^p_{mem}}$ as indicated in (2.5(C)). We sampled values for k^m_{on} between 0.2 and 2, k_f between 0 and $3k^m_{on}$, and K_p between 0 and ∞. Then we computed values for $J_{feedback}$ and mean oligomer size s at the uniform steady state and tested for spontaneous polarization as described above.

Numerical simulations to determine polarization speed

For the model with indirect positive feedback on monomer recruitment, we sampled values for α between 0.35 and 0.9 and $J_{feedback}$ between 2 and 10. We constrained $M_{ss} = 1$, set the scaled monomer diffusivity to $D = 0.00001$ and sampled values for K between 0.2 and 2. To simulate the absence of size-dependent dissociation, we scaled k^m_{off} to hold the effective dissociation rate of molecules constant as α was varied. For simulations in which oligomerization dynamics were not assumed to be infinitely fast (2.5), we assigned values to k^p_{off} as indicated in the figure legend and assigned $J_{feedback} = 5$. All other parameter values were determined by these constraints.

For the model with mutual antagonism, we sampled values for α between 0.35 and 0.9. We set $J_{feedback} = 0.64$, $k^A_{off} = k^B_{off} = 0.1\ s^{-1}$, $J_A = J_B$, and $k^A_{on} = k^B_{on} = 1s^{-1}$, $D_A = D_B = 0.1\mu m^2 s^{-1}$, concentration of A and B were scaled to their uniform steady states respectively, and all other parameters were determined by these constraints. Simulations were initiated with one compartment 3-fold more concentrated than the uniform steady state. Polarization speed was assessed as the slope of the log of the maximum concentration at the membrane when the maximum concentration was 1.5-fold higher than its minimum value in time and 2-fold lower than its maximum value in time.

Numerical simulations to determine boundary speed

In simulations to determine the boundary speed for the model with positive feedback, we sampled α between 0.35 and 0.8 and J between 2 and 10. Units for concentration, time, and length were scaled by M_{ss}, k^m_{off}, and membrane length respectively. Monomer diffusion was set to 0.00001 and k^m_{on} was randomly sampled between 0.2 and 2. If oligomerization dynamics were not assumed to be infinitely fast, k^p_{off} was set as indicated in figure panels. All other parameters were determined by these constraints. In simulations to determine boundary speed for the model with mutual antagonism, α was sampled between 0.35 and

0.8, $J_{feedback} = 0.64$, $k^A_{off} = k^B_{off} = 0.1\ s^{-1}$, $J_A = J_B$, and $k^A_{on} = k^B_{on} = 1\ s^{-1}$, $D_A = D_B = 0.1\ \mu m^2 s^{-1}$, concentration of A and B were scaled to their uniform steady states respectively, and all other parameters were determined by these constraints. In simulations that lacked size-dependent dissociation, k^m_{off} was scaled so that the effective dissociation rate of molecules off the membrane was held constant as α was varied. Simulations were initiated with an asymmetric step change distribution that was determined to be stable in the absence diffusion and where the polarized domain takes up 80 percent of the membrane length. For the model with positive feedback, this was determine by phase plane analysis (see below) and for the model with mutual antagonism this was determined through numerical simulations with $D_A = D_B = 0$. Boundary speed was determined by fitting a line to the position of the boundary over 400 time units following initiation of the simulation, defining the boundary as the inflection point of the spatial distribution.

Phase plane analysis

To identify asymmetries involving polarized domains of defined sizes that are stable without diffusion, we performed phase plane analysis. We considered a model in which the cell membrane is divided into two membrane compartments that exchange with a shared cytoplasmic pool, but we assumed no diffusive flux between membrane compartments.

$$\frac{dM_1}{dt} = F(M_1)C - G(M_1) \tag{2.57}$$

$$\frac{dM_2}{dt} = F(M_2)C - G(M_2) \tag{2.58}$$

$$C = M_{tot} - (aM_1 + (1-a)M_2) \tag{2.59}$$

where M_1 and M_2 are the concentrations of protein in the two membrane compartments and a is the length membrane compartment M_1 divided by the total length of the cell membrane. We plotted nullclines for these differential equations for defined values of a and

used the polyxpoply function in MATLAB to determine intersections between the nullclines and thus steady states.

2.5 Supporting information

Supplementary Figures

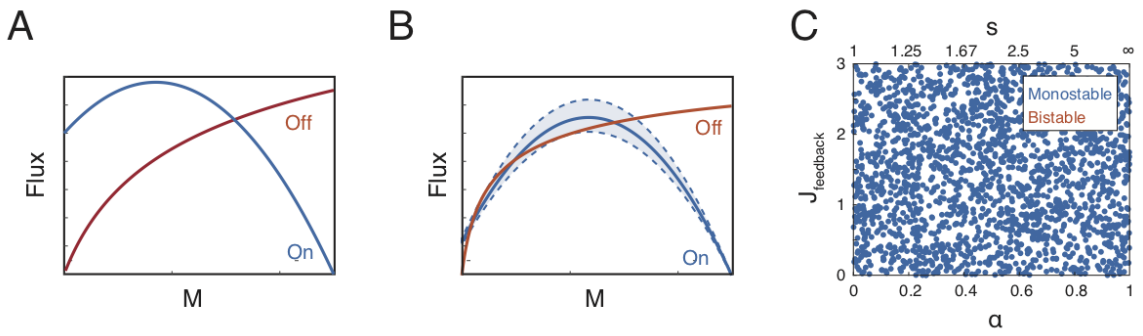

Figure 2.7: **Steady state analysis of spatially uniform distributions. (A)** Flux balance plot showing an example of a case in which there is exactly one uniform steady state. The blue line indicates flux of protein onto the membrane as a function of membrane protein concentration and the orange line indicates flux of protein off the membrane. **(B)** Flux balance plot indicating a narrow range of parameter values for which multiple uniform steady states are possible. Dotted lines indicate a range of curves that produce two uniform stable steady states, generated by varying K. **(C)** Scatter plot showing the existence of exactly one uniform steady state for the range of oligomerization strengths (α, s) and feedback strengths $\left(J_{feedback}\right)$ explored in this paper. Each point corresponds to a randomly chosen parameter set used in another analysis. Blue points have exactly one uniform steady state. There are no points that have multiple steady states.

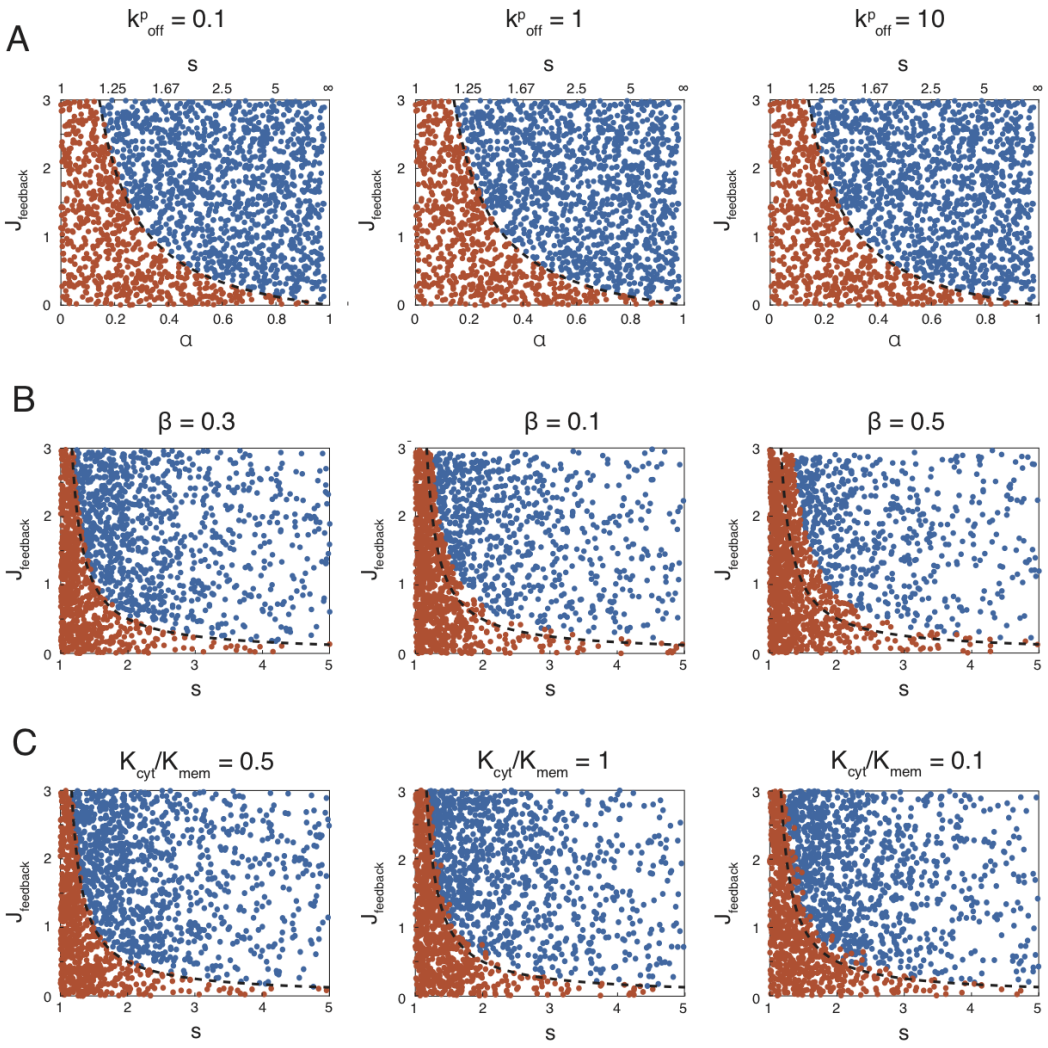

Figure 2.8: **Effects of relaxing different assumptions on polarization.** **(A)** Scatter plots showing results of simulations where the assumption that polymerization kinetics are fast relative to membrane exchange is relaxed. **(B)** Scatter plots showing results of simulations where the assumption that oligomers of size 2 and greater do not dissociate from the membrane is relaxed. In these simulations, the off rate of an oligomer of size n is equal to $k^m_{off}\beta^{n-1}$. **(C)** Scatter plots showing the results of simulations where the assumption that oligomerization only occurs on the membrane is relaxed. K_{cyt} denotes the equilibrium binding constant for oligomerization in the cytoplasm and K_{mem} denotes the equilibrium binding constant for oligomerization at the membrane. In all panels, blue dots indicate spontaneous symmetry breaking, orange dots indicate a stable uniform state, and the dotted line indicates the predicted phase boundary between these outcomes based on the ideal case. Parameters were sampled as described in the methods section.

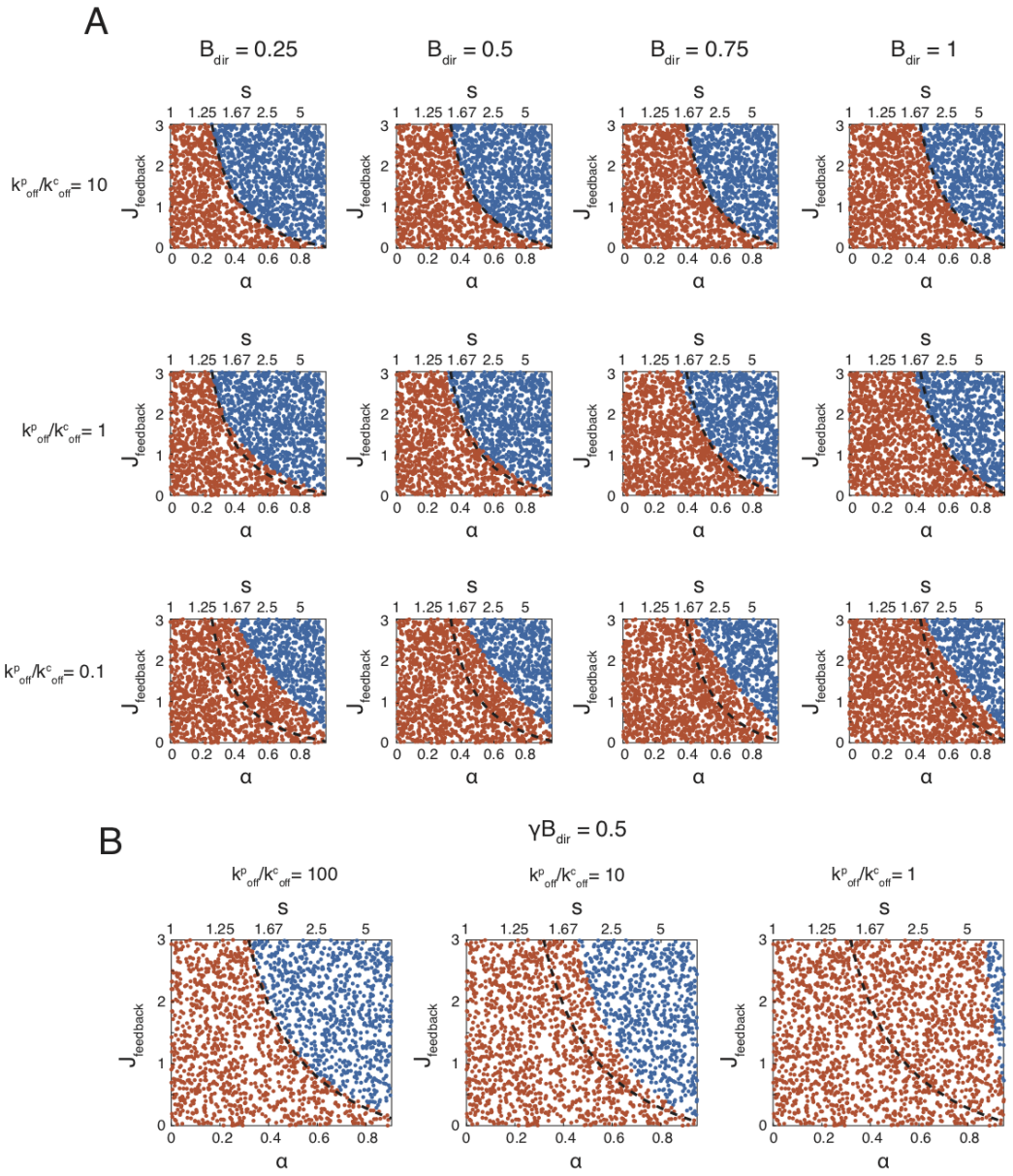

Figure 2.9: **Predictions of the full kinetic equations for scenarios involving direct binding. (A,B)** Scatter plots showing stability of the uniform steady state as a function of oligomerization (α, s) and feedback strength $\left(J_{feedback}\right)$ when **(A)**: $\gamma = 1$ for different values of B_{dir} (left to right) and $\frac{k^p_{off}}{k^c_{off}}$ (top to bottom) or **(B)**: $\gamma < 1$ and $k_f = 0$ and $\gamma B_{dir} = 0.5$, for different values of $\frac{k^p_{off}}{k^c_{off}}$ (left to right). Blue dots indicate unstable and orange dots indicate stable states. Dashed lines indicate the boundary between stable and unstable regimes derived for the one-species model.

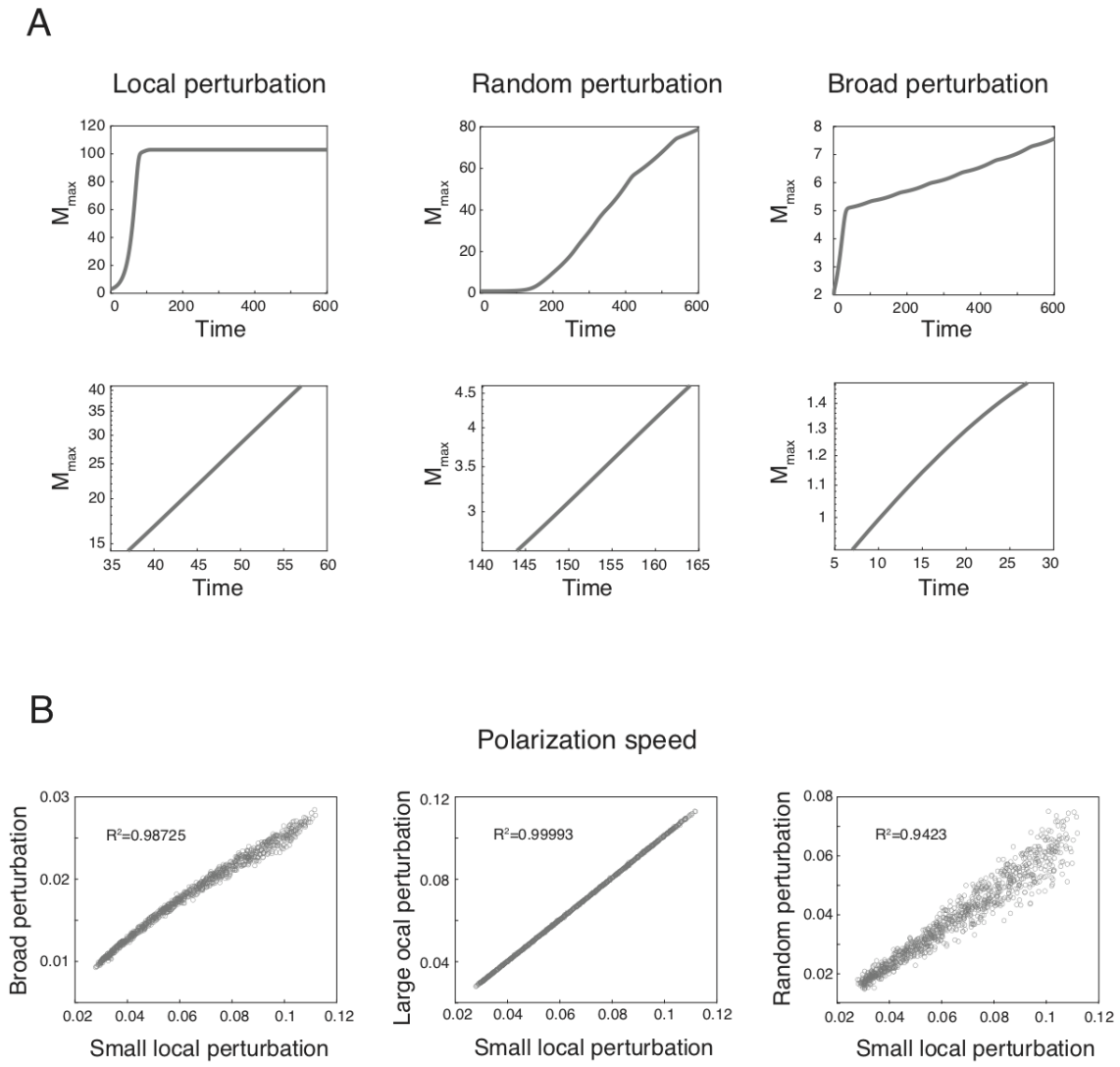

Figure 2.10: **(A)** Plots showing examples of the logarithm of the maximum local value of M (M_{max}) over time in simulations where polarization is triggered by different types of cues: a local perturbation, a spatially varying random perturbation, and a broad perturbation. While the speed of polarization differs based on the cue, all curves have a region in which M_{max} grows exponentially. **(B)** Scatter plots showing the correlation between polarization speed across different types of perturbations in simulations where $J_{feedback}$ and α were sampled randomly. Each point corresponds to a unique choice of model parameter values.

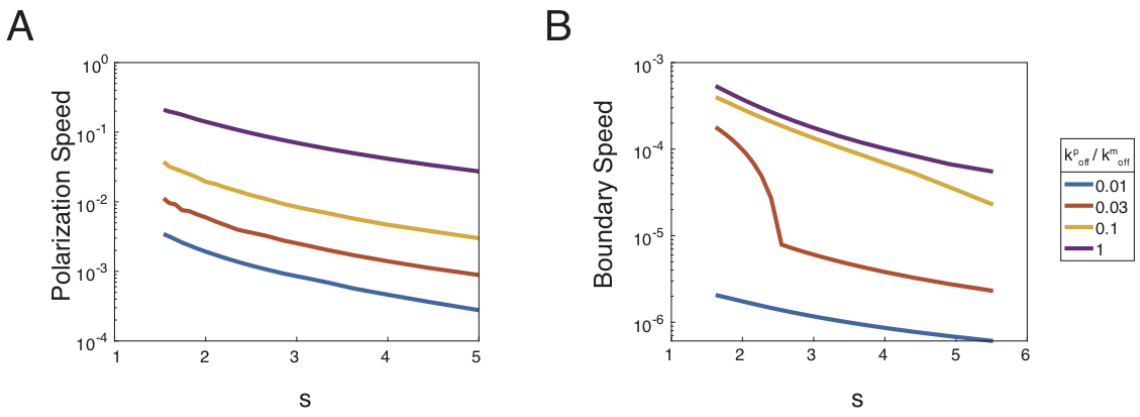

Figure 2.11: **Dependence of polarization dynamics on oligomer dissociation kinetics. (A,B)** Plots showing the effects of slowing down oligomerization dissociation kinetics $\left(k^p_{off}\right)$ on polarization speed **(A)** and boundary speed **(B)**. $J_{feedback}$ is set to 5 in these simulations, while all other parameters are sampled as described in the methods. Colored lines show the dependence of polarization speed and boundary speed on mean oligomer size s for different values of k^p_{off}.

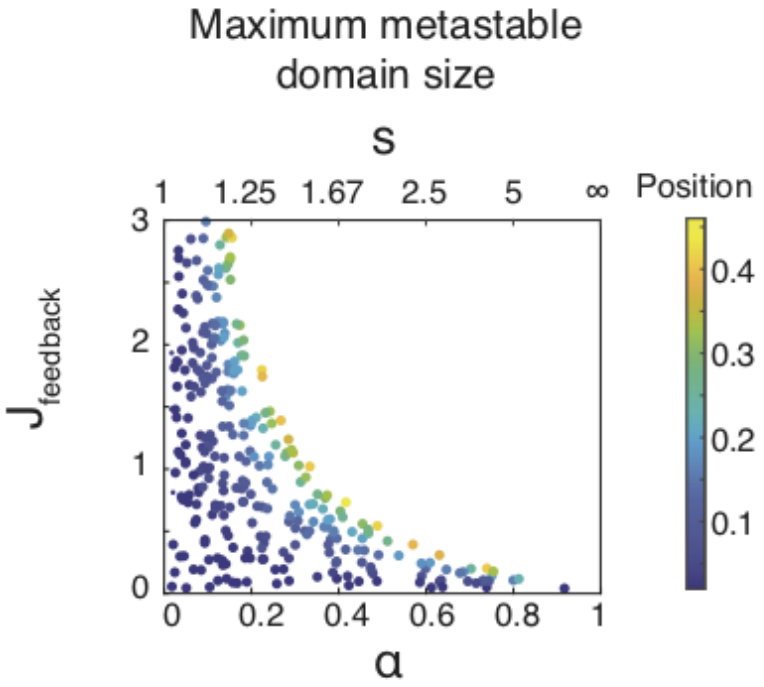

Figure 2.12: **Asymmetries that do not arise spontaneously have a maximum metastable domain size.** The maximum metastable domain size plotted as a function of α and $J_{feedback}$. The color of individual points indicates the maximum size. Maximum metastable domain size was assessed using nullcline analysis assuming no diffusion and domain boundary position ranging from 50% to 2% cell length, evaluating at increments of 1% (see methods).

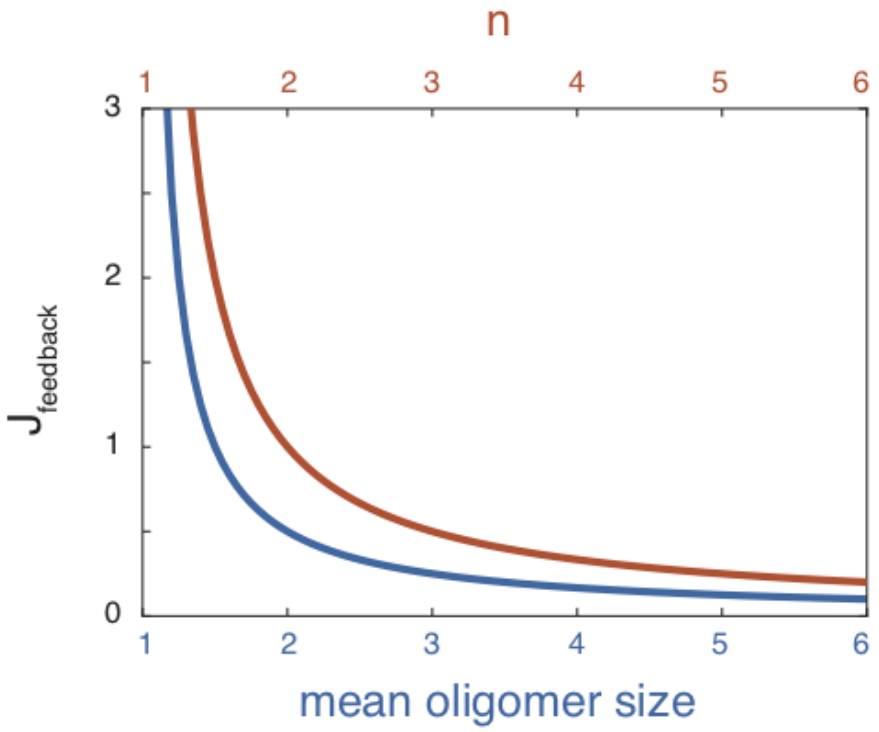

Figure 2.13: **Feedback strength and the sharpness of nonlinear dynamics determine spontaneous polarization for models with cooperative positive feedback.** The orange line shows the boundary between spontaneously polarizing and stably uniform states for a model with higher order positive feedback in phase space defined by $J_{feedback}$ and the order of the feedback (n). The blue line shows the equivalent phase boundary for a model with linear positive feedback in phase space defined by mean oligomer size and $J_{feedback}$.

CHAPTER 3

PAR-3 ASYMMETRIES ARE STABILIZED BY OLIGOMERIZATION AND BIASED RECRUITMENT OF MONOMERS TO THE MEMBRANE IN THE *C. ELEGANS* ZYGOTE

3.1 Introduction

Across metazoans, a single module of proteins called the PAR proteins is involved in cell polarization in a wide range of contexts [45]. The PAR proteins are not only required for the establishment and maintenance of cell polarity but are also themselves asymmetrically distributed at the cell membrane, and thus define polarized states. Therefore, understanding how PAR asymmetries form and are stabilized is a crucial question in cell polarity.

The PAR proteins were discovered *C. elegans*, where they are required for the asymmetric first division of the zygote. In this cell, two groups of PAR proteins become enriched in complementary membrane anterior and posterior membrane domains. The anterior PARs (aPARs) include PAR-3, PAR-6, PKC-3, and CDC-42, while the posterior PARs include PAR-1, PAR-2, CHIN-1, and LGL-1. These groups of proteins form opposing asymmetries in response to a sperm-derived cue [84]. Once established, this bipolar pattern is self-stabilizing and persists through mitosis.

Polarization of the PAR proteins is separated into distinct establishment and maintenance phases. During polarity establishment, which corresponds to interphase of the cell cycle, the combination anterior-directed transport of aPARs through actomyosin flows [23, 109, 44] and microtubule dependent recruitment of PAR-2 and PAR-1 to the posterior cortex [107, 174] provide initial symmetry-breaking cues. Both of these mechanisms depend on the microtubule organizing center (MTOC) deposited by the sperm in the posterior of the

embryo [15, 29]. During polarity maintenance, which corresponds to M phase of the cell cycle, this MTOC moves to the center of the embryo. Nonetheless complementary PAR asymmetries are dynamically maintained, despite diffusion and turnover of PAR proteins at the cell membrane [43, 125]. The current model for how these asymmetries are stabilized is that aPARs and pPARs mutually antagonize each other's cortical localization through direct interaction [32, 44, 130, 84]. PAR-1 has been shown to directly phosphorylate PAR-3 [12, 107] and CHIN-1 is a putative GAP for CDC-42 [9, 82, 130], while PKC-3 directly phosphorylates and dissociates PAR-1, PAR-2, and LGL-1 [6, 107, 58, 5, 62]. Consistent with this model, restriction of all pPARs to the posterior depends on PAR-3, PKC-3, PAR-6, and CDC-42. PAR-1 and CHIN-1 play redundant roles in restricting aPARs to the anterior cortex, but in the absence of both, the PAR-6/PKC-3 heterodimer spreads to cover the posterior cortex in maintenance phase, and CDC-42 is uniformly active at the cortex [130]. However, our lab previously showed that in the *C. elegans* zygote, PAR-3 maintains a polarized distribution at the cell cortex even when all other PARs are uniform, i.e. in *chin-1/par-1* double mutants [130]. The mechanisms that stabilize PAR-3 asymmetries in M phase are unknown.

PAR-3 is an oligomeric scaffold protein that self-associates through a conserved N-terminal domain, called the CR1 domain [11]. This CR1 domain is a PB1-like domain and assembles head to tail into helical filaments in vitro [39, 168]. While PAR-3 contains several predicted membrane binding domains [88, 101], deletion or mutation of the N-terminal domain in *C. elegans* results in a strong attenuation of PAR-3 membrane localization and embryonic polarity defects [88, 34, 126]. PAR-3 clustering plays an important role in polarity establishment by entraining PAR proteins in anterior-directed cortical actomyosin flows [34, 126, 154]. However, it is unknown whether PAR-3 clustering plays an additional role in polarity maintenance.

Here, we use single molecule imaging to measure the kinetics of PAR-3 oligomerization and membrane binding. We show that PAR-3 oligomers are larger on the anterior membrane,

and measure oligomer size-dependent membrane dissociation. This combination results in PAR-3 more stably associating with the anterior membrane than the posterior. We further show that asymmetries in the distributions of PAR-3 oligomers are dynamically maintained and that the recruitment of new PAR-3 monomers to the cell membrane exhibits an anterior bias. Using a combination of mathematical modeling and experiments, we provide evidence that the combination of feedback on monomer recruitment, dynamic oligomerization, and avidity effects enables PAR-3 asymmetries to self-stabilize, and that these processes are in turn regulated by interactions with other aPAR proteins. Finally, we show that the positions of PAR-3 domain boundaries are not encoded by a reaction diffusion system, and propose instead that oligomer size-dependent decreases in PAR-3 mobility effectively preserve arbitrary domain boundaries for the duration of polarity maintenance. Together, these results reveal a novel mechanism for stabilizing PAR-3 asymmetries in the absence of mutual antagonism.

3.2 Results

3.2.1 Asymmetries in distributions of PAR-3 oligomers are dynamically maintained in the C. elegans zygote.

As a first step to understanding how PAR-3 asymmetries are maintained in the absence of posterior inhibition by PAR-1, we characterized the sizes and dynamics of PAR-3 oligomers at the cell membrane using near-TIRF microscopy. We measured the distributions of oligomer sizes in the anterior and posterior of *par-1* mutant embryos during maintenance phase using the intensity distribution of single molecules of GFP as an internal standard (Fig. 3.1A). While the majority of PAR-3 particles on the posterior membrane are monomers, the mean size of PAR-3 particles on the anterior membrane is ~ 3.5 subunits (Fig. 3.1B). Both size distributions are roughly consistent with the steady state expectation from simple polymer-

ization kinetics $X_i = X_1\alpha^{(i-1)}$, where X_i is the concentration of particles with i subunits and α is the ratio of monomer on- and off-rates.

An anterior bias in mean oligomer size could reinforce PAR-3 asymmetries if dissociation of PAR-3 oligomers from the membrane is oligomer size-dependent, resulting in an asymmetry in the effective off-rate. To test whether PAR-3 oligomers exhibit size-dependent membrane avidity, we performed fast imaging and particle tracking analysis of mNeon::PAR-3, again using the distribution of single molecule intensities to calibrate estimates of oligomer sizes. We further improved particle tracking by conducting experiments in embryos depleted of myosin, which both increases the distance between particles by preventing polarization and decreases the movement of particles by eliminating local actomyosin contractions that jostle PAR-3 oligomers. We found that there is a sharp falloff in dissociation rate as particle size increases from monomer to dimer and that dissociation of particles with four or more subunits is negligible (Fig. 3.1C). Therefore, the asymmetry in PAR-3 oligomer sizes combined with oligomer-size dependent membrane avidity results in an asymmetry in the dynamics with which PAR-3 dissociates from the membrane.

Next, to determine whether PAR-3 asymmetries persist through maintenance phase due to slow oligomerization kinetics or whether they are dynamically maintained, we measured PAR-3 depolymerization rates. First, we used fast single molecule imaging of a sparsely labeled PAR-3::GFP to measure the residence times of PAR-3 molecules at the cell membrane. Release curves of these molecules show a prominent population that dissociates at a rate of $\sim 0.1\ s^{-1}$ after correction for the photobleaching rate (Fig. 3.1D). Second we performed fluorescence recovery after photobleaching (FRAP) experiments to measure turnover within PAR-3 oligomers at the cell membrane. The integrated fluorescence density within oligomers recovers to half maximum intensity with a mean time of ~ 8 seconds, corresponding to a dissociation rate of $\sim 0.085\ s^{-1}$ (Fig. 3.1E). Together, these results suggest PAR-3 oligomers depolymerize with a rate of $0.08 - 0.1 s^{-1}$.

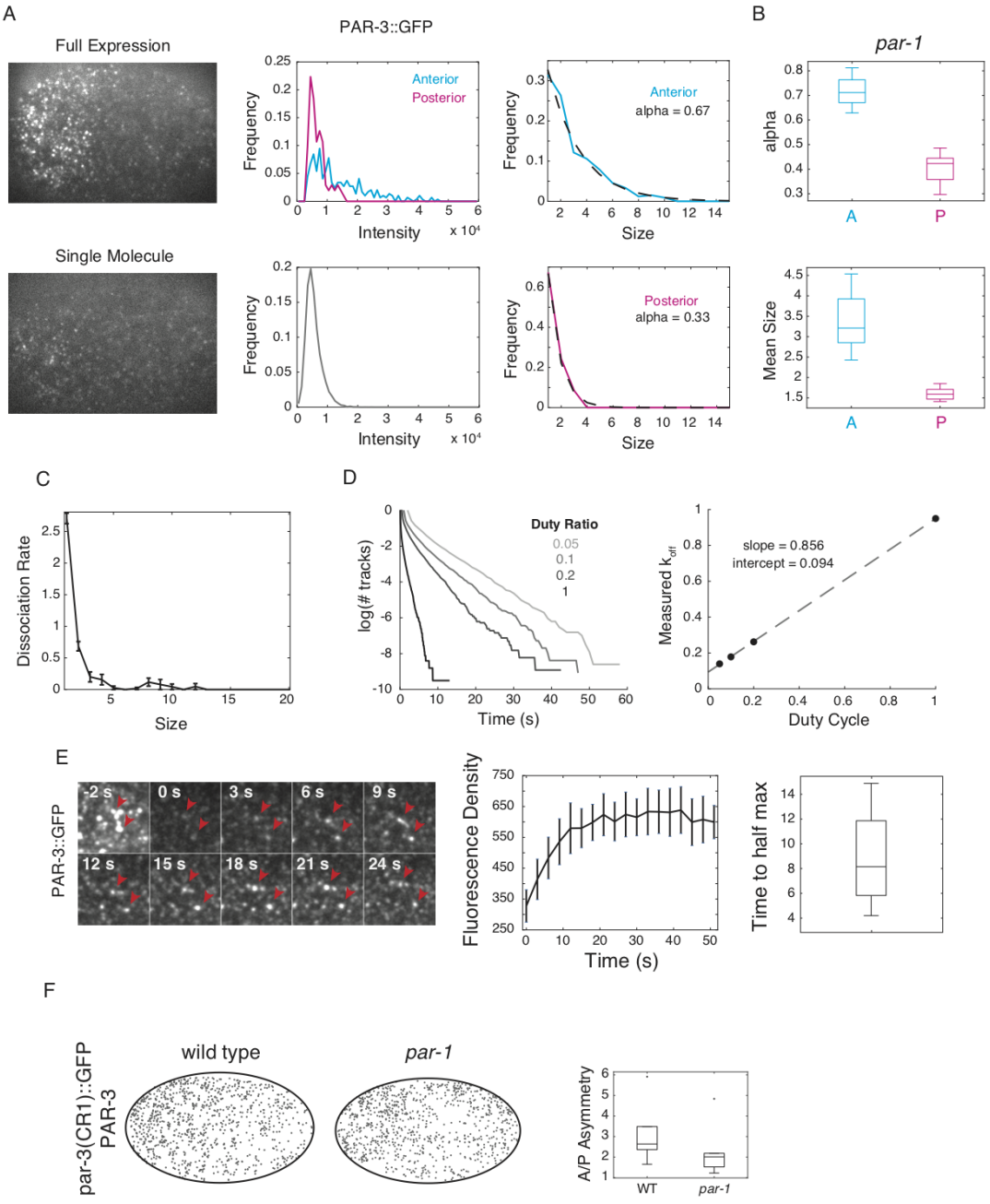

Figure 3.1: **Dynamics of PAR-3 membrane binding and oligomerization. (A)** PAR-3 speckle intensities before and after photobleaching in par-1 mutant embryos. Micrographs show near-TIRF images of PAR-3::GFP at the start of imaging (above panel) and following 30 seconds of continuous laser exposure at full power (below panel). (legend continued on next page)

Figure 3.1: (continued) Plots show representative examples of anterior (cyan) and posterior (magenta) speckle intensity distributions, as well as speckle intensities after photobleaching (gray). Plots on the right show representative examples of the inferred size distribution of PAR-3 oligomers in the anterior and posterior, based on calibrating raw intensities to the estimated intensity distribution of single molecules. **(B)** Comparison of α and mean size of PAR-3 oligomers between the anterior and posterior cortex in par-1 mutant embryos in late maintenance phase (n=8). **(C)** Dissociation rates of PAR-3 oligomers from the membrane as a function of inferred number of subunits. Error bars represent the S.E.M. (n = 3 embryos). **(D)** Dissociation rates of PAR-3 molecules from oligomers. The plot on the left shows release curves for molecules imaged at different duty ratios. The plot on the right shows the measured off rates inferred from the exponential portion of the release curves as a function of duty cycle. The slope of this line indicates the photobleaching rate, while the y-intercept indicates the true depolymerization rate. **(E)** FRAP of cortical PAR-3 oligomers in near-TIRF. Micrographs indicate representative examples of individual PAR-3 oligomers recovering fluorescence. The line graph indicates the recovery of fluorescence intensity within segmented oligomers over time (n=4). The box plot indicates the time to recover fluorescence halfway to maximum intensity (n=4). F, Binding events of oligomerization-defective PAR-3 molecules to the cell membrane, expressed over unlabeled wild-type PAR-3. Scatter plots on the left are representative examples of the distribution of binding events in space in control and par-1 mutants. Boxplots show the ratio of binding events in the anterior to posterior of the embryo (control n= 5; par-1 n = 6).

To confirm that the recovery we measured was a indeed turnover of monomers within oligomers rather than exchange of oligomers between the cytoplasm and cell membrane, we performed FRAP experiments in interphase, when PAR-3 oligomers are larger and more sparse and are thus easier to track at low image acquisition rates. We found that partially photobleached oligomers individually recover fluorescence, albeit on a slower timescale than in maintenance phase (Fig. 3.5). Qualitative analysis of this FRAP data seems to show that following photobleaching, existing puncta gradually recover fluorescence, but new bright puncta almost never appear on the cortex. This suggests that membrane-bound PAR-3 oligomers assemble locally on the cell membrane, rather than assembling in the cytoplasm and then binding to the membrane. To confirm this, we analyzed the same fast imagining data used to measure oligomer dissociation rates and inferred the number of molecules in newly bound particles. We found that the fluorescence intensity distribution of newly detected particles almost exactly matches the distribution of single mNeon::PAR-3 molecules,

suggesting that PAR-3 binds to the membrane in monomeric form and that oligomerization occurs primarily at the cell membrane (Fig 3.6). Together, these results demonstrate that PAR-3 oligomers dynamically assemble and turn over subunits at the cell membrane and that asymmetries in PAR-3 concentration and mean oligomer size are dynamically maintained.

The modeling work presented in Chapter 2 shows that oligomerization and avidity effects enable stable polarization when combined with some additional form of weak positive feedback, but are not sufficient on their own to stabilize asymmetries. To test whether feedback might exist on the recruitment of monomers to the cell membrane, we performed single molecule imaging experiments with a mutant version of PAR-3::GFP that cannot oligomerize [88] expressed over the wild-type. We found that new molecules are 2 times as likely to bind to the anterior membrane, where PAR-3 is enriched, than the posterior membrane (Fig 3.1F). Depletion of *par-1* through RNAi had only very weak effects on the recruitment asymmetry, demonstrating that this effect is unrelated to posterior inhibition by PAR-1 (Fig. 3.1F).

3.2.2 Oligomerization and positive feedback on monomer recruitment are sufficiently strong to enable stable asymmetries

In Chapter 2, I showed that in a model where oligomers assemble only at the cell membrane, dissociation of oligomers from the membrane is negligible, and monomers bind to the cell membrane much more frequently than to existing oligomers, two dimensionless quantities determine whether asymmetries will be self-stabilizing: 1) the mean oligomer size, and 2) the strength of feedback (defined as the ratio of the feedback-dependent on-rate and the basal on-rate of monomers) (Fig. 3.2A-B). We have directly measured the mean size of PAR-3 oligomers (Fig. 3.1A), and we can estimate the strength of feedback by assuming that the ratio of anterior and posterior appearance rates, which we have measured, is equal to $\frac{J_b+J_f}{J_b}$, where J_b is the basal on rate and J_f is the feedback dependent on rate. Based on these measurements, oligomerization and feedback on monomer recruitment are in principle

sufficient to stabilize PAR-3 asymmetries in the *C. elegans* zygote (Fig. 3.2B).

This model predicts that feedback on monomer recruitment will stabilize PAR-3 asymmetries only if PAR-3 oligomers are sufficiently large. Therefore, a sufficient decrease in the mean oligomer size should result in a failure to maintain polarity. To test this prediction *in vivo*, we partially depleted PAR-3 with RNAi and measured mean PAR-3 oligomer sizes and polarities of individual embryos. We found that decreasing amounts of PAR-3 at the cell membrane correlated with decreasing mean oligomer sizes (Fig. 3.7). In most embryos, we found that PAR-3 asymmetries are established prior to the onset of maintenance phase (Fig. 3.2C). However, in most embryos with a mean oligomer size of 1.5 subunits or fewer, polarity was subsequently lost over the course of maintenance phase (Fig. 3.2C,D). In these embryos, we detected no posterior flow of PAR-3 oligomers at the cortex, suggesting that loss of polarity was due to dynamic exchange between membrane-bound and fast-diffusing cytoplasmic pools rather than polarized transport (Fig. 3.2C). The decrease and eventual loss of asymmetry we observed with decreasing oligomer sizes is consistent with model predictions (Fig. 3.2D). Therefore, even in the presence of feedback on monomer recruitment, PAR-3 oligomers must be sufficiently large for polarity to be maintained.

3.2.3 PAR-6/PKC-3 and CDC-42 stabilize PAR-3 asymmetries by regulating cortical flows, PAR-3 oligomerization, and asymmetric recruitment of PAR-3 monomers.

During polarity maintenance phase, PAR-3 co-localizes to the anterior of the zygote with the aPARs PAR-6/PKC-3 and CDC-42. PAR-6/PKC-3 dimers localize to distinct pools bound directly to either PAR-3 and CDC-42 at the cell membrane. PAR-3 is required for PAR-6/PKC-3 to bind to the membrane during maintenance phase, but most of the PAR-6/PKC-3 is likely bound to CDC-42. While PAR-3 is required for polarization of aPAR proteins, it is unclear whether and how other aPARs regulate PAR-3 polarity. We found that in *par-6*

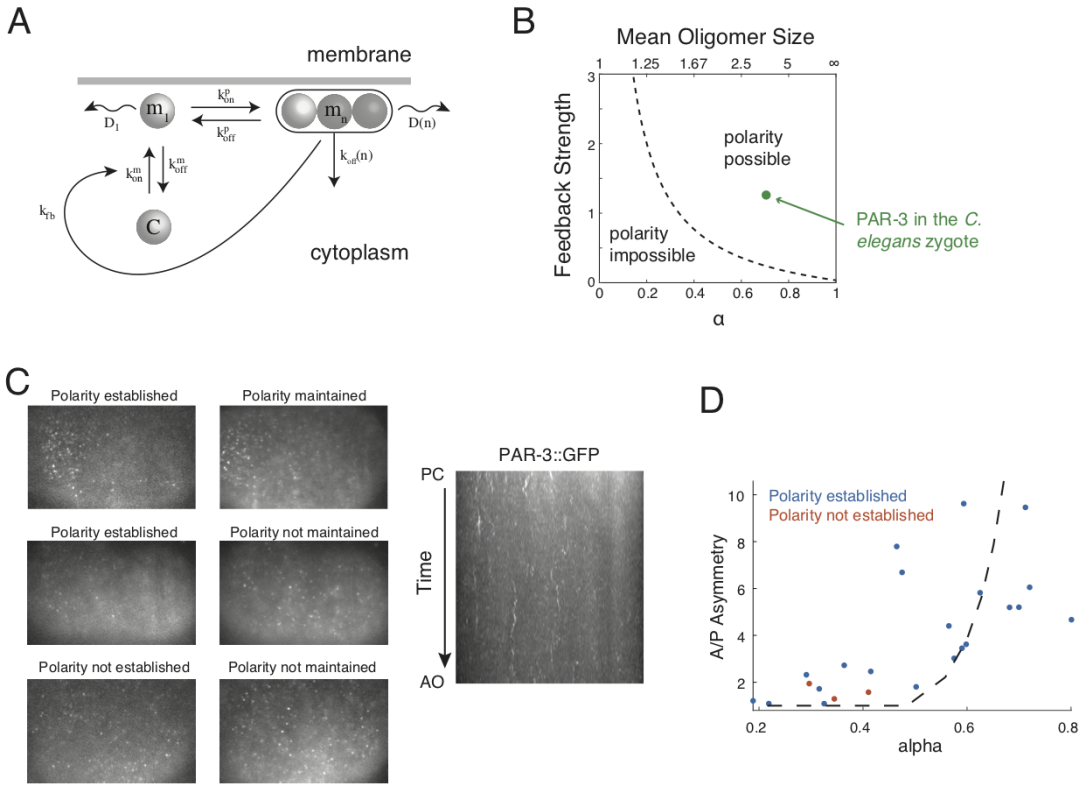

Figure 3.2: **Oligomerization and positive feedback on membrane binding are in theory sufficient to stabilize PAR-3 asymmetries. (A)** Reaction diagram of a model in which PAR-3 oligomerizes on the cell membrane and feeds back to locally promote association of PAR-3 monomers with the cell membrane. **(B)** Phase plane derived from the theoretical model in A showing the ability to polarize depends on the size distribution of oligomers (α) and the ratio of feedback dependent flux to basal flux onto the membrane (feedback strength). Experimental measurements in the *C. elegans* zygote place PAR-3 in the region of phase space polarization is possible (green dot). **(C)** Representative micrographs showing classes of embryos in experiments PAR-3 concentration is progressively reduced. The left column of micrographs shows the distribution of PAR-3 near the beginning of maintenance phase and the right column shows the distribution near the end of maintenance phase. The kymograph is derived from the embryo in the middle row of micrographs. Note the vertical streaks indicating a lack of cortical flows during this time interval. **(D)** Ratio of anterior to posterior concentration of PAR-3 near the end of maintenance phase plotted against the size distribution parameter α for embryos that have been partially depleted of PAR-3 the RNAi. Blue dots indicate embryos where PAR-3 was polarized near the beginning of maintenance phase, and orange dots indicate embryos where it was not. The dotted line shows the results of simulations where the total amount of PAR-3 is gradually decreased.

(RNAi) embryos, PAR-3 polarizes during establishment phase, although the domain boundary at the onset of maintenance phase is shifted anteriorly (Fig 3.3A). However, PAR-3 depolarizes rapidly in maintenance phase through a combination of posterior-directed flows and depolymerization of PAR-3 oligomers (Fig. 3.3A,C). Conversely, in *cdc-42 (RNAi)* embryos, PAR-3 asymmetries persist through maintenance phase and PAR-3 oligomers are roughly the same size (Fig. 3.3A,C). These opposing effects on PAR-3 oligomerization suggest that it is specifically the pool of PAR-6/PKC-3 bound to PAR-3 that promotes oligomerization. To test this, we imaged PAR-3::GFP in *cdc-37 (RNAi)* embryos. In this condition, PAR-6/PKC-3 is enriched at the cortex, but depleted from PAR-3 complexes [10]. Similar to *par-6 (RNAi)* conditions, PAR-3 asymmetries are initially established but are not maintained and PAR-3 oligomers are smaller than in WT embryos (Fig. 3.3A,C).

These results suggest that direct interaction between PAR-3 and PAR-6/PKC-3 promotes oligomerization of PAR-3. However, another possibility is that the smaller oligomers observed in *par-6 (RNAi)* conditions are an indirect effect of failure of PAR-6/PKC-3 to exclude PAR-1 from the anterior membrane, resulting in phosphorylation of anterior PAR-3 by PAR-1. To test this, we performed the same experiments in a *par-1* mutant background. We found that, similar to in the wild type background, PAR-3 depolarized in *par-6 (RNAi)* embryos and PAR-3 oligomers were smaller than controls (Fig. 3.3B,C) and PAR-3 oligomers in *cdc-42 (RNAi)* were roughly the same size as controls (Fig. 3.3B,C). However, unlike in *cdc-42 (RNAi)* embryos, PAR-3 depolarizes in *cdc-42 (RNAi)/par-1* double mutant embryos 3.3B). While in some embryos, depolarization coincides with posterior-directed flow of PAR-3 oligomers (Fig. 3.8), in others PAR-3 depolarizes without posterior directed flow (Fig. 3.3B), suggesting that depolarization is due to dynamic exchange between membrane bound and cytoplasmic pools.

To investigate why PAR-3 depolarizes in *cdc-42 (RNAi)/par-1* double mutant embryos in the absence of posterior flow or depolymerization, we measured relative rates of the

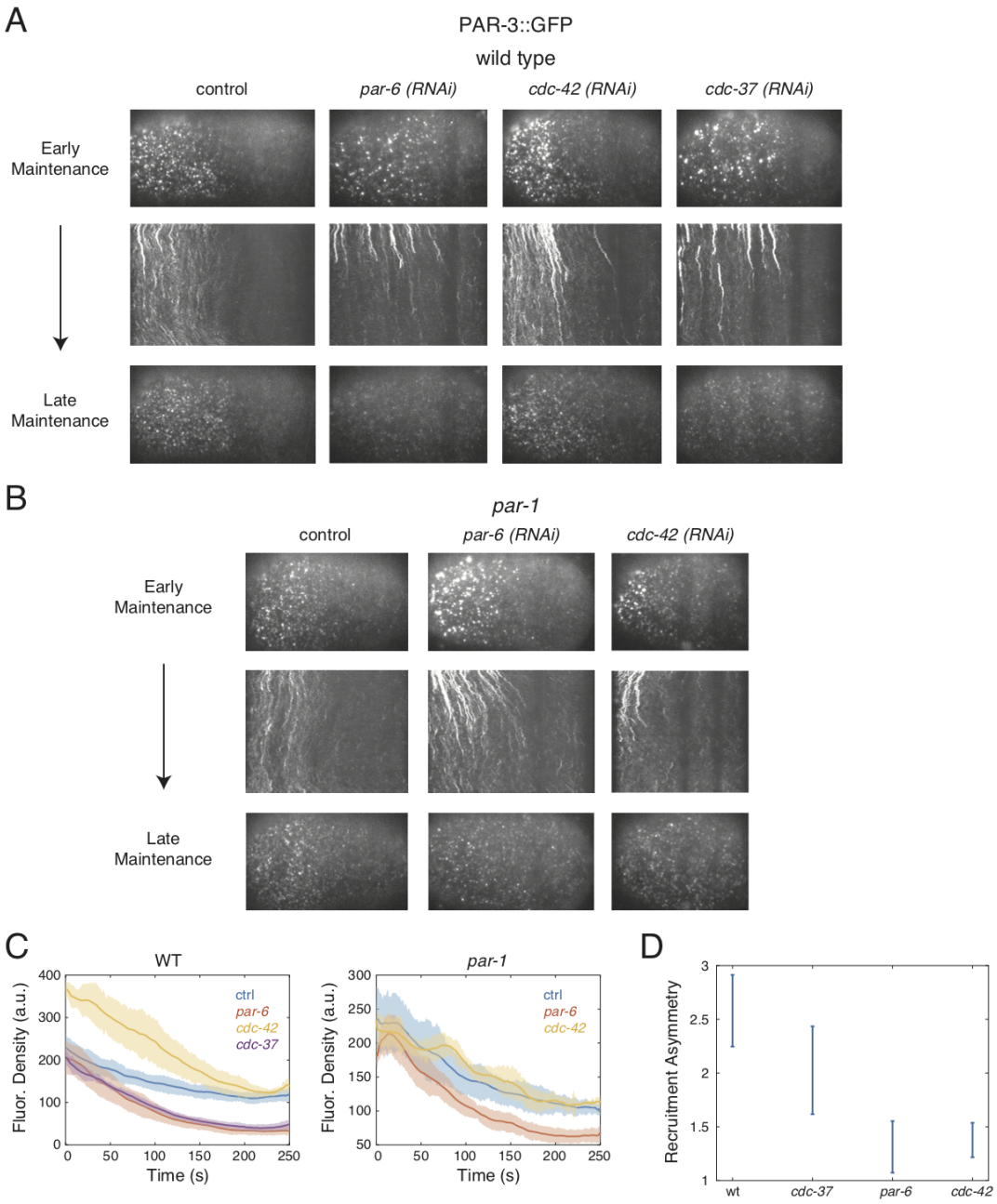

Figure 3.3: **PAR-6/PKC-3 and CDC-42 regulate PAR-3 oligomerization and polarity. A-B** Representative micrographs showing PAR-3 oligomer sizes and distribution at early and late maintenance phase in control **(A)** and par-1 mutant **(B)** backgrounds. Kymographs show how the distribution changes over the 240 seconds between these time points. Diagonal streaks in the kymographs indicate transport of PAR-3 oligomers, likely by cortical flow. (legend continued on next page)

Figure 3.3: (continued) **(B) (C)** Fluorescence density of PAR-3 within segmented speckles over polarity maintenance in control and par-1 embryos for different RNAi knockdown conditions. Bold lines indicate the mean and the shaded region indicates the standard error of the mean. **(D)** Ratio of anterior to posterior binding events of oligomerization-defective PAR-3 molecules to the cell membrane, expressed over unlabeled wild-type PAR-3. Error bars show the S.E.M.

recruitment of PAR-3 monomers to the anterior and posterior membrane in different RNAi conditions. We found that in *par-6 (RNAi)* embryos, asymmetries in PAR-3 appearance rates are significantly lower than in WT (Fig. 3.3D), consistent with overall depolarization PAR-3 in those conditions. However, even though PAR-3 asymmetries are maintained in *cdc-42 (RNAi)* conditions, the asymmetry in appearance rates is severely attenuated (Fig. 3.3D). This finding suggests that redundant PAR-1- and CDC-42-dependent feedback loops stabilize PAR-3 asymmetries, and that a combination of oligomerization and feedback are required to maintain PAR-3 asymmetries in *par-1* mutant embryos. This finding is consistent with our modeling work which shows that some form of feedback is both necessary and sufficient to stabilize asymmetries of oligomeric peripheral membrane proteins.

3.2.4 The position of the PAR-3 domain boundary is determined by actomyosin flows, not encoded by a reaction-diffusion system.

In *C. elegans* zygote, polarized PAR distributions are initially established by anterior-directed actomyosin flows, but previous studies have suggested that the stable boundary positions of polarized PAR domains are determined by the relative amount of limiting anterior and posterior PAR proteins through a reaction-diffusion mechanism called "wave-pinning" [44]. This mechanism makes a clear prediction that if the initial position of the PAR domain boundary is shifted, the reaction diffusion system alone should be sufficient to correct the boundary over the course of polarity maintenance (Fig. 3.4A). To test whether this prediction holds for PAR-3 asymmetries, we shifted the initial maintenance phase PAR-3 domain boundary posterior relative to the WT position by reducing establishment phase

contractility by partially depleting NOP-1 through RNAi. We then determined whether the aberrant boundary position persisted through maintenance phase, or dynamically shifted towards the wild-type position (Fig. 3.4A). To rule out confounding effects of maintenance phase actomyosin contractility, we performed these experiments in a *mrck-1* mutant background. We found that under these conditions, PAR-3 boundary positions change minimally over the course of maintenance phase, regardless of the initial position (Fig. 3.4B-C). Therefore, the reaction-diffusion mechanism that stabilizes PAR-3 asymmetries fails to encode a unique boundary position, and instead preserves arbitrary boundaries over the timescale of polarity maintenance.

In Chapter 2 I showed that the speed at which polarized domain boundaries shift towards steady state positions is slowed by oligomer size-dependent increases in membrane avidity and decreases in lateral diffusion and that for sufficiently large oligomers, boundary drift could be negligible over relevant timescales. To ask whether oligomerization might be slowing drift of the PAR-3 boundary, we measured PAR-3 mobility as a function of oligomer size. Consistent with previous measurements, we confirmed that lateral mobility of PAR-3 oligomers decreases sharply as a function of oligomer size (Fig. 3.4D). Based on the measured PAR-3 oligomer sizes and depolymerization rates, monomer dissociation and diffusion rates, and sharp decreases in dissociation and diffusion rates with oligomerization, our model predicts that the drift of the PAR-3 domain boundary should be negligible over the time scale ($\sim$5 minutes) of polarity maintenance (Fig. 3.4E). These findings suggest that the preservation of arbitrary PAR-3 boundary positions during maintenance phase may be a result of oligomerization-dependent decreases in PAR-3 dissociation and diffusion rates.

3.3 Discussion

In this chapter, I explored how PAR-3 asymmetries are maintained in the *C. elegans* zygote in the absence of posterior inhibition from PAR-1. I quantified asymmetries in the sizes of

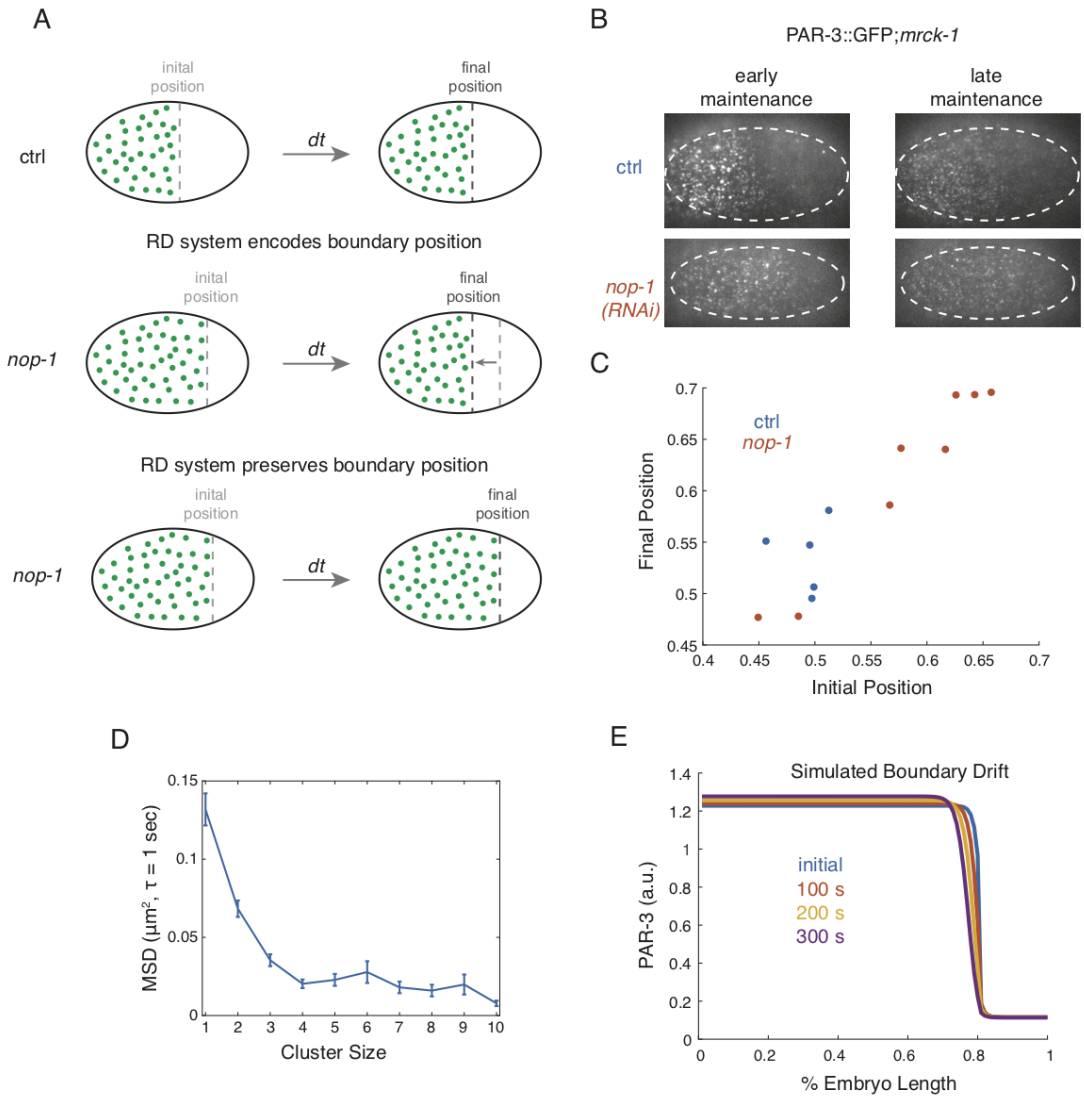

Figure 3.4: **The position of the PAR-3 domain boundary is determined by actomyosin flows, not encoded by a reaction-diffusion system. (A)** Schematic illustration two different ways the PAR protein reaction-diffusion system could influence the position of PAR-3 domain boundaries. In the middle row, the reaction diffusion system determines a unique boundary position based on reaction rates, diffusion rates, and total amounts of PAR proteins. If the boundary position is shifted posterior to its wild type position at the onset of maintenance phase, it will shift to the wild type position over the course of maintenance phase, even in the absence of cortical flows. In the bottom row, the reaction diffusion system simply preserves arbitrary boundary positions. If the position is shifted posterior to wild type at the onset of maintenance phase, it will remain at that shifted position instead of gradually "correcting" to the wild type position in the absence of cortical flow. (legend continued on next page)

Figure 3.4: (continued) **(B)** Representative micrographs showing the distribution of PAR-3 in early and late maintenance phase in mrck-1 embryos that lack maintenance phase cortical flows. Embryos in the top row are controls, and embryos in the bottom row are partially depleted of NOP-1 through RNAi, which weakens establishment phase flows and tends to position the PAR-3 domain boundary posterior to wild type embryos at the onset of maintenance phase. **(C)** Comparisons of the boundary positions in early and late maintenance phase for control (blue) and *nop-1 (RNAi)* embryos. Boundary position is defined at the position along the embryo length at which PAR-3 fluorescence density drops below the halfway point between its maximum and minimum values. **(D)** Mean squared displacement over 1 second intervals as a function of inferred PAR-3 oligomer size. Bold line indicates the mean and error bars indicate the S.E.M. (n = 3 embryos). **(E)** Simulated boundary drift for an embryos over 300 seconds using a model constrained by experimental measurements.

PAR-3 oligomers in the anterior and posterior membrane and demonstrated a size-dependent decrease in dissociation rates of PAR-3 oligomers from the membrane. I showed that asymmetries in the distributions of PAR-3 oligomers are dynamically maintained and that the recruitment of new PAR-3 monomers to the cell exhibits an anterior bias. I presented evidence that the combination of feedback on monomer recruitment, dynamic oligomerization, and avidity effects enables stable PAR-3 asymmetries, and that these processes are in turn regulated by interactions with other anterior PAR proteins. Finally, I show that the positions of PAR-3 domain boundaries are not encoded by a reaction diffusion system, as other studies have proposed, and propose that oligomer size-dependent decreases in PAR-3 mobility effectively preserve arbitrary domain boundaries for the duration of polarity maintenance.

These results challenge existing models of PAR polarity maintenance in two significant ways. First, while previous studies have shown that inhibition by posterior PARs is insufficient to robustly exclude anterior PARs from the membrane [126, 89], this is the first description a feedback mechanism for maintaining aPAR asymmetries that is independent of pPARs. Second, while most existing mathematical models of PAR asymmetries assert that PAR boundary positions are specified through a reaction-diffusion mechanism called "wave-pinning" [43, 89], we show that reaction-diffusion mechanisms preserve arbitrary boundary positions that are instead specified by patterns of actomyosin flow. The findings in this

chapter are also significant in that they show how the principles outlined in Chapter 2 are instantiated in a real cellular context. They offer empirical support for the two main ideas in Chapter 2, namely that oligomerization enables self-stabilizing asymmetries when combined with even weak positive feedback, and that oligomerization can enable a reaction-diffusion mechanism to effectively remember arbitrary boundary positions. It will be interesting in the future to determine if oligomerization endows other polarity circuits with the same properties.

Several results in this chapter strongly point to the idea that there is positive feedback on the recruitment of PAR-3 monomers. However, the molecular source of that feedback remains elusive. One tempting possibility is that it is related to asymmetries in the distribution of F-actin, or F-actin binding proteins, at the cell membrane. Support for this hypothesis comes from the observation that PAR-3 asymmetries are not maintained in embryos were F-actin is disassembled (Fig. 3.9). Further, asymmetries in PAR-3 recruitment rates are lost in embryos lacking CDC-42, which, in addition to recruiting PAR-6/PKC-3 to the membrane, promotes actin polymerization. However, in both of these conditions, PAR-3 levels increase in the posterior rather than decreasing in the anterior. This observation rules out a simple relationship between F-actin density and PAR-3 accumulation, but leaves open the possibility that differences in F-actin organization in the anterior and posterior influence the local recruitment or oligomerization of PAR-3 monomers.

In the *C. elegans* zygote, multiple redundant sources of feedback stabilize PAR protein asymmetries. This raises the question of why these redundant mechanisms exist. A simple answer may be that redundancy increases the robustness of polarity maintenance to the intrinsic noise of dynamic molecular processes. However, another possibility is that different sets of feedback mechanisms are essential for polarity establishment and/or maintenance in different cellular contexts. For example, while inhibition of PAR-3 by PAR-1 and mechanochemical feedback between aPARs and actomyosin contractility play key roles in

polarity establishment in the *C. elegans* zygote, polarized inactivation of CDC-42 is required for symmetry breaking in the 4-cell embryo. It will be interesting in the future to determine whether positive feedback on PAR-3 recruitment to the membrane plays a key role in some other context, such as the 2-cell *C. elegans* embryo where the mechanisms for polarity establishment are currently unknown.

3.4 Materials and Methods

3.4.1 C. elegans culture and RNAi

I cultured *C. elegans* strains under standard conditions [18]. EM312, EM307, and EM292 were provided by Kenneth Kemphues, EM241 came from the CGC, and EM327 came from Daniel Dickinson.

I performed RNAi experiments using the feeding method [145]. I used a 12-16 hour feeding time for *perm-1 RNAi* and a 24 hour feeding time at 25 C for all others.

3.4.2 Live imaging

For single molecule imaging experiments, I mounted embryos in egg salts containing 21 μm diameter polystyrene beads. For all other experiments, I mounted embryos in eggs salts on agarose pads.

I collected near-total internal reflection fluorescence (TIRF) images using an Olympus IX71 inverted microscope equipped with an Olympus OMAC TIRF illumination system, a 50 mW, 481 nm Sapphire laser (Coherent), and an Andor iXon3 897 EM-CCD camera. Fast single molecule imaging was conducted in streaming acquisition mode with 50 μs exposure and 100 % laser power. Slow imaging was conducted at 1 second intervals with 50 μs exposure and 30 % laser power.

3.4.3 Image analysis

All image analyses were carried out in MATLAB. Particle detection and tracking were carried out as previously described [125, 130].

3.5 Supplementary Figures

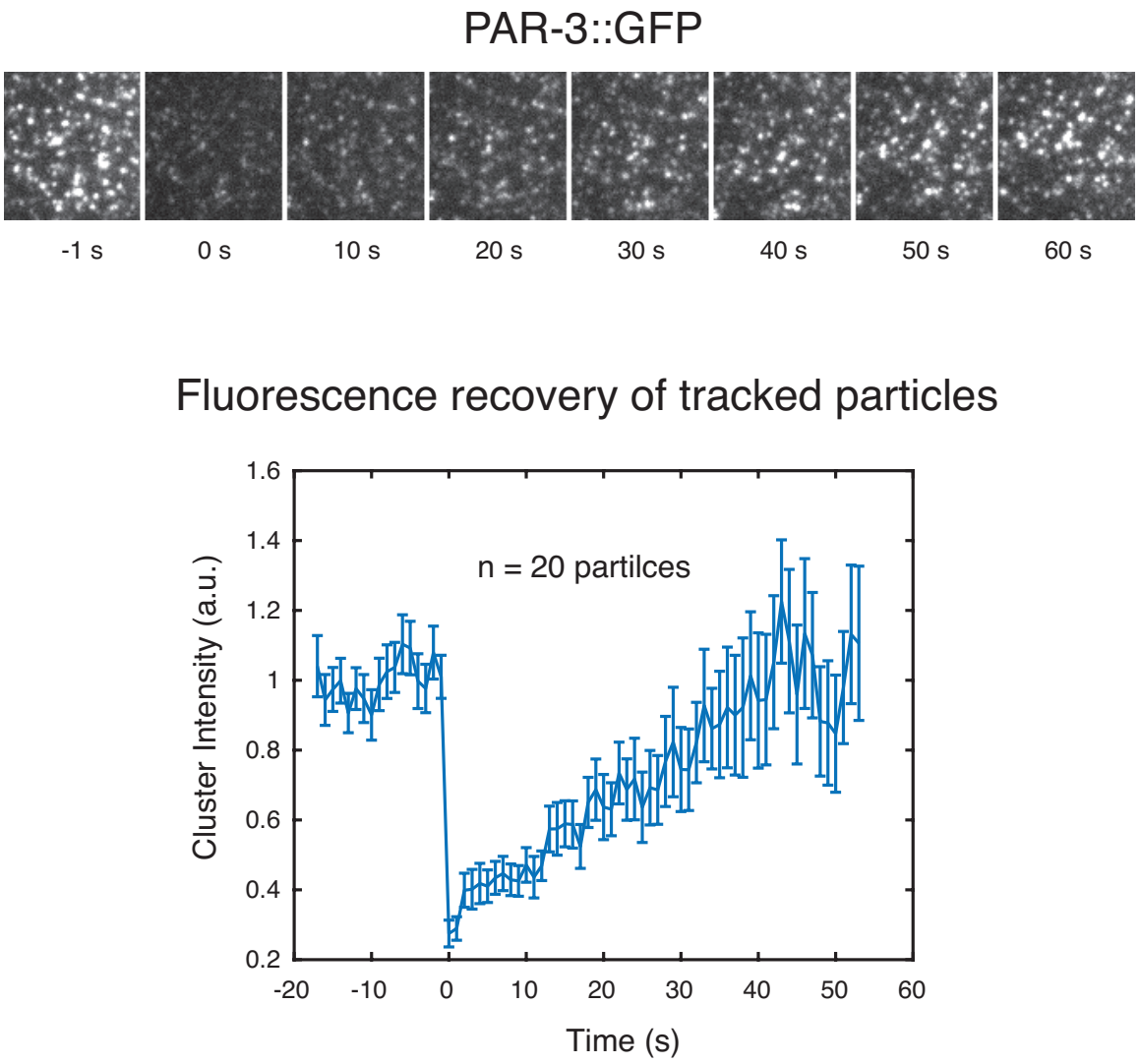

Figure 3.5: **Subunits turnover within PAR-3 oligomers.** FRAP experiment in interphase. The micrographs on top show PAR-3 oligomers directly before and after photobleaching. The graph on bottom shows the mean fluorescence intensity of 20 particles that could be tracked through photobleaching. Error bars show the S.E.M.

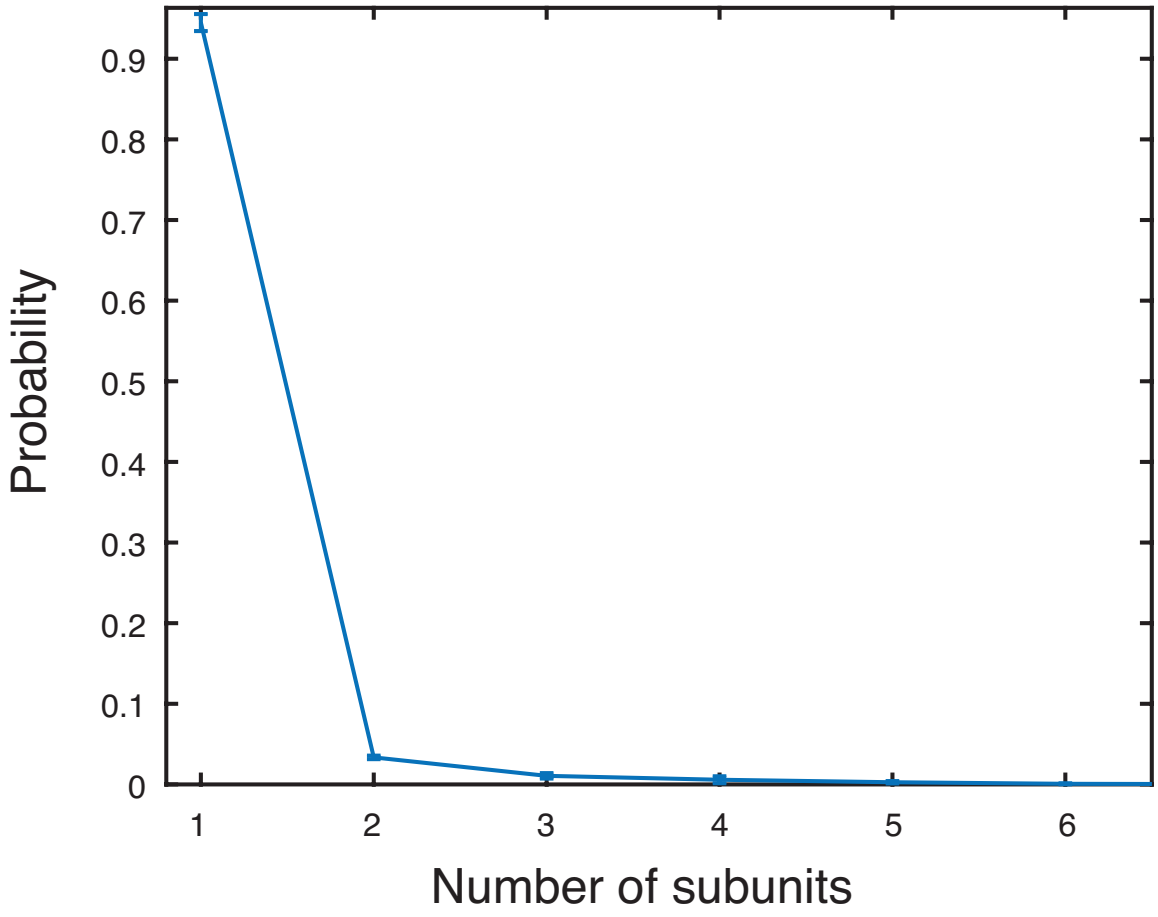

Figure 3.6: **Sizes of newly bound PAR-3 particles.** Probability distribution for the sizes of newly bound mN::PAR-3 particles, inferred from the distribution of single molecule intensities and the initial intensities of particles when they appear on the membrane.

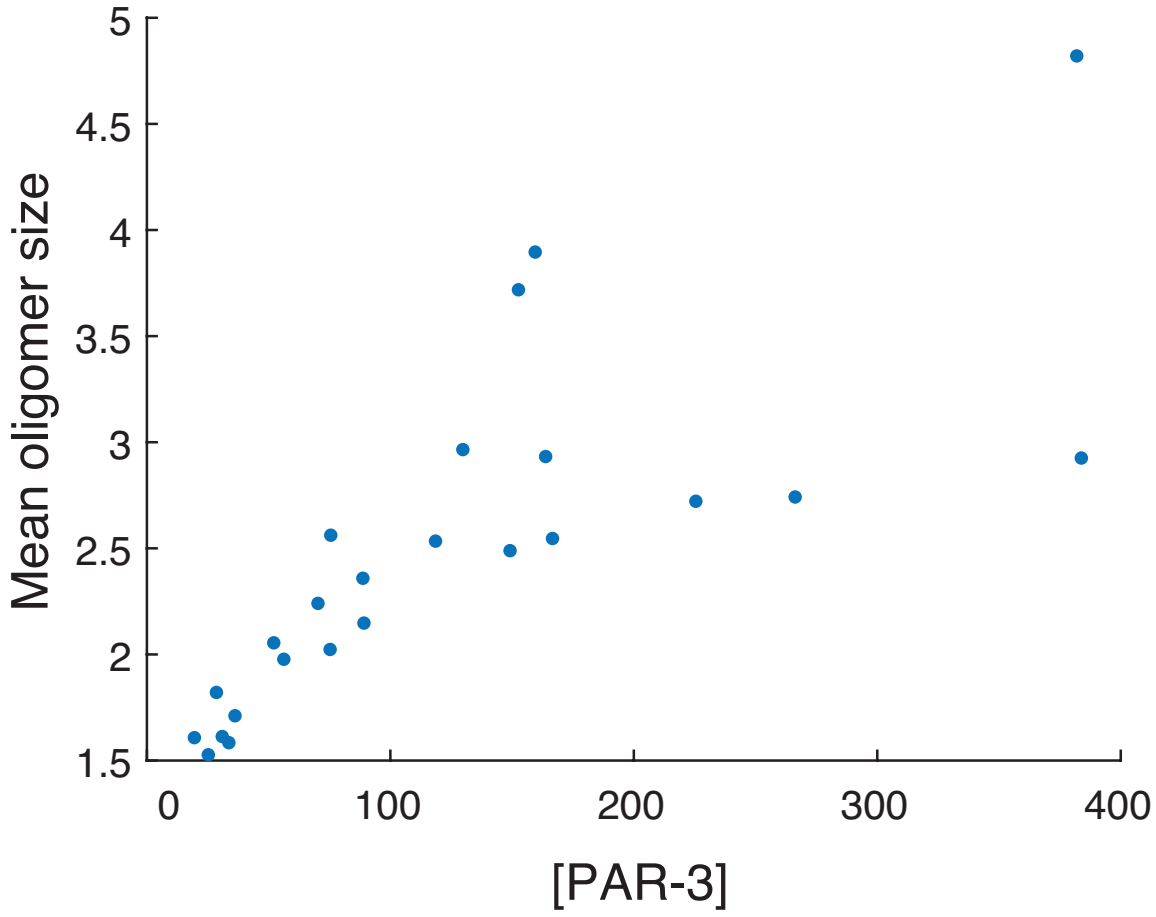

Figure 3.7: **Local PAR-3 concentration correlates with mean oligomer size.** Mean oligomers size plotted against concentration of PAR-3 (arbitrary units) in the anterior membrane of embryos with varying levels of PAR-3 depletion.

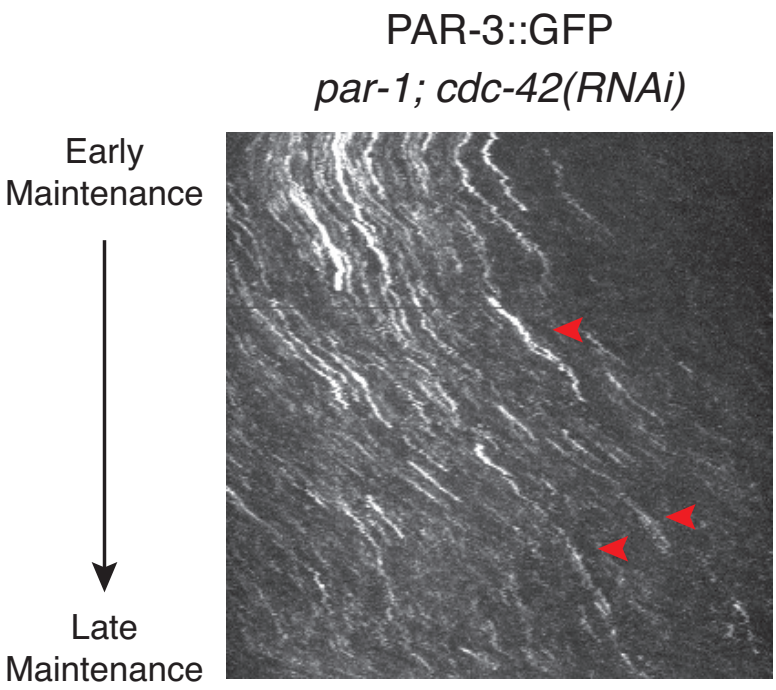

Figure 3.8: **Some *cdc-42;par-1* double mutant embryos exhibit posterior-directed cortical flows.** Example kymograph of a *par-1/cdc-42 (RNAi)* double mutant embryo with pronounced posterior-directed cortical flows. The top of the kymograph corresponds to early maintenance phase and the bottom corresponds to later maintenance phase. The left of the kymograph corresponds to the anterior of the embryo, and the right corresponds to the posterior. Diagonal streaks, marked by red arrowheads, indicate posterior flow of PAR-3 oligomers.

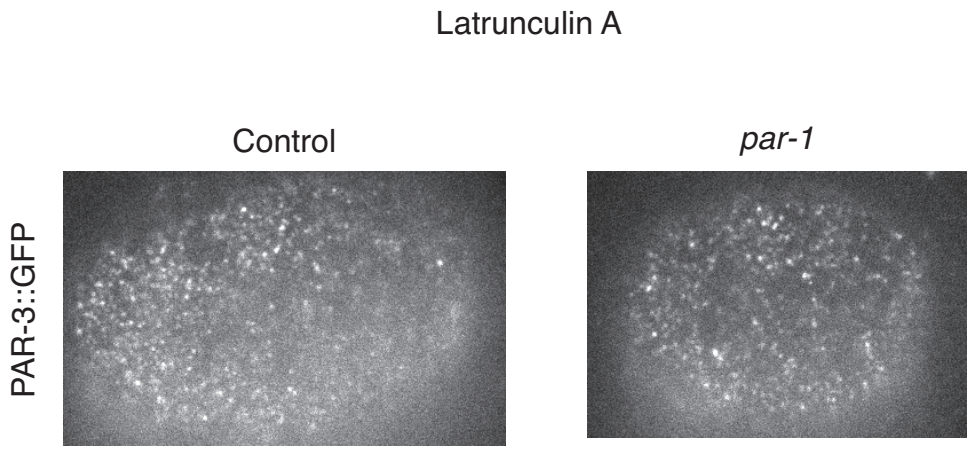

Figure 3.9: **F-actin is required for maintenance of PAR-3 asymmetries in *par-1* mutant embryos.** Representative micrographs showing that an intact actin cytoskeleton is not required to maintain PAR-3 asymmetries in control embryos, but is required in *par-1* mutants. Polarity was established prior to addition of 10 μM of the actin-depolymerizing drug Latrunculin A. Micrographs were taken 2 minutes after addition of the drug.

CHAPTER 4

OUTLOOK AND LOOSE ENDS

In this dissertation, I have discussed how cell polarity is enabled by self-stabilizing asymmetries in the distributions of key polarity proteins. I have described how these proteins interact to form core polarity circuits, and have focused on the roles protein oligomerization can play in these circuits, both in theory and in the specific example of PAR-3 asymmetries in the *C. elegans* zygote. In this final chapter, I will discuss two future directions suggested by the projects described above, as well as my views on when mathematical modeling of PAR polarity is appropriate. I will close by discussing a project that I initiated late in graduate school but did not end up pursuing on how PAR-3 distributions shape PAR-6/PKC-3 asymmetries in the *C. elegans* zygote.

4.1 Oligomeric polarity proteins in other systems

In Chapter 2 of this dissertation, I presented a modeling framework to show how oligomerization enables stable polarization of peripheral membrane proteins combined with even weak linear feedback. I used this model to explain how PAR-3 asymmetries are stabilized in Chapter 3, but there are at least two other systems where this modeling framework may apply.

The first system is SOSEKI protein polarity in plants. The SOSEKI proteins are a family of peripheral membrane binding proteins that oligomerize through a DIX domain [167]. Discovered in *Arabidopsis*, they are widely conserved in plants and are asymmetrically localized at the surfaces of a range of different cell types [167, 151]. Although the feedback mechanisms that stabilize SOSEKI asymmetries are unknown, mutations that impair oligomerization abolish polarity. It is therefore tempting to speculate that oligomerization and avidity effects introduce nonlinearities to the feedback circuit that polarizes these proteins.

The second system is the PCP proteins. Here, integral membrane proteins are clustered upon binding to oligomeric cytoplasmic proteins, and clustering has been shown to amplify PCP protein asymmetries. In this system, avidity effects are unlikely to meaningfully increase residence time, since turnover of integral membrane proteins is primarily mediated by endocytosis. However, if a negative relationship exists between cluster size and endocytosis rates, clustering in this system could play an analogous role to avidity effects in peripheral membrane protein polarity, and a similar model to the one I used in my work could be employed. Additionally, it would be interesting to use models to investigate whether role size-dependent cluster mobility could play any role in amplifying or stabilizing PCP protein polarity.

4.2 Feedback on PAR-3 accumulation

Previous studies of PAR polarity have focused on feedback through mutual antagonism. In my work, I have provided evidence for positive feedback on the local binding rates of PAR-3 to the membrane. While this feedback mechanism appears to be redundant in the *C. elegans* zygote, there may be other contexts where it plays a more central role. For example, as discussed above, different feedback mechanisms are utilized in polarizing the 4-cell embryo and the zygote. Positive feedback on PAR-3 binding rates may be required for polarization of other blastomeres, such as in the 2-cell embryo where the mechanisms for polarization are unknown. Further, outside of the *C. elegans* embryo, positive feedback on PAR-3 binding may be required for stabilizing monopolar PAR asymmetries in contexts where there is no evidence of mutual antagonism between PAR proteins, such as *Drosophila* neuroblasts or neurons.

While I provide evidence for the existence of feedback on PAR-3 binding rates, I was unable to identify the mechanism. One possibility, discussed above, is that feedback is mediated by the local architecture of the actin cytoskeleton or some actin binding protein.

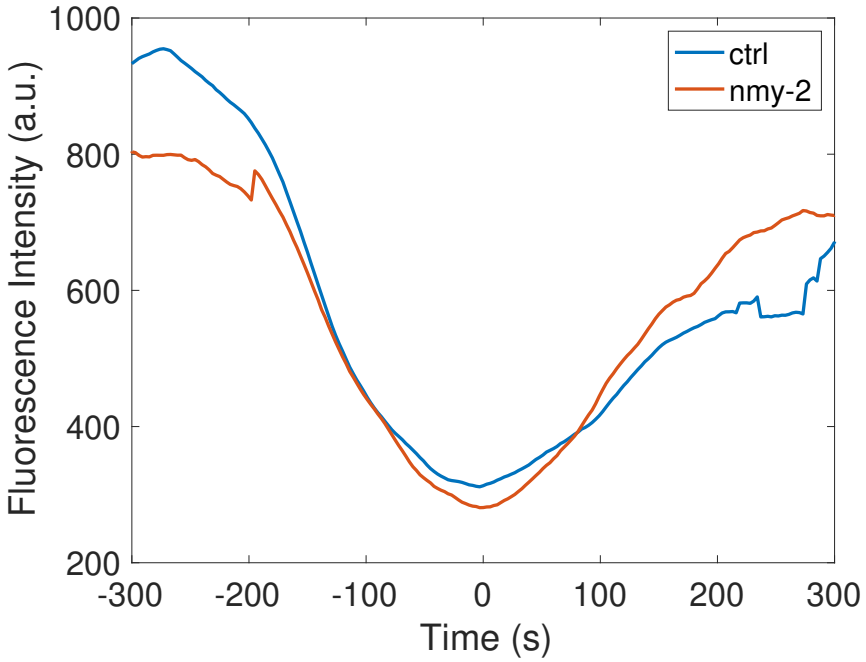

Figure 4.1: **Actomyosin contractility does not regulate PAR-3 oligomerization.** Integrated fluorescence density of PAR-3 puncta in WT versus *nmy-2* embryos, aligned to the onset of maintenance phase (t=0 s).

This is supported by the observations that PAR-3 polarity is lost in *par-1* embryos when F-actin is depolymerized (Fig. 3.9) or when CDC-42, an regulator of actin polymerization, is depleted (Fig. 3.3). This hypothesis is worth pursuing, but further evidence is required.

Another possibility is that feedback involves mechanical forces. One previous study showed evidence that actomyosin contractility promotes PAR-3 oligomerization [154]. Since PAR-3 locally promotes contractility, this could be a possible feedback mechanism. However, I failed to reproduce the findings of this paper in identical experiments (Fig. 4.1) and therefore think this type of feedback is unlikely.

A third possibility is that feedback comes through direct binding of cytoplasmic PAR-3 monomers to membrane-bound oligomers. In the second chapter of this dissertation, I showed that direct binding can constitute a form of positive feedback if detailed balance is broken in such a way that there is net flux of molecules from the cytoplasm into oligomers.

Detailed balance could be broken in this system by, for example, irreversible phosphorylation of PAR-3 by PKC-3 at the cell membrane. While this hypothesis is hard to test, it could be supported by measuring the fraction of PAR-3 monomers that are recruited to the cell surface by binding directly to PAR-3 oligomers versus to the cell membrane. Further, a role for PAR-3 phosphorylation by PKC-3 in promoting feedback could be tested using small molecule inhibitors of PKC-3 kinase activity.

4.3 Mathematical modeling of PAR polarity in the *C. elegans* zygote: when is it useful?

Mathematical modeling has become increasingly ubiquitous in papers on *C. elegans* blastomere polarity [44, 130, 5, 51, 69, 89, 21]. In some of these cases mathematical modeling is necessary to illustrate a novel theoretical idea, formalize a complex hypothesis or interpret a puzzling result. For example, modeling is necessary to explain the idea of wave-pinning in Goehring et al. [44], which they invoke to explain the result that PAR boundaries shift anterior and posterior when aPARs and pPARs are respectively depleted. While I do not think that wave-pinning mechanisms determine boundary positions in the *C. elegans* zygote (see chapter 3), this was a reasonable hypothesis at the time, and a novel idea which would not be intuitively understood without a model. In other cases, a combination of experimental measurements and modeling can be used to effectively show that specific theoretical conditions are satisfied in the *C. elegans* zygote. For example, Sailer et al. combine modeling and experimental measurements to demonstrate bistable dynamics in a feedback circuit between aPARs and CHIN-1 [130]. However, there are other examples where the modeling is unnecessary and even misleading.

One such example is the modeling performed in Lim et al. [89]. In this paper, the authors use careful and clever experiments to show that altering the relative amounts of aPARs and pPARs in the *C. elegans* embryo can induce ectopic polarization of the AB blastomere, which

is unpolarized in wild type embryos. This is an interesting finding, and is consistent with the established principle that models with nonlinear feedback through mutual antagonism and finite pools of polarity proteins will only exhibit bistability if the relative amounts of opposing proteins fall within some range of values. Instead of simply pointing out that the result is consistent with a very general class of models, the authors constructed a specific and complicated model that they claimed was constrained by experimental measurements. However, their specific model contains several unsubstantiated assumptions and the ability of their model to explain this experimental result is not dependent on the parameters that they were actually able to constrain. Rather, the ability to reproduce this finding was treated as a constraint on model parameters. Therefore, the success of their model in reproducing this finding is in no way a vindication of their specific model assumptions, a confirmation of the accuracy of any of their measured parameter values, or an indication that further predictions of the model would be accurate. A toy model would have sufficed to interpret their data, and would not have misled readers into thinking that their specific model had predictive power. Going forward, I do not think it is worthwhile for researchers in this field to perform mathematical modeling unless the purpose is either to introduce a new theoretical principle to the field, or to present independent parameter measurements that demonstrate that some established theoretical principle applies to PAR polarity.

4.4 Coupling between PAR-3 and PAR-6/PKC-3 asymmetries in the *C. elegans* zygote

My dissertation adds to the existing body of work showing how PAR-3 and CDC-42 are concentrated in the anterior membrane in maintenance phase. However, it is yet unclear how PAR-3 and CDC-42 asymmetries shape the distribution of PAR-6/PKC-3. We know that PAR-6/PKC-3 asymmetries are maintained through asymmetries in membrane binding rates, not dissociation rates [125, 130]. Further, we know that PAR-6 binds directly to active

CDC-42, and that a majority of PAR-6/PKC-3 is bound to CDC-42 during maintenance phase. Therefore, one would expect that in *chin-1* mutants, where CDC-42 is uniform at the membrane, PAR-6/PKC-3 asymmetries would be lost. However, previous work from our lab shows asymmetries in PAR-6 binding events are unchanged under those conditions, suggesting that cytoplasmic PAR-6/PKC-3 dimers cannot bind directly to active CDC-42 at the membrane.

Classical studies have shown that PAR-6/PKC-3 localizes to the cortex in two distinct pools: one diffuse and one punctate [10]. CDC-42 is required for the diffuse pool and PAR-3 is required for the punctate pool, presumably because they consist of PAR-6/PKC-3 dimers bound directly to CDC-42 and PAR-3 respectively [10]. However, PAR-3 is also required for the diffuse pool, suggesting that PAR-3 somehow promotes the binding of PAR-6 to CDC-42 [10]. This result is consistent with the finding that PAR-6 binding events are symmetrically distributed in *chin-1/par-1* double mutants, where active CDC-42 is uniform and PAR-3 levels are increased relative to wild type [130, discussed in chapter 1]. Interestingly, this result is also consistent with the observation in epithelia that apical domains enriched in PAR-6/aPKC require PAR-3, even though PAR-3 and PAR-6/aPKC distributions overlap minimally.

One general class of models that has been proposed to explain this observation is that binding of PAR-6/PKC-3 to PAR-3 at the cell membrane enables it to be subsequently transferred to active CDC-42 [126, 108] (Fig. 4.2A). There are many possible molecular mechanisms for how this could work. For example, the chaperone protein CDC-37 blocks association of PAR-6/PKC-3 with CDC-42, but not PAR-3, and one could imagine a scenario where binding to PAR-3 displaces CDC-37 and allows PAR-6 to bind CDC-42. However, any model requires that there is net flux of PAR-6/PKC-3 from a PAR-3 bound state to CDC-42 bound state. Failure to observe directional flux would falsify this model. I believe I have collected data that could be used to infer flux of PAR-6/PKC-3 between different

binding states at the membrane.

At the end of my time in the Munro lab, I used single molecule imaging measure mobilities of PAR-6 molecules bound to either PAR-3 or CDC-42. To isolate the pool bound to PAR-3, I imaged a PAR-6::GFP transgene with a mutation in its semi-CRIB domain that prevents it from binding to CDC-42. To isolate the CDC-42 bound pool, I imaged PAR-6::GFP in *cdc-37 (RNAi)* embryos. I found that the mean frame-to-frame displacements of PAR-3-bound molecules were significantly shorter than those of CDC-42-bound molecules, while wild type molecules exhibited intermediate displacements (Fig. 4.2B). Based on this observation, it seems possible to infer the binding state of a molecule at a given time point based on its displacement in space from the previous time point. However, although the mean displacements are starkly different, the distributions of displacements for these two pool overlap substantially (Fig. 4.2C). Therefore, use of a statistical model such as a Hidden Markov model may be necessary to infer the most likely binding state [31, 117]. In this framework, the hidden state would be the binding partner and the emission probabilities would be empirically determined distributions of displacements. This model could be used to estimate transition probabilities, which could in turn be used to infer the relative fluxes between states. While I was unable to follow through on this project, it seems like challenging yet straightforward analysis for someone to do that could shed light on a fundamental question in the field.

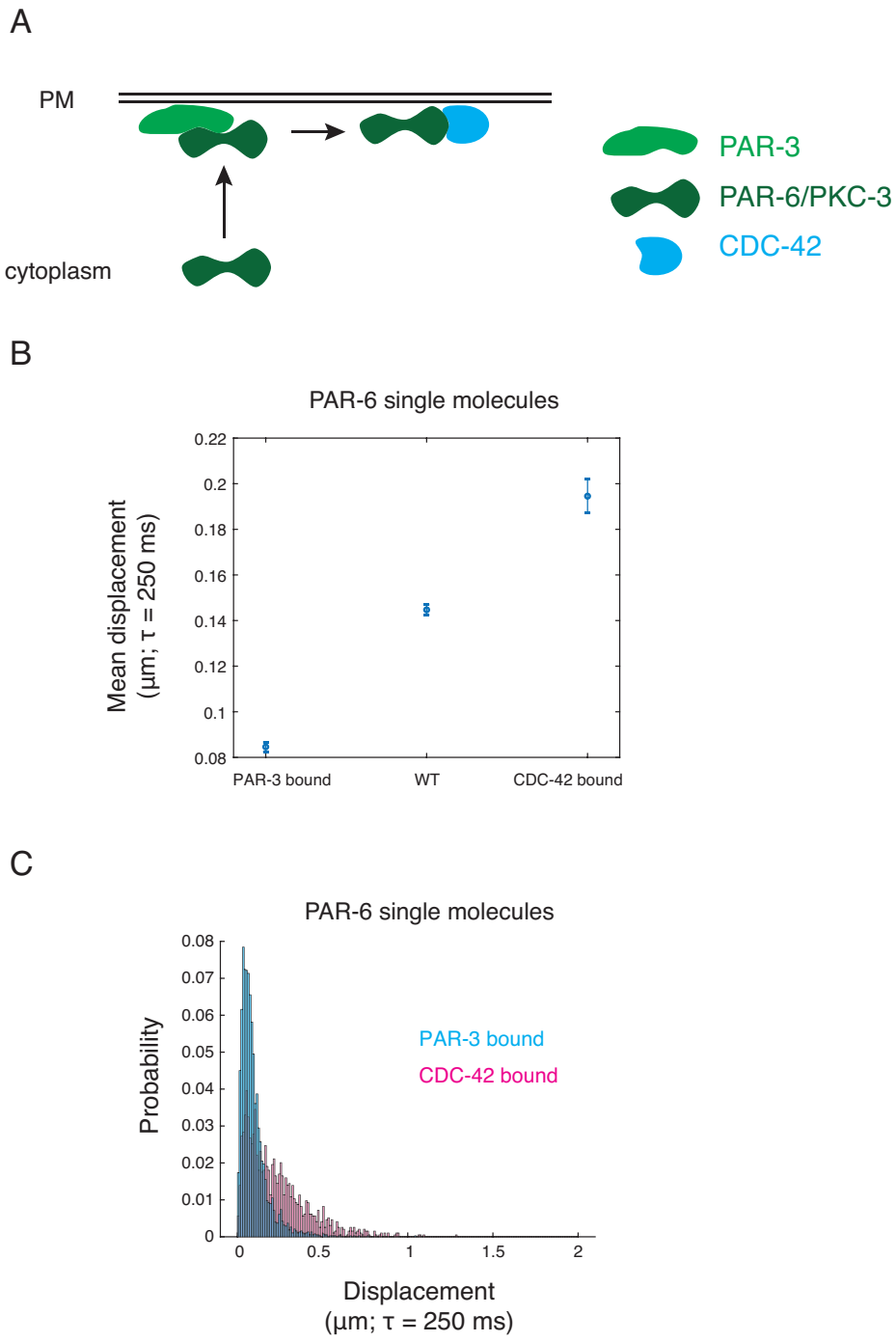

Figure 4.2: **PAR-3 loads PAR-6 onto the membrane.(A)** Schematic illustrating the hypothesis that PAR-6/PKC-3 must first form a complex with PAR-3 at the cell membrane in order to bind to CDC-42. **(B)** Mean displacement of single molecules of PAR-6 in WT conditions, as well as in genetic conditions that cause them to be bound exclusively to PAR-3 and CDC-42. **(C)** Histograms of the displacements of single PAR-6 molecules bound to PAR-3 and CDC-42.

REFERENCES

[1] D. Aceto, M. Beers, and K. J. Kemphues. Interaction of PAR-6 with CDC-42 is required for maintenance but not establishment of PAR asymmetry in C. elegans. *Dev Biol*, 299(2):386–397, Nov 2006.

[2] S. J. Altschuler, S. B. Angenent, Y. Wang, and L. F. Wu. On the spontaneous emergence of cell polarity. *Nature*, 454(7206):886–889, Aug 2008.

[3] K. Amonlirdviman, N. A. Khare, D. R. Tree, W. S. Chen, J. D. Axelrod, and C. J. Tomlin. Mathematical modeling of planar cell polarity to understand domineering nonautonomy. *Science*, 307(5708):423–426, Jan 2005.

[4] D. C. Anderson, J. S. Gill, R. M. Cinalli, and J. Nance. Polarization of the C. elegans embryo by RhoGAP-mediated exclusion of PAR-6 from cell contacts. *Science*, 320(5884):1771–1774, Jun 2008.

[5] Y. Arata, M. Hiroshima, C. G. Pack, R. Ramanujam, F. Motegi, K. Nakazato, Y. Shindo, P. W. Wiseman, H. Sawa, T. J. Kobayashi, H. B. Brandão, T. Shibata, and Y. Sako. Cortical Polarity of the RING Protein PAR-2 Is Maintained by Exchange Rate Kinetics at the Cortical-Cytoplasmic Boundary. *Cell Rep*, 16(8):2156–2168, 08 2016.

[6] M. J. Bailey and K. E. Prehoda. Establishment of Par-Polarized Cortical Domains via Phosphoregulated Membrane Motifs. *Dev Cell*, 35(2):199–210, Oct 2015.

[7] R. M. Barry, A. F. Bitbol, A. Lorestani, E. J. Charles, C. H. Habrian, J. M. Hansen, H. J. Li, E. P. Baldwin, N. S. Wingreen, J. M. Kollman, and Z. Gitai. Large-scale filament formation inhibits the activity of CTP synthetase. *Elife*, 3:e03638, Jul 2014.

[8] A. Beatty, D. Morton, and K. Kemphues. The C. elegans homolog of Drosophila Lethal giant larvae functions redundantly with PAR-2 to maintain polarity in the early embryo. *Development*, 137(23):3995–4004, Dec 2010.

[9] A. Beatty, D. G. Morton, and K. Kemphues. PAR-2, LGL-1 and the CDC-42 GAP CHIN-1 act in distinct pathways to maintain polarity in the C. elegans embryo. *Development*, 140(9):2005–2014, May 2013.

[10] M. Beers and K. Kemphues. Depletion of the co-chaperone CDC-37 reveals two modes of PAR-6 cortical association in C. elegans embryos. *Development*, 133(19):3745–3754, Oct 2006.

[11] R. Benton and D. St Johnston. A conserved oligomerization domain in drosophila Bazooka/PAR-3 is important for apical localization and epithelial polarity. *Curr Biol*, 13(15):1330–1334, Aug 2003.

[12] R. Benton and D. St Johnston. Drosophila PAR-1 and 14-3-3 inhibit Bazooka/PAR-3 to establish complementary cortical domains in polarized cells. *Cell*, 115(6):691–704, Dec 2003.

[13] H. C. Berg and E. M. Purcell. Physics of chemoreception. *Biophys J*, 20(2):193–219, Nov 1977.

[14] C. C. Bicho, D. A. Kelly, H. A. Snaith, A. B. Goryachev, and K. E. Sawin. A catalytic role for Mod5 in the formation of the Tea1 cell polarity landmark. *Curr Biol*, 20(19):1752–1757, Oct 2010.

[15] D. Bienkowska and C. R. Cowan. Centrosomes can initiate a polarity axis from any position within one-cell C. elegans embryos. *Curr Biol*, 22(7):583–589, Apr 2012.

[16] L. Boyd, S. Guo, D. Levitan, D. T. Stinchcomb, and K. J. Kemphues. PAR-2 is asymmetrically distributed and promotes association of P granules and PAR-1 with the cortex in C. elegans embryos. *Development*, 122(10):3075–3084, Oct 1996.

[17] C. P. Brangwynne, C. R. Eckmann, D. S. Courson, A. Rybarska, C. Hoege, J. Gharakhani, F. Jülicher, and A. A. Hyman. Germline P granules are liquid droplets that localize by controlled dissolution/condensation. *Science*, 324(5935):1729–1732, Jun 2009.

[18] S. Brenner. The genetics of Caenorhabditis elegans. *Genetics*, 77(1):71–94, May 1974.

[19] M. T. Butler and J. B. Wallingford. Planar cell polarity in development and disease. *Nat Rev Mol Cell Biol*, 18(6):375–388, 06 2017.

[20] L. B. Case, X. Zhang, J. A. Ditlev, and M. K. Rosen. Stoichiometry controls activity of phase-separated clusters of actin signaling proteins. *Science*, 363(6431):1093–1097, 03 2019.

[21] Yiran Chang and Daniel J. Dickinson. A particle size threshold governs diffusion and segregation of par-3 during cell polarization. *Cell Reports*, 39(2), Apr 2022.

[22] A. H. Chau, J. M. Walter, J. Gerardin, C. Tang, and W. A. Lim. Designing synthetic regulatory networks capable of self-organizing cell polarization. *Cell*, 151(2):320–332, Oct 2012.

[23] R. J. Cheeks, J. C. Canman, W. N. Gabriel, N. Meyer, S. Strome, and B. Goldstein. C. elegans PAR proteins function by mobilizing and stabilizing asymmetrically localized protein complexes. *Curr Biol*, 14(10):851–862, May 2004.

[24] S. Chen, J. Chen, H. Shi, M. Wei, D. R. Castaneda-Castellanos, R. S. Bultje, X. Pei, A. R. Kriegstein, M. Zhang, and S. H. Shi. Regulation of microtubule stability and organization by mammalian Par3 in specifying neuronal polarity. *Dev Cell*, 24(1):26–40, Jan 2013.

[25] W. S. Chen, D. Antic, M. Matis, C. Y. Logan, M. Povelones, G. A. Anderson, R. Nusse, and J. D. Axelrod. Asymmetric homotypic interactions of the atypical cadherin flamingo mediate intercellular polarity signaling. *Cell*, 133(6):1093–1105, Jun 2008.

[26] J. G. Chiou, K. D. Moran, and D. J. Lew. How cells determine the number of polarity sites. *Elife*, 10, 04 2021.

[27] J. G. Chiou, S. A. Ramirez, T. C. Elston, T. P. Witelski, D. G. Schaeffer, and D. J. Lew. Principles that govern competition or co-existence in Rho-GTPase driven polarization. *PLoS Comput Biol*, 14(4):e1006095, 04 2018.

[28] B. Cho, G. Pierre-Louis, A. Sagner, S. Eaton, and J. D. Axelrod. Clustering and negative feedback by endocytosis in planar cell polarity signaling is modulated by ubiquitinylation of prickle. *PLoS Genet*, 11(5):e1005259, May 2015.

[29] C. R. Cowan and A. A. Hyman. Centrosomes direct cell polarity independently of microtubule assembly in C. elegans embryos. *Nature*, 431(7004):92–96, Sep 2004.

[30] A. A. Cuenca, A. Schetter, D. Aceto, K. Kemphues, and G. Seydoux. Polarization of the C. elegans zygote proceeds via distinct establishment and maintenance phases. *Development*, 130(7):1255–1265, Apr 2003.

[31] R. Das, C. W. Cairo, and D. Coombs. A hidden Markov model for single particle tracks quantifies dynamic interactions between LFA-1 and the actin cytoskeleton. *PLoS Comput Biol*, 5(11):e1000556, Nov 2009.

[32] A. T. Dawes and E. M. Munro. PAR-3 oligomerization may provide an actin-independent mechanism to maintain distinct par protein domains in the early Caenorhabditis elegans embryo. *Biophys J*, 101(6):1412–1422, Sep 2011.

[33] E. Denker, I. Bocina, and D. Jiang. Tubulogenesis in a simple cell cord requires the formation of bi-apical cells through two discrete Par domains. *Development*, 140(14):2985–2996, Jul 2013.

[34] D. J. Dickinson, F. Schwager, L. Pintard, M. Gotta, and B. Goldstein. A Single-Cell Biochemistry Approach Reveals PAR Complex Dynamics during Cell Polarization. *Dev Cell*, 42(4):416–434, 08 2017.

[35] E. Dine, A. A. Gil, G. Uribe, C. P. Brangwynne, and J. E. Toettcher. Protein Phase Separation Provides Long-Term Memory of Transient Spatial Stimuli. *Cell Syst*, 6(6):655–663, 06 2018.

[36] J. A. Ditlev, A. R. Vega, D. V. Köster, X. Su, T. Tani, A. M. Lakoduk, R. D. Vale, S. Mayor, K. Jaqaman, and M. K. Rosen. A composition-dependent molecular clutch between T cell signaling condensates and actin. *Elife*, 8, 07 2019.

[37] J. Dodgson, A. Chessel, M. Yamamoto, F. Vaggi, S. Cox, E. Rosten, D. Albrecht, M. Geymonat, A. Csikasz-Nagy, M. Sato, and R. E. Carazo-Salas. Spatial segregation of polarity factors into distinct cortical clusters is required for cell polarity control. *Nat Commun*, 4:1834, 2013.

[38] B. Etemad-Moghadam, S. Guo, and K. J. Kemphues. Asymmetrically distributed PAR-3 protein contributes to cell polarity and spindle alignment in early C. elegans embryos. *Cell*, 83(5):743–752, Dec 1995.

[39] W. Feng, H. Wu, L. N. Chan, and M. Zhang. The Par-3 NTD adopts a PB1-like structure required for Par-3 oligomerization and membrane localization. *EMBO J*, 26(11):2786–2796, Jun 2007.

[40] M. Feric and C. P. Brangwynne. A nuclear F-actin scaffold stabilizes ribonucleoprotein droplets against gravity in large cells. *Nat Cell Biol*, 15(10):1253–1259, Oct 2013.

[41] M. Fiedler, C. Mendoza-Topaz, T. J. Rutherford, J. Mieszczanek, and M. Bienz. Dishevelled interacts with the DIX domain polymerization interface of Axin to interfere with its function in down-regulating β-catenin. *Proc Natl Acad Sci U S A*, 108(5):1937–1942, Feb 2011.

[42] A. W. Folkmann, A. Putnam, C. F. Lee, and G. Seydoux. Regulation of biomolecular condensates by interfacial protein clusters. *Science*, 373(6560):1218–1224, 09 2021.

[43] N. W. Goehring, C. Hoege, S. W. Grill, and A. A. Hyman. PAR proteins diffuse freely across the anterior-posterior boundary in polarized C. elegans embryos. *J Cell Biol*, 193(3):583–594, May 2011.

[44] N. W. Goehring, P. K. Trong, J. S. Bois, D. Chowdhury, E. M. Nicola, A. A. Hyman, and S. W. Grill. Polarization of PAR proteins by advective triggering of a pattern-forming system. *Science*, 334(6059):1137–1141, Nov 2011.

[45] B. Goldstein and I. G. Macara. The PAR proteins: fundamental players in animal cell polarization. *Dev Cell*, 13(5):609–622, Nov 2007.

[46] D. S. Goodsell and A. J. Olson. Structural symmetry and protein function. *Annu Rev Biophys Biomol Struct*, 29:105–153, 2000.

[47] A. B. Goryachev and M. Leda. Many roads to symmetry breaking: molecular mechanisms and theoretical models of yeast cell polarity. *Mol Biol Cell*, 28(3):370–380, Feb 2017.

[48] A. B. Goryachev and A. V. Pokhilko. Dynamics of Cdc42 network embodies a Turing-type mechanism of yeast cell polarity. *FEBS Lett*, 582(10):1437–1443, Apr 2008.

[49] M. Gotta, M. C. Abraham, and J. Ahringer. CDC-42 controls early cell polarity and spindle orientation in C. elegans. *Curr Biol*, 11(7):482–488, Apr 2001.

[50] E. E. Griffin, D. J. Odde, and G. Seydoux. Regulation of the MEX-5 gradient by a spatially segregated kinase/phosphatase cycle. *Cell*, 146(6):955–968, Sep 2011.

[51] P. Gross, K. V. Kumar, N. W. Goehring, J. S. Bois, C. Hoege, F. Jülicher, and S. W. Grill. Guiding self-organized pattern formation in cell polarity establishment. *Nat Phys*, 15(3):293–300, Jul 2019.

[52] S. Guo and K. J. Kemphues. par-1, a gene required for establishing polarity in C. elegans embryos, encodes a putative Ser/Thr kinase that is asymmetrically distributed. *Cell*, 81(4):611–620, May 1995.

[53] S. Guo and K. J. Kemphues. Molecular genetics of asymmetric cleavage in the early Caenorhabditis elegans embryo. *Curr Opin Genet Dev*, 6(4):408–415, Aug 1996.

[54] O. Hachet, M. Berthelot-Grosjean, K. Kokkoris, V. Vincenzetti, J. Moosbrugger, and S. G. Martin. A phosphorylation cycle shapes gradients of the DYRK family kinase Pom1 at the plasma membrane. *Cell*, 145(7):1116–1128, Jun 2011.

[55] J. Halatek, F. Brauns, and E. Frey. Self-organization principles of intracellular pattern formation. *Philos Trans R Soc Lond B Biol Sci*, 373(1747), 05 2018.

[56] D. R. Hamill, A. F. Severson, J. C. Carter, and B. Bowerman. Centrosome maturation and mitotic spindle assembly in C. elegans require SPD-5, a protein with multiple coiled-coil domains. *Dev Cell*, 3(5):673–684, Nov 2002.

[57] B. Han, K. R. Antkowiak, X. Fan, M. Rutigliano, S. P. Ryder, and E. E. Griffin. Polo-like Kinase Couples Cytoplasmic Protein Gradients in the C. elegans Zygote. *Curr Biol*, 28(1):60–69, 01 2018.

[58] Y. Hao, L. Boyd, and G. Seydoux. Stabilization of cell polarity by the C. elegans RING protein PAR-2. *Dev Cell*, 10(2):199–208, Feb 2006.

[59] T. J. Harris and M. Peifer. Adherens junction-dependent and -independent steps in the establishment of epithelial cell polarity in Drosophila. *J Cell Biol*, 167(1):135–147, Oct 2004.

[60] T. J. C. Harris. Protein clustering for cell polarity: Par-3 as a paradigm. *F1000Res*, 6:1620, 2017.

[61] G. K. A. Hochberg, Y. Liu, E. G. Marklund, B. P. H. Metzger, A. Laganowsky, and J. W. Thornton. A hydrophobic ratchet entrenches molecular complexes. *Nature*, 588(7838):503–508, 12 2020.

[62] C. Hoege, A. T. Constantinescu, A. Schwager, N. W. Goehring, P. Kumar, and A. A. Hyman. LGL can partition the cortex of one-cell Caenorhabditis elegans embryos into two domains. *Curr Biol*, 20(14):1296–1303, Jul 2010.

[63] W. R. Holmes, M. A. Mata, and L. Edelstein-Keshet. Local perturbation analysis: a computational tool for biophysical reaction-diffusion models. *Biophys J*, 108(2):230–236, Jan 2015.

[64] A. R. Houk, A. Jilkine, C. O. Mejean, R. Boltyanskiy, E. R. Dufresne, S. B. Angenent, S. J. Altschuler, L. F. Wu, and O. D. Weiner. Membrane tension maintains cell polarity by confining signals to the leading edge during neutrophil migration. *Cell*, 148(1-2):175–188, Jan 2012.

[65] M. Howard. How to build a robust intracellular concentration gradient. *Trends Cell Biol*, 22(6):311–317, Jun 2012.

[66] A. S. Howell, N. S. Savage, S. A. Johnson, I. Bose, A. W. Wagner, T. R. Zyla, H. F. Nijhout, M. C. Reed, A. B. Goryachev, and D. J. Lew. Singularity in polarization: rewiring yeast cells to make two buds. *Cell*, 139(4):731–743, Nov 2009.

[67] W. Y. Huang, Q. Yan, W. C. Lin, J. K. Chung, S. D. Hansen, S. M. Christensen, H. L. Tu, J. Kuriyan, and J. T. Groves. Phosphotyrosine-mediated LAT assembly on membranes drives kinetic bifurcation in recruitment dynamics of the Ras activator SOS. *Proc Natl Acad Sci U S A*, 113(29):8218–8223, 07 2016.

[68] W. Y. C. Huang, S. Alvarez, Y. Kondo, Y. K. Lee, J. K. Chung, H. Y. M. Lam, K. H. Biswas, J. Kuriyan, and J. T. Groves. A molecular assembly phase transition and kinetic proofreading modulate Ras activation by SOS. *Science*, 363(6431):1098–1103, 03 2019.

[69] L. Hubatsch, F. Peglion, J. D. Reich, N. T. Rodrigues, N. Hirani, R. Illukkumbura, and N. W. Goehring. A cell size threshold limits cell polarity and asymmetric division potential. *Nat Phys*, 15(10):1075–1085, Jun 2019.

[70] R. Iino, I. Koyama, and A. Kusumi. Single molecule imaging of green fluorescent proteins in living cells: E-cadherin forms oligomers on the free cell surface. *Biophys J*, 80(6):2667–2677, Jun 2001.

[71] J. E. Irazoqui, A. S. Gladfelter, and D. J. Lew. Scaffold-mediated symmetry breaking by Cdc42p. *Nat Cell Biol*, 5(12):1062–1070, Dec 2003.

[72] A. Jenny, J. Reynolds-Kenneally, G. Das, M. Burnett, and M. Mlodzik. Diego and Prickle regulate Frizzled planar cell polarity signalling by competing for Dishevelled binding. *Nat Cell Biol*, 7(7):691–697, Jul 2005.

[73] T. Jiang, R. F. McKinley, M. A. McGill, S. Angers, and T. J. Harris. A Par-1-Par-3-Centrosome Cell Polarity Pathway and Its Tuning for Isotropic Cell Adhesion. *Curr Biol*, 25(20):2701–2708, Oct 2015.

[74] A. Jilkine, S. B. Angenent, L. F. Wu, and S. J. Altschuler. A density-dependent switch drives stochastic clustering and polarization of signaling molecules. *PLoS Comput Biol*, 7(11):e1002271, Nov 2011.

[75] P. J. Kang, A. Sanson, B. Lee, and H. O. Park. A GDP/GTP exchange factor involved in linking a spatial landmark to cell polarity. *Science*, 292(5520):1376–1378, May 2001.

[76] K. J. Kemphues, J. R. Priess, D. G. Morton, and N. S. Cheng. Identification of genes required for cytoplasmic localization in early C. elegans embryos. *Cell*, 52(3):311–320, Feb 1988.

[77] K. Klinkert, N. Levernier, P. Gross, C. Gentili, L. von Tobel, M. Pierron, C. Busso, S. Herrman, S. W. Grill, K. Kruse, and P. Gönczy. . *Elife*, 8, 02 2019.

[78] D. Klompstra, D. C. Anderson, J. Y. Yeh, Y. Zilberman, and J. Nance. An instructive role for C. elegans E-cadherin in translating cell contact cues into cortical polarity. *Nat Cell Biol*, 17(6):726–735, Jun 2015.

[79] J. D. Knight, M. G. Lerner, J. G. Marcano-Velázquez, R. W. Pastor, and J. J. Falke. Single molecule diffusion of membrane-bound proteins: window into lipid contacts and bilayer dynamics. *Biophys J*, 99(9):2879–2887, Nov 2010.

[80] D. Koch. Homo-Oligomerisation in Signal Transduction: Dynamics, Homeostasis, Ultrasensitivity, Bistability. *J Theor Biol*, 499:110305, 08 2020.

[81] D. F. Kucik, E. L. Elson, and M. P. Sheetz. Cell migration does not produce membrane flow. *J Cell Biol*, 111(4):1617–1622, Oct 1990.

[82] K. T. Kumfer, S. J. Cook, J. M. Squirrell, K. W. Eliceiri, N. Peel, K. F. O'Connell, and J. G. White. CGEF-1 and CHIN-1 regulate CDC-42 activity during asymmetric division in the Caenorhabditis elegans embryo. *Mol Biol Cell*, 21(2):266–277, Jan 2010.

[83] A. Kusumi, K. Suzuki, and K. Koyasako. Mobility and cytoskeletal interactions of cell adhesion receptors. *Curr Opin Cell Biol*, 11(5):582–590, Oct 1999.

[84] C. F. Lang and E. Munro. The PAR proteins: from molecular circuits to dynamic self-stabilizing cell polarity. *Development*, 144(19):3405–3416, 10 2017.

[85] C. F. Lang and E. M. Munro. Oligomerization of peripheral membrane proteins provides tunable control of cell surface polarity. *bioRxiv*, 2022.

[86] M. A. Lemmon. Membrane recognition by phospholipid-binding domains. *Nat Rev Mol Cell Biol*, 9(2):99–111, Feb 2008.

[87] E. D. Levy and S. Teichmann. Structural, evolutionary, and assembly principles of protein oligomerization. *Prog Mol Biol Transl Sci*, 117:25–51, 2013.

[88] B. Li, H. Kim, M. Beers, and K. Kemphues. Different domains of C. elegans PAR-3 are required at different times in development. *Dev Biol*, 344(2):745–757, Aug 2010.

[89] Y. W. Lim, F. L. Wen, P. Shankar, T. Shibata, and F. Motegi. A balance between antagonizing PAR proteins specifies the pattern of asymmetric and symmetric divisions in C. elegans embryogenesis. *Cell Rep*, 36(1):109326, 07 2021.

[90] W. C. Lo, H. O. Park, and C. S. Chou. Mathematical analysis of spontaneous emergence of cell polarity. *Bull Math Biol*, 76(8):1835–1865, Aug 2014.

[91] M. Loose, E. Fischer-Friedrich, J. Ries, K. Kruse, and P. Schwille. Spatial regulators for bacterial cell division self-organize into surface waves in vitro. *Science*, 320(5877):789–792, May 2008.

[92] M. Lynch. Evolutionary diversification of the multimeric states of proteins. *Proc Natl Acad Sci U S A*, 110(30):E2821–2828, Jul 2013.

[93] D. Ma, C. H. Yang, H. McNeill, M. A. Simon, and J. D. Axelrod. Fidelity in planar cell polarity signalling. *Nature*, 421(6922):543–547, Jan 2003.

[94] W. Ma, M. Chen, H. Kang, Z. Steinhart, S. Angers, X. He, and M. W. Kirschner. Single-molecule dynamics of Dishevelled at the plasma membrane and Wnt pathway activation. *Proc Natl Acad Sci U S A*, 117(28):16690–16701, 07 2020.

[95] P. Maiuri, J. F. Rupprecht, S. Wieser, V. Ruprecht, O. Bénichou, N. Carpi, M. Coppey, S. De Beco, N. Gov, C. P. Heisenberg, C. Lage Crespo, F. Lautenschlaeger, M. Le Berre, A. M. Lennon-Dumenil, M. Raab, H. R. Thiam, M. Piel, M. Sixt, and R. Voituriez. Actin flows mediate a universal coupling between cell speed and cell persistence. *Cell*, 161(2):374–386, Apr 2015.

[96] S. G. Martin, W. H. McDonald, J. R. Yates, and F. Chang. Tea4p links microtubule plus ends with the formin for3p in the establishment of cell polarity. *Dev Cell*, 8(4):479–491, Apr 2005.

[97] F. Martin-Belmonte, A. Gassama, A. Datta, W. Yu, U. Rescher, V. Gerke, and K. Mostov. PTEN-mediated apical segregation of phosphoinositides controls epithelial morphogenesis through Cdc42. *Cell*, 128(2):383–397, Jan 2007.

[98] J. Mata and P. Nurse. tea1 and the microtubular cytoskeleton are important for generating global spatial order within the fission yeast cell. *Cell*, 89(6):939–949, Jun 1997.

[99] M. Mayer, M. Depken, J. S. Bois, F. Jülicher, and S. W. Grill. Anisotropies in cortical tension reveal the physical basis of polarizing cortical flows. *Nature*, 467(7315):617–621, Sep 2010.

[100] R. F. McKinley and T. J. Harris. Displacement of basolateral Bazooka/PAR-3 by regulated transport and dispersion during epithelial polarization in Drosophila. *Mol Biol Cell*, 23(22):4465–4471, Nov 2012.

[101] R. F. McKinley, C. G. Yu, and T. J. Harris. Assembly of Bazooka polarity landmarks through a multifaceted membrane-association mechanism. *J Cell Sci*, 125(Pt 5):1177–1190, Mar 2012.

[102] A. P. Minton. Effects of excluded surface area and adsorbate clustering on surface adsorption of proteins. II. Kinetic models. *Biophys J*, 80(4):1641–1648, Apr 2001.

[103] M. Mittasch, P. Gross, M. Nestler, A. W. Fritsch, C. Iserman, M. Kar, M. Munder, A. Voigt, S. Alberti, S. W. Grill, and M. Kreysing. Non-invasive perturbations of intracellular flow reveal physical principles of cell organization. *Nat Cell Biol*, 20(3):344–351, 03 2018.

[104] E. Morais-de Sá, V. Mirouse, and D. St Johnston. aPKC phosphorylation of Bazooka defines the apical/lateral border in Drosophila epithelial cells. *Cell*, 141(3):509–523, Apr 2010.

[105] Y. Mori, A. Jilkine, and L. Edelstein-Keshet. Wave-pinning and cell polarity from a bistable reaction-diffusion system. *Biophys J*, 94(9):3684–3697, May 2008.

[106] F. Motegi and A. Sugimoto. Sequential functioning of the ECT-2 RhoGEF, RHO-1 and CDC-42 establishes cell polarity in Caenorhabditis elegans embryos. *Nat Cell Biol*, 8(9):978–985, Sep 2006.

[107] F. Motegi, S. Zonies, Y. Hao, A. A. Cuenca, E. Griffin, and G. Seydoux. Microtubules induce self-organization of polarized PAR domains in Caenorhabditis elegans zygotes. *Nat Cell Biol*, 13(11):1361–1367, Oct 2011.

[108] E. Munro. Protein Clustering Shapes Polarity Protein Gradients. *Dev Cell*, 42(4):309–311, 08 2017.

[109] E. Munro, J. Nance, and J. R. Priess. Cortical flows powered by asymmetrical contraction transport PAR proteins to establish and maintain anterior-posterior polarity in the early C. elegans embryo. *Dev Cell*, 7(3):413–424, Sep 2004.

[110] M. Nakaya, A. Fukui, Y. Izumi, K. Akimoto, M. Asashima, and S. Ohno. Meiotic maturation induces animal-vegetal asymmetric distribution of aPKC and ASIP/PAR-3 in Xenopus oocytes. *Development*, 127(23):5021–5031, Dec 2000.

[111] K. F. O'Connell, K. N. Maxwell, and J. G. White. The spd-2 gene is required for polarization of the anteroposterior axis and formation of the sperm asters in the Caenorhabditis elegans zygote. *Dev Biol*, 222(1):55–70, Jun 2000.

[112] C. H. Oon and K. E. Prehoda. Asymmetric recruitment and actin-dependent cortical flows drive the neuroblast polarity cycle. *Elife*, 8, 05 2019.

[113] C. H. Oon and K. E. Prehoda. Phases of cortical actomyosin dynamics coupled to the neuroblast polarity cycle. *Elife*, 10, 11 2021.

[114] M. Otsuji, S. Ishihara, C. Co, K. Kaibuchi, A. Mochizuki, and S. Kuroda. A mass conserved reaction-diffusion system captures properties of cell polarity. *PLoS Comput Biol*, 3(6):e108, Jun 2007.

[115] F. Peglion and N. W. Goehring. Switching states: dynamic remodelling of polarity complexes as a toolkit for cell polarization. *Curr Opin Cell Biol*, 60:121–130, 10 2019.

[116] Y. Peng and J. D. Axelrod. Asymmetric protein localization in planar cell polarity: mechanisms, puzzles, and challenges. *Curr Top Dev Biol*, 101:33–53, 2012.

[117] F. Persson, M. Lindén, C. Unoson, and J. Elf. Extracting intracellular diffusive states and transition rates from single-molecule tracking data. *Nat Methods*, 10(3):265–269, Mar 2013.

[118] R. Ramanujam, Z. Han, Z. Zhang, P. Kanchanawong, and F. Motegi. Establishment of the PAR-1 cortical gradient by the aPKC-PRBH circuit. *Nat Chem Biol*, 14(10):917–927, 10 2018.

[119] S. Ranganathan and E. I. Shakhnovich. Dynamic metastable long-living droplets formed by sticker-spacer proteins. *Elife*, 9, 06 2020.

[120] D. M. Raskin and P. A. de Boer. MinDE-dependent pole-to-pole oscillation of division inhibitor MinC in Escherichia coli. *J Bacteriol*, 181(20):6419–6424, Oct 1999.

[121] P. Recouvreux and P. F. Lenne. Molecular clustering in the cell: from weak interactions to optimized functional architectures. *Curr Opin Cell Biol*, 38:18–23, Feb 2016.

[122] P. Recouvreux, T. R. Sokolowski, A. Grammoustianou, P. R. ten Wolde, and M. Dogterom. Chimera proteins with affinity for membranes and microtubule tips polarize in the membrane of fission yeast cells. *Proc Natl Acad Sci U S A*, 113(7):1811–1816, Feb 2016.

[123] S. A. Rincon, P. Bhatia, C. Bicho, M. Guzman-Vendrell, V. Fraisier, W. E. Borek, F. d. e. L. Alves, F. Dingli, D. Loew, J. Rappsilber, K. E. Sawin, S. G. Martin, and A. Paoletti. Pom1 regulates the assembly of Cdr2-Mid1 cortical nodes for robust spatial control of cytokinesis. *J Cell Biol*, 206(1):61–77, Jul 2014.

[124] K. Ritchie, R. Iino, T. Fujiwara, K. Murase, and A. Kusumi. The fence and picket structure of the plasma membrane of live cells as revealed by single molecule techniques (Review). *Mol Membr Biol*, 20(1):13–18, 2003.

[125] F. B. Robin, W. M. McFadden, B. Yao, and E. M. Munro. Single-molecule analysis of cell surface dynamics in Caenorhabditis elegans embryos. *Nat Methods*, 11(6):677–682, Jun 2014.

[126] J. Rodriguez, F. Peglion, J. Martin, L. Hubatsch, J. Reich, N. Hirani, A. G. Gubieda, J. Roffey, A. R. Fernandes, D. St Johnston, J. Ahringer, and N. W. Goehring. aPKC Cycles between Functionally Distinct PAR Protein Assemblies to Drive Cell Polarity. *Dev Cell*, 42(4):400–415, 08 2017.

[127] L. Rose and P. Gönczy. Polarity establishment, asymmetric division and segregation of fate determinants in early C. elegans embryos. *WormBook*, pages 1–43, Dec 2014.

[128] L. S. Rose, M. L. Lamb, S. N. Hird, and K. J. Kemphues. Pseudocleavage is dispensable for polarity and development in C. elegans embryos. *Dev Biol*, 168(2):479–489, Apr 1995.

[129] S. Saha, C. A. Weber, M. Nousch, O. Adame-Arana, C. Hoege, M. Y. Hein, E. Osborne-Nishimura, J. Mahamid, M. Jahnel, L. Jawerth, A. Pozniakovski, C. R. Eckmann, F. Jülicher, and A. A. Hyman. Polar Positioning of Phase-Separated Liquid Compartments in Cells Regulated by an mRNA Competition Mechanism. *Cell*, 166(6):1572–1584, Sep 2016.

[130] A. Sailer, A. Anneken, Y. Li, S. Lee, and E. Munro. Dynamic Opposition of Clustered Proteins Stabilizes Cortical Polarity in the C. elegans Zygote. *Dev Cell*, 35(1):131–142, Oct 2015.

[131] T. E. Saunders, K. Z. Pan, A. Angel, Y. Guan, J. V. Shah, M. Howard, and F. Chang. Noise reduction in the intracellular pom1p gradient by a dynamic clustering mechanism. *Dev Cell*, 22(3):558–572, Mar 2012.

[132] N. S. Savage, A. T. Layton, and D. J. Lew. Mechanistic mathematical model of polarity in yeast. *Mol Biol Cell*, 23(10):1998–2013, May 2012.

[133] T. Schwarz-Romond, M. Fiedler, N. Shibata, P. J. Butler, A. Kikuchi, Y. Higuchi, and M. Bienz. The DIX domain of Dishevelled confers Wnt signaling by dynamic polymerization. *Nat Struct Mol Biol*, 14(6):484–492, Jun 2007.

[134] T. Schwarz-Romond, C. Metcalfe, and M. Bienz. Dynamic recruitment of axin by Dishevelled protein assemblies. *J Cell Sci*, 120(Pt 14):2402–2412, Jul 2007.

[135] M. P. Sheetz, S. Turney, H. Qian, and E. L. Elson. Nanometre-level analysis demonstrates that lipid flow does not drive membrane glycoprotein movements. *Nature*, 340(6231):284–288, Jul 1989.

[136] Amit R. Singh, Travis Leadbetter, and Brian A. Camley. Sensing the shape of a cell: reaction-diffusion and energy minimization. *arXiv*, 2021.

[137] J. Smith, D. Calidas, H. Schmidt, T. Lu, D. Rasoloson, and G. Seydoux. Spatial patterning of P granules by RNA-induced phase separation of the intrinsically-disordered protein MEG-3. *Elife*, 5, 12 2016.

[138] E. V. Soriano, M. E. Ivanova, G. Fletcher, P. Riou, P. P. Knowles, K. Barnouin, A. Purkiss, B. Kostelecky, P. Saiu, M. Linch, A. Elbediwy, S. Kjær, N. O'Reilly, A. P. Snijders, P. J. Parker, B. J. Thompson, and N. Q. McDonald. aPKC Inhibition by Par3 CR3 Flanking Regions Controls Substrate Access and Underpins Apical-Junctional Polarization. *Dev Cell*, 38(4):384–398, 08 2016.

[139] H. Strutt, J. Gamage, and D. Strutt. Robust Asymmetric Localization of Planar Polarity Proteins Is Associated with Organization into Signalosome-like Domains of Variable Stoichiometry. *Cell Rep*, 17(10):2660–2671, 12 2016.

[140] H. Strutt, J. Gamage, and D. Strutt. Reciprocal action of Casein Kinase Iϵ on core planar polarity proteins regulates clustering and asymmetric localisation. *Elife*, 8, 05 2019.

[141] H. Strutt, S. J. Warrington, and D. Strutt. Dynamics of core planar polarity protein turnover and stable assembly into discrete membrane subdomains. *Dev Cell*, 20(4):511–525, Apr 2011.

[142] A. Suzuki and S. Ohno. The PAR-aPKC system: lessons in polarity. *J Cell Sci*, 119(Pt 6):979–987, Mar 2006.

[143] Y. Tabuse, Y. Izumi, F. Piano, K. J. Kemphues, J. Miwa, and S. Ohno. Atypical protein kinase C cooperates with PAR-3 to establish embryonic polarity in Caenorhabditis elegans. *Development*, 125(18):3607–3614, Sep 1998.

[144] J. Taylor, N. Abramova, J. Charlton, and P. N. Adler. Van Gogh: a new Drosophila tissue polarity gene. *Genetics*, 150(1):199–210, Sep 1998.

[145] L. Timmons, D. L. Court, and A. Fire. Ingestion of bacterially expressed dsRNAs can produce specific and potent genetic interference in Caenorhabditis elegans. *Gene*, 263(1-2):103–112, Jan 2001.

[146] P. Tomancak, F. Piano, V. Riechmann, K. C. Gunsalus, K. J. Kemphues, and A. Ephrussi. A Drosophila melanogaster homologue of Caenorhabditis elegans par-1 acts at an early step in embryonic-axis formation. *Nat Cell Biol*, 2(7):458–460, Jul 2000.

[147] D. R. Tree, J. M. Shulman, R. Rousset, M. P. Scott, D. Gubb, and J. D. Axelrod. Prickle mediates feedback amplification to generate asymmetric planar cell polarity signaling. *Cell*, 109(3):371–381, May 2002.

[148] Y. C. Tse, M. Werner, K. M. Longhini, J. C. Labbe, B. Goldstein, and M. Glotzer. RhoA activation during polarization and cytokinesis of the early Caenorhabditis elegans embryo is differentially dependent on NOP-1 and CYK-4. *Mol Biol Cell*, 23(20):4020–4031, Oct 2012.

[149] K. Tsujita, T. Takenawa, and T. Itoh. Feedback regulation between plasma membrane tension and membrane-bending proteins organizes cell polarity during leading edge formation. *Nat Cell Biol*, 17(6):749–758, Jun 2015.

[150] A. M. Turing. The chemical basis of morphogenesis. *Philosophical Transactions of the Royal Society of London. Series B, Biological Sciences*, 237(641):37–72, 1952.

[151] M. van Dop, M. Fiedler, S. Mutte, J. de Keijzer, L. Olijslager, C. Albrecht, C. Y. Liao, M. E. Janson, M. Bienz, and D. Weijers. DIX Domain Polymerization Drives Assembly of Plant Cell Polarity Complexes. *Cell*, 180(3):427–439, 02 2020.

[152] C. R. Vinson and P. N. Adler. Directional non-cell autonomy and the transmission of polarity information by the frizzled gene of Drosophila. *Nature*, 329(6139):549–551, 1987.

[153] J. B. Wallingford. Planar cell polarity and the developmental control of cell behavior in vertebrate embryos. *Annu Rev Cell Dev Biol*, 28:627–653, 2012.

[154] S. C. Wang, T. Y. F. Low, Y. Nishimura, L. Gole, W. Yu, and F. Motegi. Cortical forces and CDC-42 control clustering of PAR proteins for Caenorhabditis elegans embryonic polarization. *Nat Cell Biol*, 19(8):988–995, Aug 2017.

[155] Y. C. Wang, Z. Khan, M. Kaschube, and E. F. Wieschaus. Differential positioning of adherens junctions is associated with initiation of epithelial folding. *Nature*, 484(7394):390–393, Mar 2012.

[156] O. Wartlick, A. Kicheva, and M. González-Gaitán. Morphogen gradient formation. *Cold Spring Harb Perspect Biol*, 1(3):a001255, Sep 2009.

[157] J. L. Watts, B. Etemad-Moghadam, S. Guo, L. Boyd, B. W. Draper, C. C. Mello, J. R. Priess, and K. J. Kemphues. par-6, a gene involved in the establishment of asymmetry in early C. elegans embryos, mediates the asymmetric localization of PAR-3. *Development*, 122(10):3133–3140, Oct 1996.

[158] A. Wodarz, A. Ramrath, U. Kuchinke, and E. Knust. Bazooka provides an apical cue for Inscuteable localization in Drosophila neuroblasts. *Nature*, 402(6761):544–547, Dec 1999.

[159] I. Y. Wong, M. L. Gardel, D. R. Reichman, E. R. Weeks, M. T. Valentine, A. R. Bausch, and D. A. Weitz. Anomalous diffusion probes microstructure dynamics of entangled F-actin networks. *Phys Rev Lett*, 92(17):178101, Apr 2004.

[160] C. F. Wu and D. J. Lew. Beyond symmetry-breaking: competition and negative feedback in GTPase regulation. *Trends Cell Biol*, 23(10):476–483, Oct 2013.

[161] H. Wu. Higher-order assemblies in a new paradigm of signal transduction. *Cell*, 153(2):287–292, Apr 2013.

[162] M. Wu and M. A. Herman. Asymmetric localizations of LIN-17/Fz and MIG-5/Dsh are involved in the asymmetric B cell division in C. elegans. *Dev Biol*, 303(2):650–662, Mar 2007.

[163] Y. Wu, B. Han, T. J. Gauvin, J. Smith, A. Singh, and E. E. Griffin. Single-molecule dynamics of the P granule scaffold MEG-3 in the Caenorhabditis elegans zygote. *Mol Biol Cell*, 30(3):333–345, 02 2019.

[164] Y. Wu, B. Han, Y. Li, E. Munro, D. J. Odde, and E. E. Griffin. zygote. *Proc Natl Acad Sci U S A*, 115(36):E8440–E8449, 09 2018.

[165] Y. Wu, H. Zhang, and E. E. Griffin. Coupling between cytoplasmic concentration gradients through local control of protein mobility in the Caenorhabditis elegans zygote. *Mol Biol Cell*, 26(17):2963–2970, Sep 2015.

[166] H. Yamanaka and E. Nishida. Wnt11 stimulation induces polarized accumulation of Dishevelled at apical adherens junctions through Frizzled7. *Genes Cells*, 12(8):961–967, Aug 2007.

[167] S. Yoshida, A. van der Schuren, M. van Dop, L. van Galen, S. Saiga, M. Adibi, B. Möller, C. A. Ten Hove, P. Marhavy, R. Smith, J. Friml, and D. Weijers. A SOSEKI-based coordinate system interprets global polarity cues in Arabidopsis. *Nat Plants*, 5(2):160–166, 02 2019.

[168] Y. Zhang, W. Wang, J. Chen, K. Zhang, F. Gao, B. Gao, S. Zhang, M. Dong, F. Besenbacher, W. Gong, M. Zhang, F. Sun, and W. Feng. Structural insights into the intrinsic self-assembly of Par-3 N-terminal domain. *Structure*, 21(6):997–1006, Jun 2013.

[169] P. Zhao, X. Teng, S. N. Tantirimudalige, M. Nishikawa, T. Wohland, Y. Toyama, and F. Motegi. Aurora-A Breaks Symmetry in Contractile Actomyosin Networks Independently of Its Role in Centrosome Maturation. *Dev Cell*, 48(5):631–645, 03 2019.

[170] Y. Zheng, A. Bender, and R. A. Cerione. Interactions among proteins involved in bud-site selection and bud-site assembly in Saccharomyces cerevisiae. *J Biol Chem*, 270(2):626–630, Jan 1995.

[171] M. Zhu, J. Cornwall-Scoones, P. Wang, C. E. Handford, J. Na, M. Thomson, and M. Zernicka-Goetz. Developmental clock and mechanism of de novo polarization of the mouse embryo. *Science*, 370(6522), 12 2020.

[172] B. P. Ziemba and J. J. Falke. Lateral diffusion of peripheral membrane proteins on supported lipid bilayers is controlled by the additive frictional drags of (1) bound lipids and (2) protein domains penetrating into the bilayer hydrocarbon core. *Chem Phys Lipids*, 172-173:67–77, 2013.

[173] C. Zmurchok and W. R. Holmes. Biophysical Models of PAR Cluster Transport by Cortical Flow in C. elegans Early Embryogenesis. *Bull Math Biol*, 84(3):40, Feb 2022.

[174] S. Zonies, F. Motegi, Y. Hao, and G. Seydoux. Symmetry breaking and polarization of the C. elegans zygote by the polarity protein PAR-2. *Development*, 137(10):1669–1677, May 2010.

[175] D. Zwicker, A. A. Hyman, and F. Jülicher. Suppression of Ostwald ripening in active emulsions. *Phys Rev E Stat Nonlin Soft Matter Phys*, 92(1):012317, Jul 2015.